# Forest Monitoring and Fire Regime in South Sudan

Project report
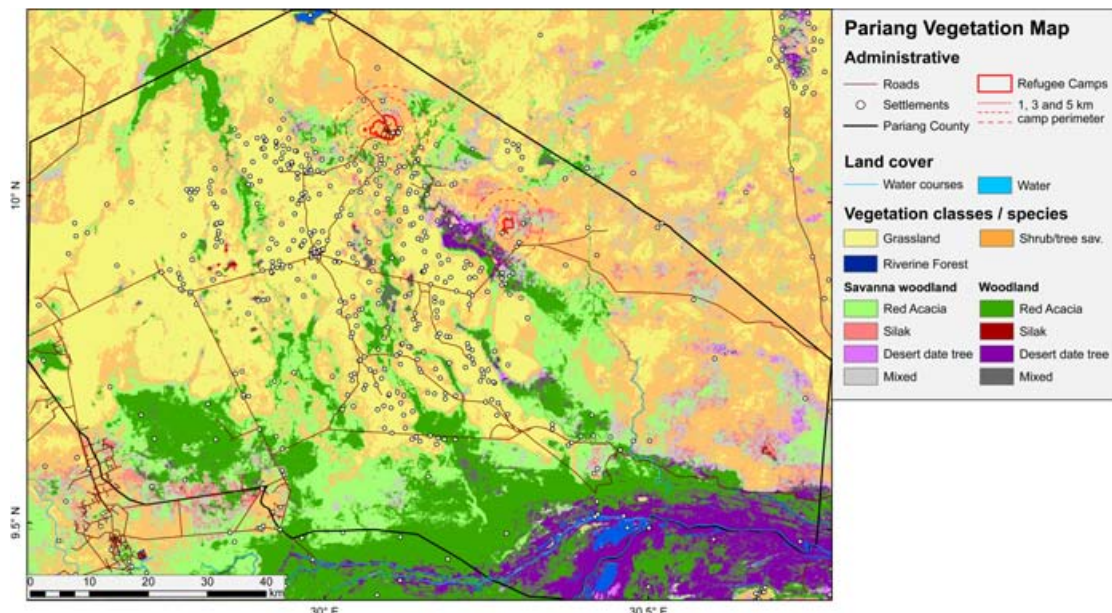
Prepared by:

      Hendrik Wulf, RSL/NPOC, Zurich, Switzerland
      Philip Jörg, RSL/NPOC, Zurich, Switzerland
      Reik Leiterer, RSL/NPOC, Zurich, Switzerland

Approved by:

      DEZA/HH, Berne

Released by:

      Philip Jörg

Version:

      Version 02,
      Zurich, 16.01.2015

Acknowledgements

Content

Abbreviations and Definitions

Abbreviation	Description
BRDF	Bidirectional reflectance distribution function
GPS	Global Positioning System
GSD	Ground sampling distance
L8	Landsat 8
ML	Maximum likelihood (classification algorithm)
NBR	Normalized Burn Ratio
NDVI	Normalized Difference Vegetation Index
NIR	Near Infrared
NPOC	Swiss National Point of Contact for Satellite Images (npoc.ch)
NPV	Non-photosynthetic vegetation
RSL	Remote Sensing Laboratories at the Department of Geography of the University of Zürich (http://www.geo.uzh.ch/en/units/rsl)
SAM	Spectral Angle Mapper (classification algorithm)
SDC	Swiss Agency for Development and Cooperation
SWIR	Short-wavelength infrared
SVM	Support Vector Machines (classification algorithm)
TOA	Top-of-atmosphere
UNHCR	The Office of the United Nations High Commissioner for Refugees
UTM	Universal Transverse Mercator projection
WRS	World Reference System
WV2	WorldView-2

Term	Definition
Data composite	Combination of different 2D data layers with data gaps to generate a complete 2D data layer without data gaps.
Data stack	Combination of various 2D data layers in a 3D data cube.
Landsat	The Landsat program is the longest running enterprise for acquisition of satellite imagery of Earth from 1972 onwards. For example, Landsat 7 data has eight spectral bands with spatial resolutions ranging from 15 to 60 meters; the temporal resolution is 16 days.
MODIS	The Moderate-resolution Imaging Spectroradiometer (MODIS) is a payload remote sensing instrument launched into Earth orbit by NASA in 1999 on board the Terra (EOS AM) Satellite, and in 2002 on board the Aqua (EOS PM) satellite. The instruments capture data in 36 spectral bands ranging in wavelength from 0.4 µm to 14.4 µm and at varying spatial resolutions (250 m, 500 m, and 1 km).

Nadir	The nadir is the direction pointing directly below a particular location.
Object-oriented classification	While pixel-based image analysis is based on the information in each pixel, object-based image analysis is based on information from a set of similar pixels called objects or image objects. More specifically, image objects are groups of pixels that are similar to one another based on a measure of spectral properties (i.e., color), size, shape, and texture, as well as context from a neighborhood surrounding the pixels.
Pansharpened image	Pansharpening is a process of merging high-resolution panchromatic and lower resolution multispectral imagery to create a single high-resolution color image.
Tree/shrub cover	Percentage of the soil surface covered by vertically projected tree and shrub crowns; synonym: canopy cover
TRMM	The Tropical Rainfall Measuring Mission (TRMM) is a joint space NASA and JAXA mission designed to monitor and study tropical rainfall. The satellite was launched on November 27, 1997.
UNOSAT	UNOSAT is the United Nations Institute for Training and Research (UNITAR) Operational Satellite Applications Programme. It is a technology-intensive programme delivering imagery analysis and satellite solutions to relief and development organisations within and outside the UN system.
WorldView-2	WorldView-2 is a commercial Earth observation satellite owned by DigitalGlobe launched in 2009. It provides panchromatic imagery of 0.46 m resolution, and eight-band multispectral imagery with 1.84 m resolution.

Summary

This report summarizes the background, methodology and findings of the "*forest monitoring*" and "*fire regime*" projects carried out from January to December 2014 by the NPOC team composed of Dr. Hendrik Wulf, Dr. Philip Jörg, and Reik Leiterer.

Since September 2011 UNHCR has set up refugee camps in the South Sudanese Counties of Maban and Pariang for about 200,000 people. Their need for building materials, domestic energy and agricultural land led to rapid deforestation within and around the refugee camps. In an effort to assess the environmental impact and to manage the natural resources sustainably between host and refugee communities, UNHCR elaborated an environmental action plan. For this UNHCR requested specific environmental expertize from SDC through the deployment of standby personnel from the Swiss Humanitarian Aid Unit (Dr. Urs Bloesch). In this frame SDC additionally mandated the NPOC to assist the initiative of UNHCR in the establishment of a forest inventory in both refugee-hosting Counties based on remote sensing data. To further understand the extent and impact of fires on different land cover and ecosystems in South Sudan, we analyze their spatiotemporal distribution and assess the impact of rainfall on annual variations in burned areas.

Our approach to establish the forest inventory combines the analysis of remote sensing satellite data along with ground-based observations gathered by Dr. Urs Bloesch and his team during a vegetation survey in April/May 2014. These datasets comprise 80 freely available scenes of Landsat 5, 7 and 8, 37 survey site description on vegetation characteristics and land cover as well as seven WorldView-2 scenes provides by UNOSAT under the US Department of State, Humanitarian Information Unit, NextView License. Preprocessing of remote sensing data included their radiometric calibration, atmospheric correction, cloud and other data gap identification, geographic projection, mosaicking and co-registration. In preparation of the vegetation survey the NPOC provided detailed preliminary maps and data on vegetation cover and potential field survey sites.

The forest inventory mapping comprises map products on vegetation cover, tree species, and vegetation changes. For the vegetation cover products, we used two adapted approaches for WorldView-2 and Landsat data to generate vegetation masks and vegetation cover products. The WorldView-2 approach is based on a field data optimized NDVI thresholds and supervised SVM image classification, whereas the Landsat approach exclusively utilizes acquisitions after the onset of the dry season, detected by satellite rainfall data, to better distinguish between dried up grasslands and shrub/tree vegetation. Exploiting the linear relation between Landsat NDVI and WorldView-2 canopy cover, we convert Landsat NDVI data to canopy cover. Based on the canopy cover percentages, we distinguish between grassland, shrub/tree savanna, savanna woodland, and woodland vegetation classes. These approaches provide reasonable results (R^2 = 0.45 - 0.5) but include woodland misclassifications in evergreen wetlands.

For the tree species products, we distinguished between the Red acacia, the Desert date tree, the Doum palm, and the Silak. The classification in Maban is based on an extended calibration and validation dataset, to train and validate the supervised classification approach that yielded an overall accuracy of 62.6%. The lower ground data and WorldView-2 data availability in Pariang facilitated simply a supervised classification approach without validation. We combined the data on the vegetation classes and vegetation species to a vegetation map product. In addition, we distinguish in the vegetation map riverine forest along watercourses and mixed savanna woodland and mixed woodland that exhibits less than 70% monospecific stands. Furthermore, spatial data on watercourses, roads, settlements and refugee camps is illustrated. The vegetation dynamics products indicate vegetation reductions within and in the surroundings of refugee camps based on two NDVI change detection approaches using Landsat data.

The analysis of the fire regime reveals that substantial areas in South Sudan (52.8%), Upper Nile (52.6%), Unity (51.7%), Maban (57.9%), and Pariang (67.0%) are burnt on average each year. We analyzed the spatial and temporal distribution of fires and investigated potential relationships with rainfall characteristics (seasonal rainfall magnitudes and duration). Multiple linear regression analysis did not reveal significant direct links between both variables in Maban and Pariang, which indicates a more complex or random fire-spread mechanism. However, optimal fire spread conditions appear to be limited to climatic zones with annual rainfall ranging between 0.6 and 1.4 m/yr. The subsequent analysis of burnt areas in relation with land cover types indicated that (a) urban and frequently flooded land cover types are hardly affected by fires, (b) the frequently burnt land cover classes (frequency > 0.5 fire per year) account for almost 80% of the total area; (c) fires tend to occur more often in densely vegetated regions as compared to less dense vegetated regions, with the exception of forests.

Final recommendations for potential future studies include the targeted use of multi-temporal WorldView-2 data for vegetation change analysis at the refugee camp scale and object-oriented classification approaches for tree species identification.

# 1.	Introduction

## 1.1	Context

Since July 2011 fighting in the Sudanese states of South Kordofan and Blue Nile led to the flight of about 200,000 people to South Sudan. UNHCR's emergency response for these Sudanese refugees started in September 2011 by setting up refugee camps in Pariang County in Unity State and Maban County in Upper Nile State of South Sudan (Fig. 1). Further escalating violence in South Sudan during December 2013 displaced more than 1 million people internally and led to the arrival of new refugees in these camps. Given the sparse population of ca. 36,000 and 83,000 inhabitants in Maban and Pariang County, respectively [*Tiller and Healy*, 2013], the refugees are by far outnumbering the local host communities [*Bloesch et al.*, 2013].

In an effort to assess the environment impact of the refugee on the ecosystem three major challenges have been identified [*Bloesch et al.*, 2013]:

1) The permanent need of the refugees for building materials for shelter and latrines (wooden poles and sticks) and for their daily domestic energy consumption (cooking, heating and lighting) led to rapid deforestation around the refugee camps. Tree cutting is greatly accelerated by illegal charcoal making. The impact of tree cutting on the local ecosystems is locally significant in the surroundings of the camps/settlement. Within a radius of about 2 km from the Yida refugee camp most of the trees are chopped down. Generally, the radius of deforestation around the settlements is steadily increasing while the cutting rate decreases with increasing distance from the camps/settlement.
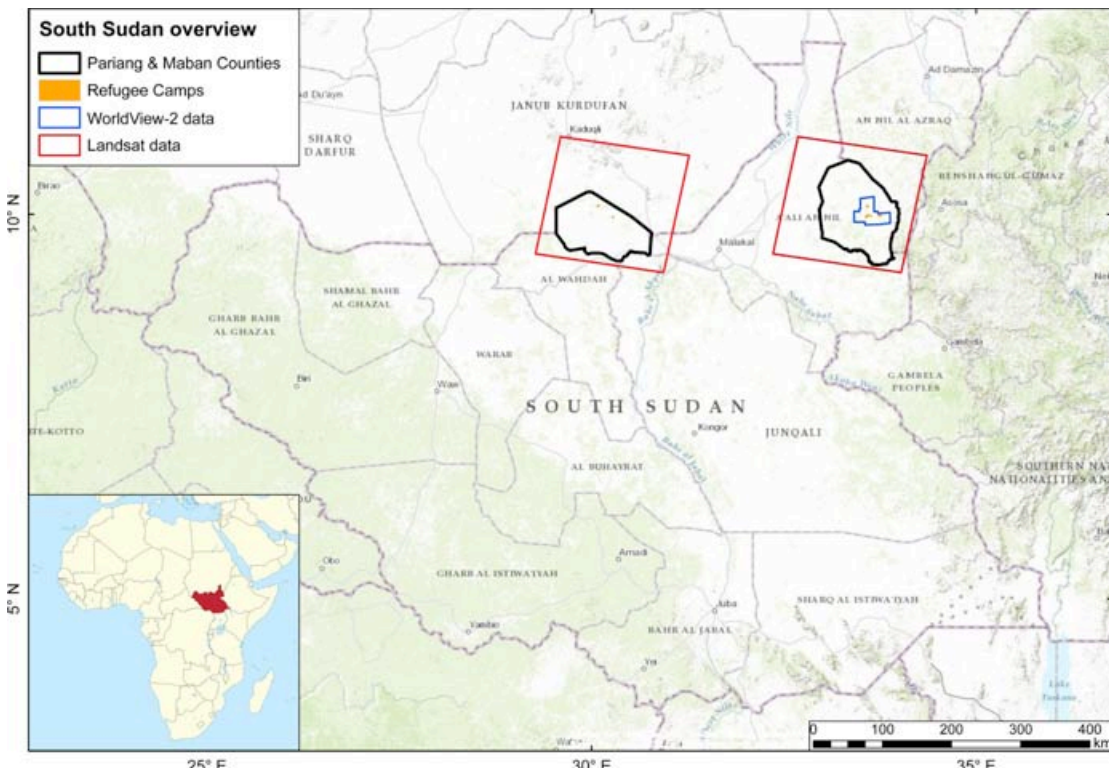
Fig. 1. Overview of South Sudan and the location of both counties Pariang and Maban (black outlines) in the states Unity and Upper Nile, respectively. Red squares indicate the coverage of respective Landsat acquisitions according to the WRS-2. Blue outlines indicate the WorldView-2 coverage.

2) The additional needs of the Sudanese refugees for natural resources including water, pasture and agricultural land put an additional burden on the local ecosystems with an inherent risk of overstressing their carrying capacity. Host communities see their natural resources increasingly depleted in the surroundings of the refugee camps, which causes additional tensions between refugees and host communities.

3) Large parts of the refugee-hosting areas are annually burnt during the dry season. This combustion of biomass released large amounts of greenhouse gases, while late dry season fires may also kill the trees and shrubs thereby opening the savannas.

1.2   Aims

In view of a sustainable supply of wood for both communities a forest mapping and inventory has been recommended for the refugee hosting areas in Maban County (Upper Nile) and Pariang County (Unity) by both, the multi-party rapid environmental assessment in November 2012 and UNHCR's environmental inception mission in June 2013 [*Bloesch et al.* 2013].

The aim of the forest mapping/inventory is to estimate the total amount of accessible wood resources for defining a sustainable use of poles and fuelwood for the Sudanese refugees and local communities. The forest maps and inventories will serve as a basis for identifying potential harvest areas and for defining a community forest management where the locals take the lead in the sustainable management of their wood resources. This approach will also contribute to reduce the conflict potential between refugees and locals competing for the same natural resources. Furthermore, it is of interest to assess the status of the forest prior to the first refugee influx in 2011 as a baseline in comparison with the current situation.

In addition to the "Forest Monitoring" project the need emerged to analyze the annually burnt areas in South Sudan in more detail. Initial aerial observations during the field campaign by Dr. Urs Bloesch and his team in May 2014 indicated that more than 50% of the areas in Maban and Pariang counties experienced recent fires [*Bloesch*, 2014]. Given the importance of fires for the terrestrial ecosystems and the land use and considering the lack of previous studies analyzing burnt area patterns in South Sudan, an initial analysis on the spatiotemporal distribution of burnt areas aims to fill this knowledge gap.

1.3   Approach

The RSL from the University of Zurich has been mandated by SDC to carry out the remote sensing part of the forest mapping/inventory in Maban and Pariang counties. The RSL has identified typical sites for the field verification (ground truthing). In total 49 vegetation sites and 33 land cover sites nearby the refugee camps (settlement) and along the access roads have been located on digital map sections using high resolution WorldView-2 satellite data provided by UNOSAT (for Maban County) and Landsat-5, 7 & 8 satellite data for both counties (Fig. 2, Fig. 3).

As far as possible, the species composition will be considered in the classification of the vegetation types. The locally dominant tree species, including the Doum palm (*Hyphaene thebaica*), the Red acacia (*Acacia seyal*), Silak (*Anogeissus leiocarpus*) and the Dessert date tree (*Balanites aegyptiaca*), may form virtually monospecific vegetation units [*Bloesch et al.*, 2013].

The analysis of the fire regime is based on freely available remote sensing products from MODIS and TRMM sensors, which detect burned areas and precipitation, respectively. In addition, we will include data on land cover to elaborate links between fire occurrences and land cover types. In general, will analyze spatial and temporal relations between predominant fire occurrences, rainfall patterns and land cover types.

1.4   Scope and structure of this document

This document presents the methodology, results and limitations of the approaches undertaken to generate a vegetation map for the counties Maban and Pariang in South Sudan. These vegetation maps comprise data on shrub/tree surface cover and tree species data in both counties. In addition to the forest monitoring project, we describe in chapter 4 our approaches and results of the fire regime analysis in South Sudan.

In Chapter 2, we introduce the steps taken from data acquisition to pre- and post-processing. These processing techniques are needed to convert raw data into physically meaningful, geocoded and corrected units that can be compared and analyzed against each other. This chapter also introduces the maps and data used for the field campaign (vegetation survey) lead by Dr. Urs Bloesch in April/May 2014. Furthermore, it also provides an overview of the data collected during this campaign, which served as ground control and calibration data for the tree species classification approach.

In Chapter 3, we present the methodology, results and limitations of the data products, which include maps on (a) vegetation cover, (b) tree species, (c) land cover/vegetation classes and (d) vegetation dynamics. Our approach for each data product is described in detail and illustrated in respective sections and subsections.

In Chapter 4, we present the analysis of the fire regime in South Sudan. First, we present the spatiotemporal distribution of burnt areas and rainfall on a national state and county scale. In a second step we investigate potential relations of burnt areas, rainfall patterns and land cover.

We conclude this report in Chapter 5 and provide recommendations for potential future tasks to improve and build on the products of this project.

2. Forest monitoring data processing

2.1 Data acquisition

The datasets used for the forest inventory analysis and for illustration purposes comprise WordView-2 and Landsat 5, 7 and 8-satellite imagery (Table A1-Table A8), survey site descriptions on vegetation characteristics including GPS-based photography of individual tree species, vector data of refugee camps, infrastructure and administrative borders of South Sudan (Fig. 1).

Landsat data, which are freely available, were acquired from the "EarthExplorer" web-portal (http://earthexplorer.usgs.gov/). Data selection generally aimed at obtaining Landsat scenes covering different times of the dry (Nov.-Apr.) and rainy (May-Oct.) season with minimum cloud cover. Given the low data availability of the recently launched Landsat-8 sensor (Feb. 2013) also data with high cloud cover percentages (Table A1-Table A2) were used to compute Landsat data composites.

Within the Landsat-based WorldReferenceSystem-2 (WRS-2), both counties, Maban (path: 172, row: 53) and Pariang (path: 174, row: 53), are covered by one Landsat tile, respectively (Fig. 2, Fig. 3).

WorldView-2 satellite data were made available by UNOSAT under the US Department of State, Humanitarian Information Unit, NextView License (Fig. 4).
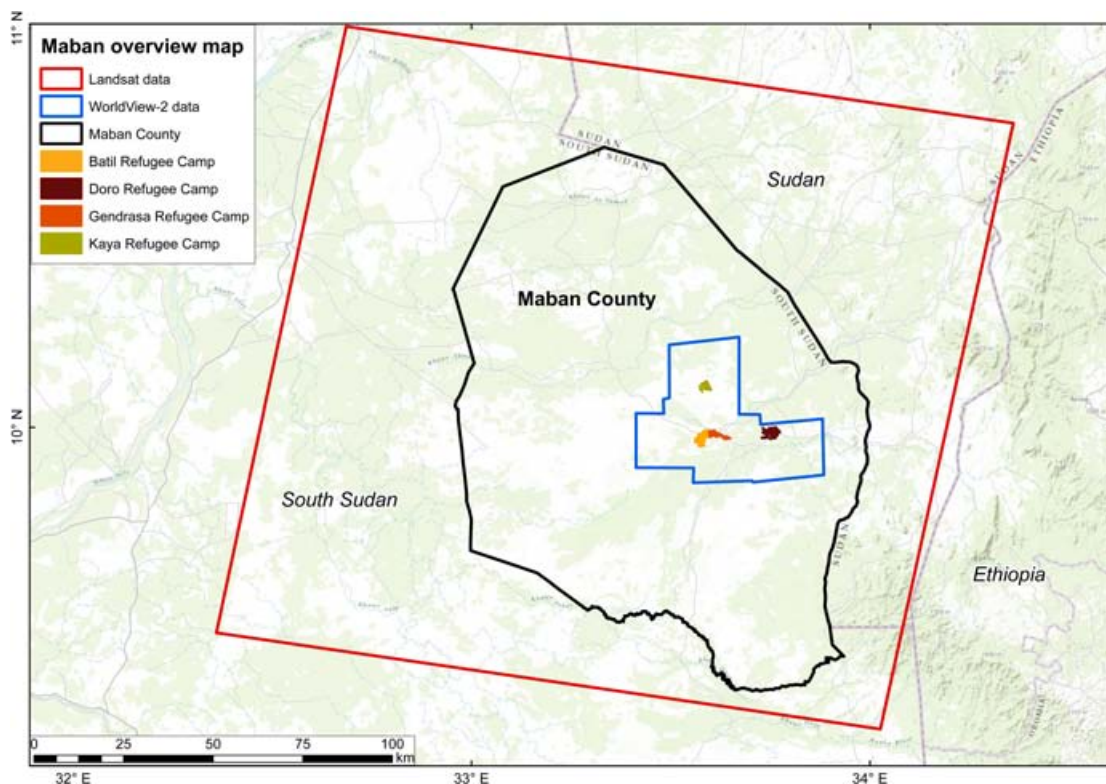
Fig. 2. Overview map of Maban County, Upper Nile, South Sudan highlighting the extent of available Landsat and WorldView-2 data covering the refugee camps.
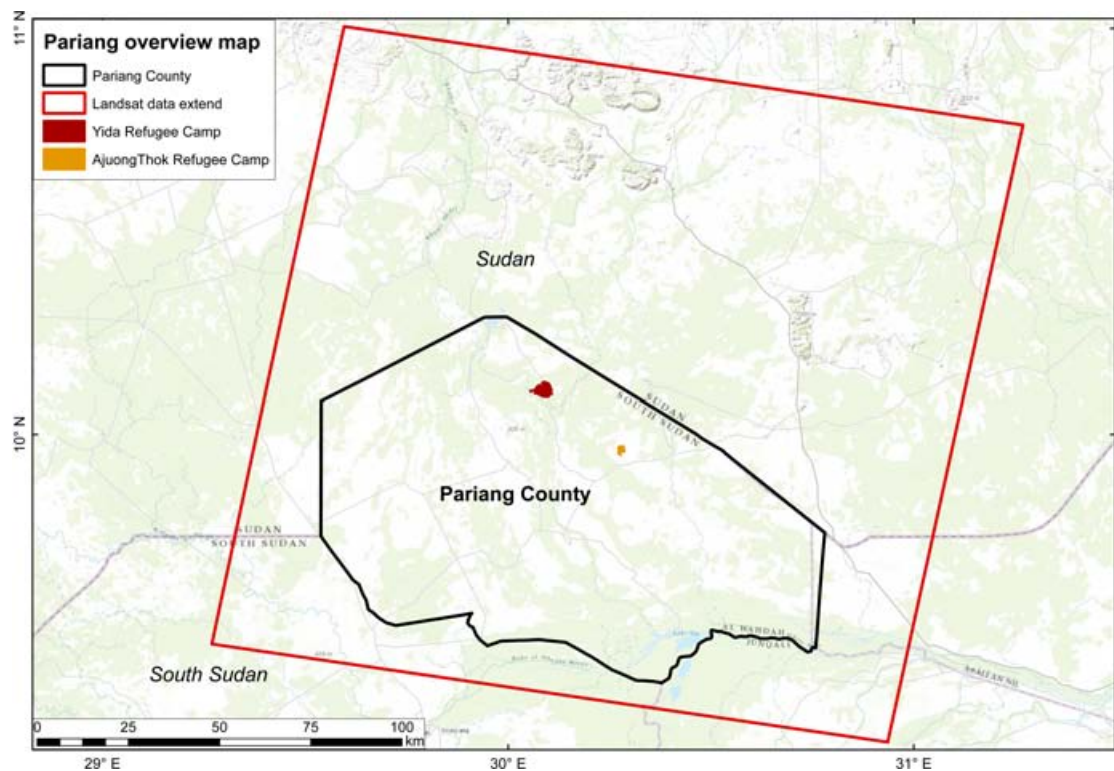
Fig. 3 Overview map of Pariang County, Unity, South Sudan highlighting the extent of available Landsat data covering the refugee camps.
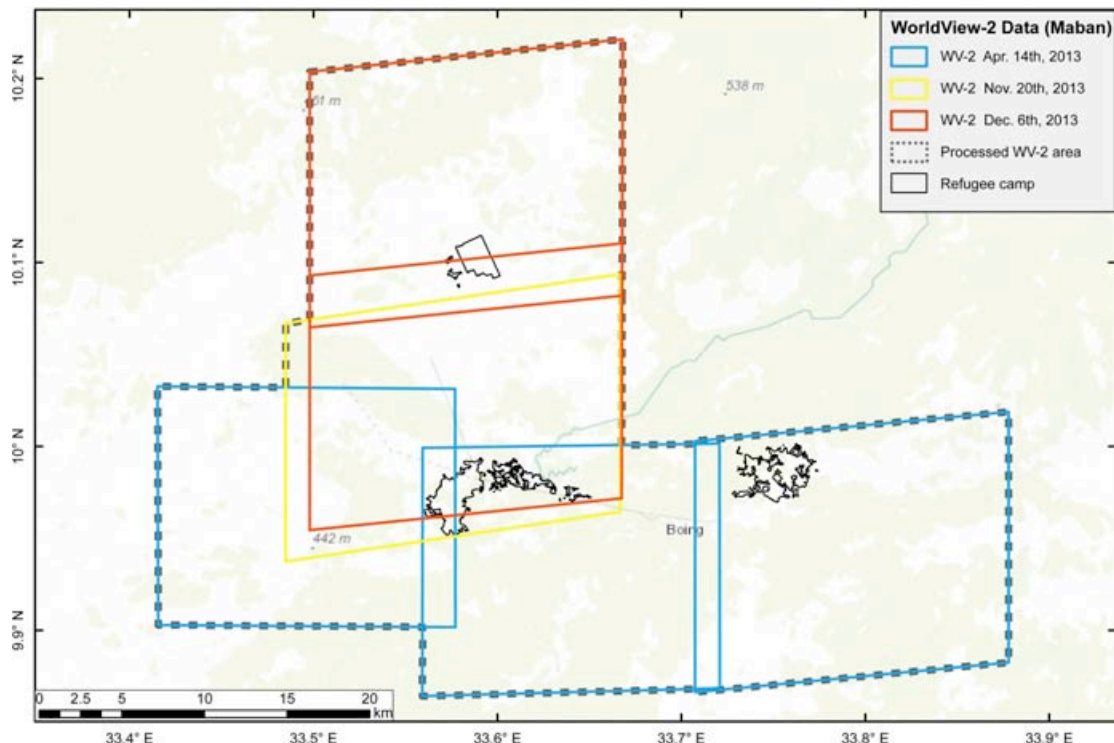
Fig. 4. Overview of WorldView-2 (WV) data coverage and timing in Maban County, South Sudan.

13
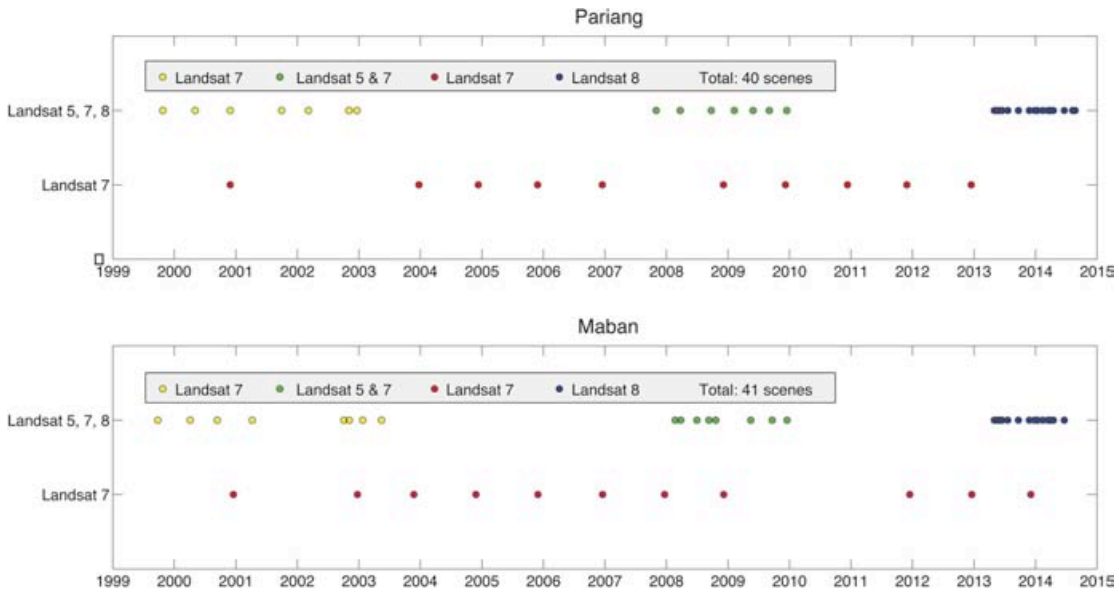
Fig. 5. Timing of Landsat 5, 7 and 8 acquisitions in Maban and Pariang County, South Sudan. The first dataset represents Landsat 7 acquisitions (red circles) at the beginning of the dry season. The second dataset represents Landsat 5, 7 and 8 acquisitions that cluster around the years 2002 (yellow circles), 2008 (green circles) and 2014 (blue circles).

Whereas Landsat data covers multiple dates (16-day repeat cycle) over the past decades (Table A1-Table A8, Fig. 5), WorldView-2 data was acquired at the beginning (Nov./Dec. 2013) and the end (Apr. 2013) of the dry season in 2013 (Fig. 4).

2.2   Data pre-processing

2.2.1   Radiometric calibration

The WorldView-2 and Landsat raw imagery (digital number format = no calibrated physically meaningful units) was calibrated and converted to top-of-atmosphere spectral radiance and reflectance to perform spectral analysis [*Updike and Comp*, 2010]. This radiometric calibration is a common pre-processing step to compensate for radiometric errors from sensor defects, variations in scan angle, and system noise to produce an image that represents true spectral radiance at the sensor [*ENVI*, 2014]. Radiance is the amount of radiation reflected from the surface, bounced in from neighboring pixels, and reflected from clouds above the area of the pixel.

For quantitative analysis of multispectral image data, radiance images are typically corrected to reflectance images. Reflectance is the proportion of the radiation striking a surface to the radiation reflected off of it.

2.2.2   Atmospheric correction

To retrieve the surface reflectance, which characterizes the surface properties, from remotely sensed imagery we additionally removed atmospheric effects. This atmospheric correction compensates for atmospheric effects caused by water vapor and aerosols using inversion procedures based on radiative transfer algorithms and the atmospheric optical properties [*ENVI*, 2014].

To circumvent several license issues for WorldView-2 data (provided in ntf-format) we employed the following radiometric calibration workflow to convert digital

numbers to atmospherically corrected surface reflectance data using the software programs ArcGIS®, ENVI® and Matlab®:

1) Import multispectral and panchromatic WorldView-2 data in '.ntf'-format in ArcGIS® (version 10.3) to export the respective files in '.geotiff'-format.

2) Import multispectral and panchromatic WorldView-2 data in '.geotiff'-format in ENVI® (version 5.0 classic) to perform radiometric calibration and atmospheric correction of multispectral data

3) Conversion of panchromatic radiance data to top-of-atmosphere reflectance data using Matlab® (version 2012a) to implement calibration and correction procedures described by Updike and Comp [*2010*].

Preprocessing of Landsat 5, 7 and 8 imagery was implemented using established preprocessing tools (radiometric calibration and atmospheric correction) in ENVI® (version 5.1):

1) Radiometric calibration Landsat data to convert digital numbers to top-of-atmosphere reflectance data

2) TOA reflectance to surface reflectance data using the quick atmospheric correction (QUAC) tool

Preprocessing of Landsat 7 scenes between 1999 and 2003 was carried out based on services provided by the USGS Earth Resources Observation and Science (EROS) Center Science Processing Architecture (ESPA) On Demand Interface (https://espa.cr.usgs.gov/).
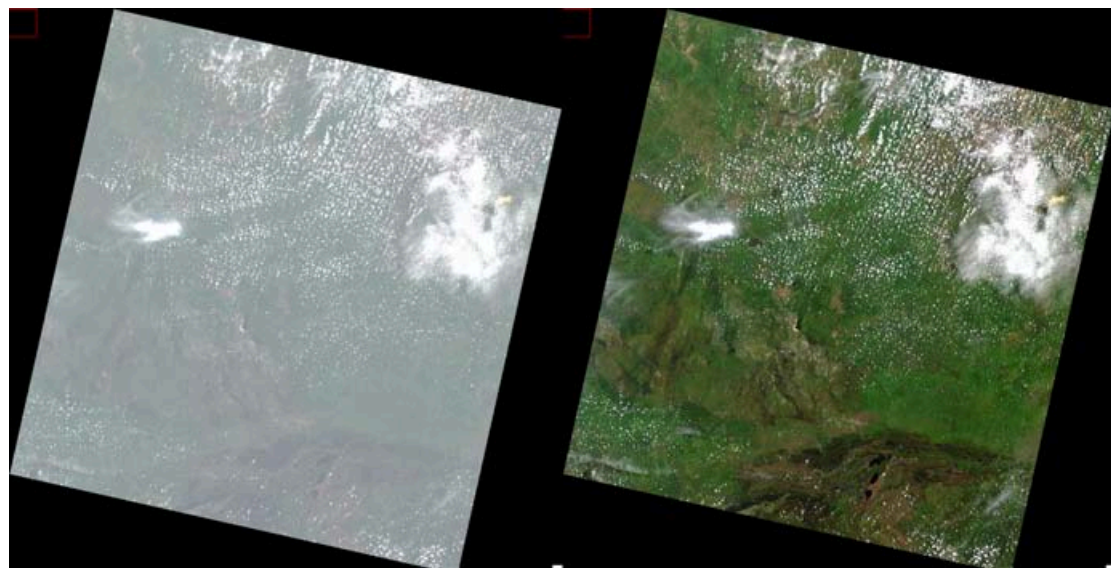
Fig. 6. Example of Landsat 8 data in Pariang displayed in a 2% linear stretch mode of the raw data in DN (left) and with radiometric calibration and atmospheric correction (right).

2.2.3 Data gaps

WorldView-2 data used in this study is cloud-free and without missing data, resulting in a complete coverage of the recorded area.

Data gaps in Landsat 7 data were introduced by the failure of the Scan Line Corrector on May 31, 2003, which compensates for the forward motion of satellite. An estimated 22% of any given scene is lost due to this malfunction.

Furthermore, data gaps are introduced by clouds and clouds shadows, which mask or alter the spectral response of the underlying land cover. We used the software Fmask (Function of mask) as stand alone version and implemented in MATLAB® to detect and mask clouds and associated cloud shadow regions in Landsat imagery [*Zhu et al.*, 2012]. The overall accuracy of Fmask to detect clouds and cloud shadows is 96.4% but detection problems may be associated with thin cirrus clouds and smoke arising from active fires [*Zhu et al.*, 2012].

Next to clouds, we additionally filtered recently burned areas in Landsat data acquired at the beginning of the dry season, when fire activity is high. Background and aim of this processing step is further explained in subsection 3.1.2.

2.2.4 Geographic Projection

To integrate and combine information from different datasets, we first needed to assure that each dataset inherits the same geographical projection. For example, Landsat data is provided in the Universal Transverse Mercator (UTM) conformal projection, which represents a 2-dimensional Cartesian coordinate system with constant lengths, angles, and areas across the two dimensions. In contrast, WorldView-2 data is provided in a geographic coordinate system with a standard spheroidal reference surface measured in latitude and longitude. Commonly, local to regional maps are represented in a projected coordinate system with a Cartesian coordinate plane to preserve and compare lengths and angles throughout the map. Thus we transferred the all data given in a geographic coordinate system (e.g., WorldView-2, administrative shapefiles, field data) to the UTM projection. In both our study areas (i.e. Maban and Pariang) this projection is defined as the grid zone 36 in the northern hemisphere.

2.2.5 Mosaicking

Due to the significant temporal difference between the WorldView-2 tiles acquired at the beginning and at the end of the dry season in 2013, the vegetation cover exhibits differences in foliation and phenological stages. To account for these differences, we analyzed the acquisitions from April and November/December separately and mosaicked individual WorldView-2 tiles according to their temporal cluster. The results of each analysis were consolidated in a last step by mosaicking the final product.

2.2.6 Co-registration

Co-registration is the process of ensuring that different spatial data sets are properly aligned so that the same geographical locations in each data set are aligned to the same points. This procedure is an essential prerequisite to overlay analysis and is based on a common geographic projection of the datasets.

In particular, we co-registrated Landsat data, which is characterized by slide offsets of individual scenes within the same WRS-2 tile. Co-registration was carried out in MATLAB® by subsetting/clipping each Landsat scene to the spatial boundaries of the respective county using the *inpolygon* function. As a result we created data stacks of the same spatial extend that could be compared on a pixelwise basis.

2.3   Satellite data spectral indices

For this study we relied on two spectral indices, the Normalized Difference Vegetation Index (NDVI - eq. 1) and normalized burn ratio (NBR2 - eq. 2) to discriminate photosynthetic vegetation from its surrounding (including non-photosynthetic vegetation - NPV) and recently burned areas from unburned areas:

$$NDVI = \frac{NIR-RED}{NIR+RED} \qquad\qquad \text{(Eq. 1)}$$

$$NBR2 = \frac{SWIR1-SWIR2}{SWIR1+SWIR2} \qquad\qquad \text{(Eq. 2)}$$

In these equations NIR represents the near infrared (ca. 0.86 µm), RED the red wavelengths (ca. 0.66 µm) of the visible spectrum, SWIR1 the short-wavelength infrared around 1.6 µm and SWIR2 the short-wavelength infrared around 2.2 µm.

As the spectral band configuration varies from sensor to sensor, sensor bands in the required wavelength range in the electromagnetic spectrum need to be defined individually.
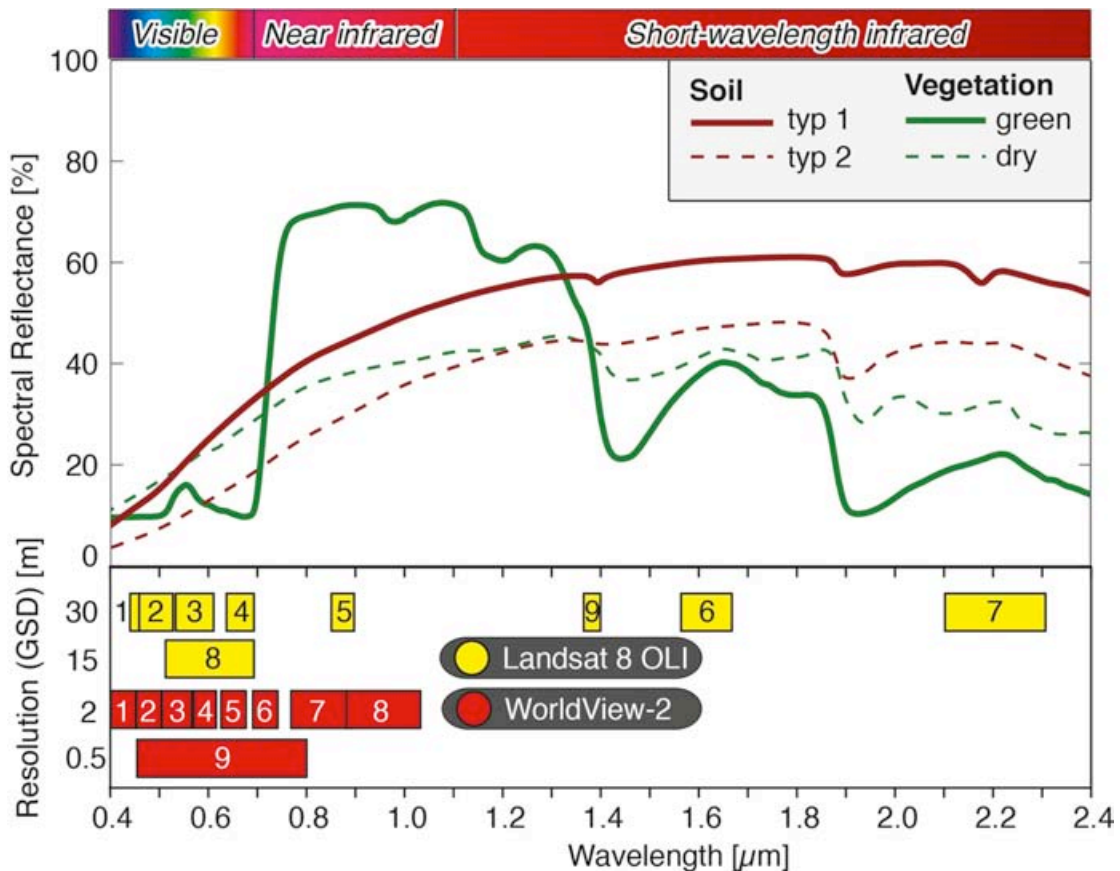
Fig. 7. Wavelength regions and respective spatial resolutions of Landsat 8 (yellow) and WorldView-2 (red) spectral bands with their respective band numbers in the lower panel. The panel above indicates the spectral reflectance curves of soils with different mineralogical compositions (type 1 & 2) and green/dry vegetation.

The spectral reflectances (section 2.2.2) are themselves ratios of the reflected over the incoming radiation in each spectral band individually; hence, they take on values between 0.0 and 1.0 or 0 to 100%. By design, the NDVI and NBR2 thus vary between -1.0 and +1.0.

17

In general, if there is much more reflected radiation in near-infrared wavelengths than in visible wavelengths, then that pixel is likely represent vegetation indicated by NDVI values ranging between 0.3 and 0.8. Previous work revealed that the NDVI is directly related to the photosynthetic capacity and hence energy absorption of plant canopies [*Myneni et al.*, 1995].

The formula for the NBR2 is very similar to that of NDVI and highlights areas that have burned while indicating the severity of a burn. We then used the index to select high-severity burned areas with a threshold of 0.1.

2.4 Vegetation survey preparation maps

In preparation and support of the field campaign by Dr. Urs Bloesch in April/May 2014 the NPOC provided preliminary maps of vegetation cover, vegetation density and potential field survey sites in close proximity to the refugee camps and roads (Fig. 8 and Fig. 10). In total 49 vegetation sites and 33 land-cover sites have been identified (Table 1 - Table 4).

The maps were provided in digital format (geocoded "pdf" files) that were transferred to a GPS enabled tablet-PC (Samsung Galaxy Tab3) in order to support on-site orientation and map-interpretation. Maps for Maban are based on pansharpened WorldView-2 data and maps for Pariang are based on pansharpened Landsat 8 data (Fig. 9 and Fig. 11).
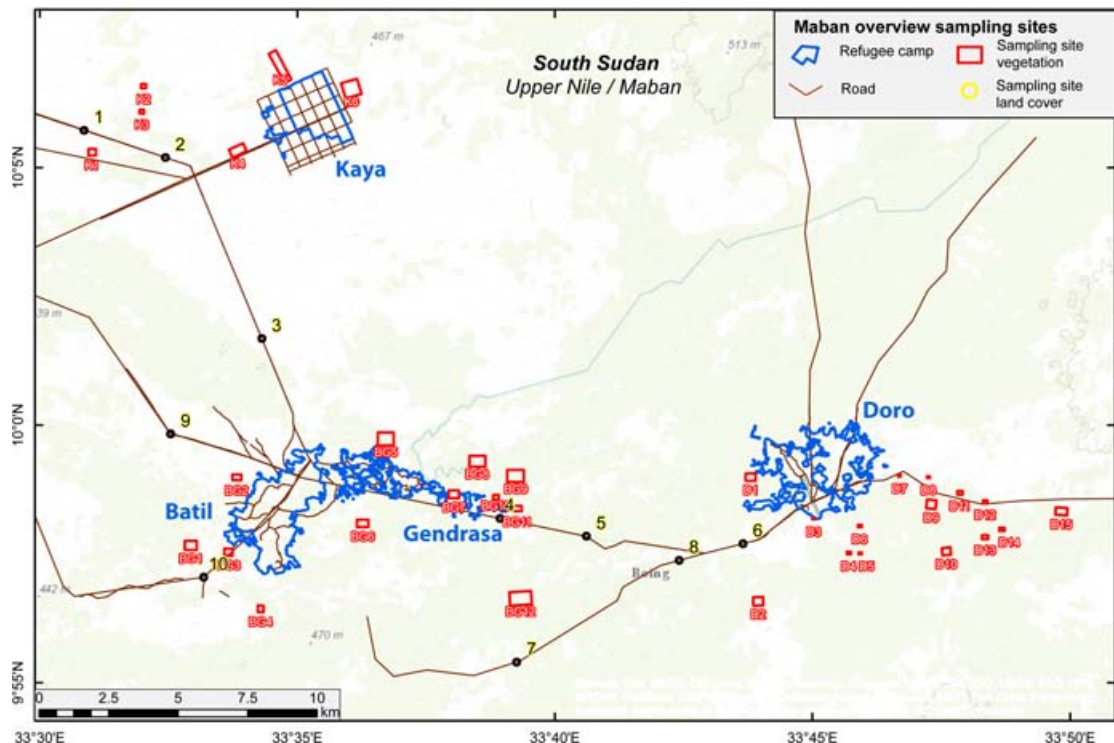
Fig. 8. Overview map on potential vegetation (red) and landcover (yellow) survey-sites in the vicinity of refugee camps in Maban.

Table 1: List on vegetation survey sites in Maban.

County	Camp	ID	Longitude	Latitude	Lon			Lat			Distance road
			DD	DD	D	M	S	D	M	S	m
Maban	Kaya	K1	10.0883	33.51691	10	5	17.88	33	31	0.876	100
Maban	Kaya	K2	10.1097	33.53355	10	6	34.92	33	32	0.78	2060
Maban	Kaya	K3	10.10148	33.53296	10	6	5.328	33	31	58.656	1190
Maban	Kaya	K4	10.08892	33.56402	10	5	20.112	33	33	50.472	10
Maban	Kaya	K5	10.11603	33.57774	10	6	57.708	33	34	39.864	160
Maban	Kaya	K6	10.10892	33.60078	10	6	32.112	33	36	2.808	160
Maban	Batil-Gen.	BG1	9.9611	33.54881	9	57	39.96	33	32	55.716	880
Maban	Batil-Gen.	BG2	9.98315	33.56369	9	58	59.34	33	33	49.284	670
Maban	Batil-Gen.	BG3	9.95892	33.56101	9	57	32.112	33	33	39.636	0
Maban	Batil-Gen.	BG4	9.94061	33.57145	9	56	26.196	33	34	17.22	1080
Maban	Batil-Gen.	BG5	9.99555	33.61191	9	59	43.98	33	36	42.876	400
Maban	Batil-Gen.	BG6	9.96823	33.60442	9	58	5.628	33	36	15.912	1000
Maban	Batil-Gen.	BG7	9.97766	33.63393	9	58	39.576	33	38	2.148	330
Maban	Batil-Gen.	BG8	9.98832	33.64153	9	59	17.952	33	38	29.508	1520
Maban	Batil-Gen.	BG9	9.98361	33.65394	9	59	0.996	33	39	14.184	1330
Maban	Batil-Gen.	BG10	9.97674	33.64755	9	58	36.264	33	38	51.18	610
Maban	Batil-Gen.	BG11	9.97301	33.65449	9	58	22.836	33	39	16.164	340
Maban	Batil-Gen.	BG12	9.94398	33.65551	9	56	38.328	33	39	19.836	1490
Maban	Doro	D1	9.98318	33.72994	9	58	59.448	33	43	47.784	1160
Maban	Doro	D2	9.94302	33.73241	9	56	34.872	33	43	56.676	1950
Maban	Doro	D3	9.96975	33.7503	9	58	11.1	33	45	1.08	330
Maban	Doro	D4	9.95863	33.76171	9	57	31.068	33	45	42.156	2040
Maban	Doro	D5	9.95855	33.76541	9	57	30.78	33	45	55.476	2280
Maban	Doro	D6	9.96739	33.76529	9	58	2.604	33	45	55.044	1320
Maban	Doro	D7	9.98371	33.77809	9	59	1.356	33	46	41.124	30
Maban	Doro	D8	9.98323	33.78747	9	58	59.628	33	47	14.892	260
Maban	Doro	D9	9.97437	33.78841	9	58	27.732	33	47	18.276	260
Maban	Doro	D10	9.95921	33.79332	9	57	33.156	33	47	35.952	1770
Maban	Doro	D11	9.9781	33.7977	9	58	41.16	33	47	51.72	120
Maban	Doro	D12	9.97522	33.80588	9	58	30.792	33	48	21.168	10
Maban	Doro	D13	9.96379	33.80581	9	57	49.644	33	48	20.916	1120
Maban	Doro	D14	9.96631	33.81131	9	57	58.716	33	48	40.716	900
Maban	Doro	D15	9.97213	33.83051	9	58	19.668	33	49	49.836	280

Table 2: List on land cover survey sites in Maban.

| County	Camp	ID	Longitude	Latitude	Lon			Lat			Road distance
			DD	DD	D	M	S	D	M	S	m
Maban	Kaya	1	33.51427	10.09542	33	30	51.372	10	5	43.512	0
Maban	Kaya	2	33.54062	10.08662	33	32	26.232	10	5	11.832	0
Maban	Batil-Gen.	3	33.57182	10.02807	33	34	18.552	10	1	41.052	0
Maban	Batil-Gen.	4	33.64891	9.96986	33	38	56.076	9	58	11.496	0
Maban	Batil-Gen.	5	33.67682	9.96411	33	40	36.552	9	57	50.796	0
Maban	Doro	6	33.72749	9.96167	33	43	38.964	9	57	42.012	0
Maban	Batil-Gen.	7	33.65424	9.92336	33	39	15.264	9	55	24.096	0
Maban	Doro	8	33.70685	9.95628	33	42	24.66	9	57	22.608	0
Maban	Batil-Gen.	9	33.54228	9.99721	33	32	32.208	9	59	49.956	0
Maban	Batil-Gen.	10	33.55299	9.95085	33	33	10.764	9	57	3.06	0
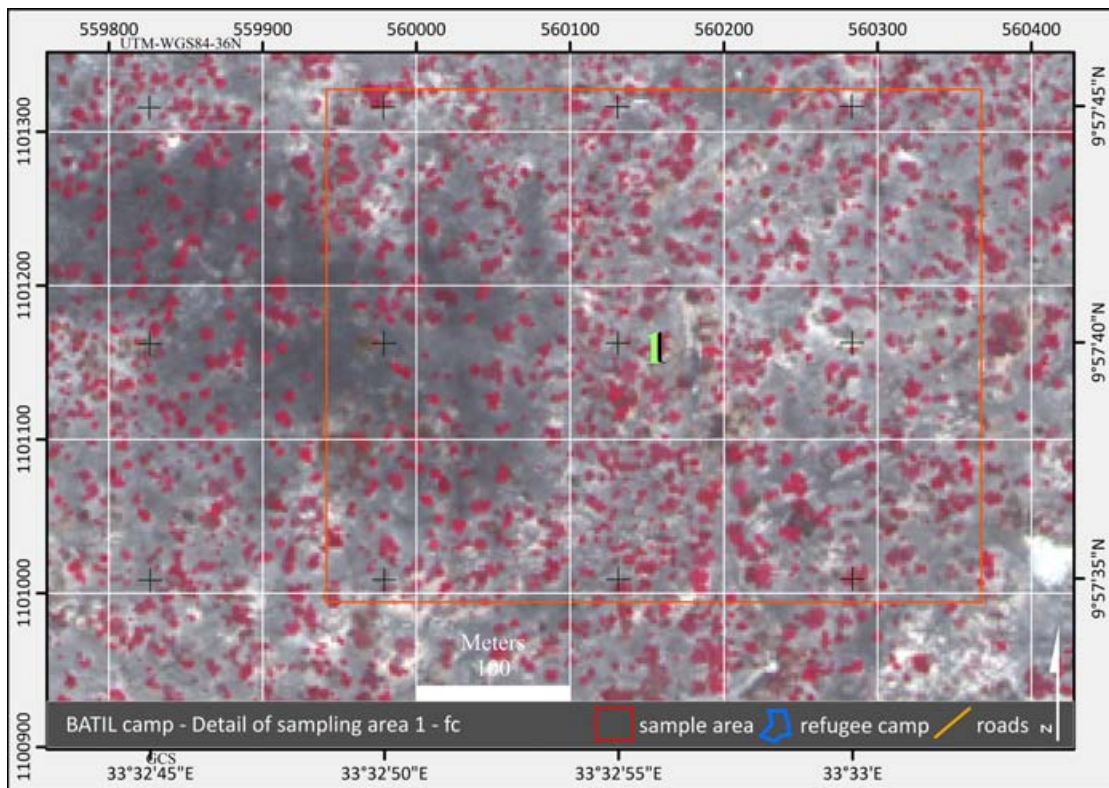
Fig. 9. Example of a potential vegetation survey site map in the vicinity of Batil refugee camp based on WorldView-2 data.
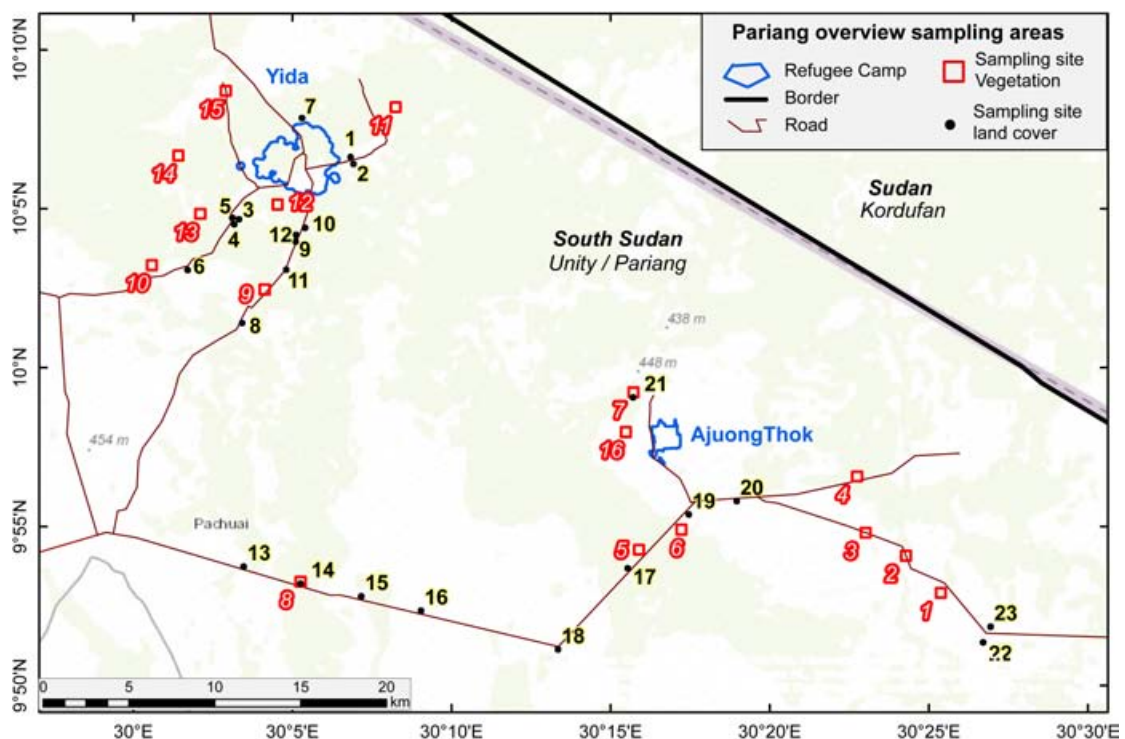

Fig. 10. Overview map on potential vegetation (red) and land cover (yellow) survey-sites in the vicinity of refugee camps in Pariang.

20

Table 3: List on vegetation survey sites in Pariang.

County	Camp	ID	Longitude	Latitude	Lon			Lat			Distance road	Vegetation cover (%)					
			DD	DD	D	M	S	D	M	S	m	13.2.14	17.3.14	2.5.13	2.6.13	22.9.13	25.11.13
Pariang	AjuongThok	1	9.88198	30.42311	9	52	55.128	30	25	23.196	520	24	22	25	48	85	40
Pariang	AjuongThok	2	9.90143	30.4048	9	54	5.148	30	24	17.28	0	16	18	12	32	66	51
Pariang	AjuongThok	3	9.91355	30.38365	9	54	48.78	30	23	1.14	0	2	6	11	46	90	30
Pariang	AjuongThok	4	9.94306	30.37925	9	56	35.016	30	22	45.3	260	4	5	21	56	87	31
Pariang	AjuongThok	5	9.90451	30.26492	9	54	16.236	30	15	53.712	450	19	8	27	59	81	42
Pariang	AjuongThok	6	9.9151	30.28729	9	54	54.36	30	17	14.244	540	10	10	16	42	88	28
Pariang	AjuongThok	7	9.98719	30.26218	9	59	13.884	30	15	43.848	1110	9	9	24	63	88	39
Pariang	AjuongThok	8	9.88776	30.08774	9	53	15.936	30	5	15.864	250	7	12	0	1	73	64
Pariang	Yida	9	10.04111	30.06889	10	2	27.996	30	4	8.004	180	17	22	15	39	86	32
Pariang	Yida	10	10.05384	30.00976	10	3	13.824	30	0	35.136	690	17	25	14	35	88	45
Pariang	Yida	11	10.13665	30.13753	10	8	11.94	30	8	15.108	1370	37	29	29	35	73	59
Pariang	Yida	12	10.08561	30.07567	10	5	8.196	30	4	32.412	1080	15	22	12	32	73	37
Pariang	Yida	13	10.08073	30.03522	10	4	50.628	30	2	6.792	1750	21	29	16	43	91	56
Pariang	Yida	14	10.11131	30.02368	10	6	40.716	30	1	25.248	3130	25	35	23	47	71	58
Pariang	Yida	15	10.14521	30.04851	10	8	42.756	30	2	54.636	10	15	22	15	24	82	43
Pariang	AjuongThok	16	9.9663	30.25816	9	57	58.68	30	15	29.376	1380	16	15	15	54	100	36

Table 4: List on land cover survey sites in Pariang.

| County	Camp	ID	Longitude	Latitude	Lon			Lat			Road distance
			DD	DD	D	M	S	D	M	S	m
Pariang	Yida	1	10.11055	30.11392	10	6	37.98	30	6	50.112	190
Pariang	Yida	2	10.10686	30.11541	10	6	24.696	30	6	55.476	240
Pariang	Yida	3	10.07787	30.05546	10	4	40.332	30	3	19.656	450
Pariang	Yida	4	10.07519	30.05293	10	4	30.684	30	3	10.548	190
Pariang	Yida	5	10.07867	30.05198	10	4	43.212	30	3	7.128	70
Pariang	Yida	6	10.05122	30.02857	10	3	4.392	30	1	42.852	230
Pariang	Yida	7	10.13104	30.08846	10	7	51.744	30	5	18.456	790
Pariang	Yida	8	10.02346	30.05705	10	1	24.456	30	3	25.38	130
Pariang	Yida	9	10.06618	30.08513	10	3	58.248	30	5	6.468	50
Pariang	Yida	10	10.07343	30.09006	10	4	24.348	30	5	24.216	150
Pariang	Yida	11	10.05142	30.08019	10	3	5.112	30	4	48.684	40
Pariang	Yida	12	10.06974	30.08531	10	4	11.064	30	5	7.116	180
Pariang	AjuongThok	13	9.89569	30.05788	9	53	44.484	30	3	28.368	150
Pariang	AjuongThok	14	9.88676	30.08774	9	53	12.336	30	5	15.864	140
Pariang	AjuongThok	15	9.8801	30.11951	9	52	48.36	30	7	10.236	190
Pariang	AjuongThok	16	9.87261	30.1508	9	52	21.396	30	9	2.88	190
Pariang	AjuongThok	17	9.89486	30.25906	9	53	41.496	30	15	32.616	190
Pariang	AjuongThok	18	9.85226	30.22254	9	51	8.136	30	13	21.144	160
Pariang	AjuongThok	19	9.92305	30.29107	9	55	22.98	30	17	27.852	240
Pariang	AjuongThok	20	9.93007	30.31617	9	55	48.252	30	18	58.212	160
Pariang	AjuongThok	21	9.98444	30.26192	9	59	3.984	30	15	42.912	1010
Pariang	AjuongThok	22	9.85595	30.44526	9	51	21.42	30	26	42.936	570
Pariang	AjuongThok	23	9.86416	30.44918	9	51	50.976	30	26	57.048	370
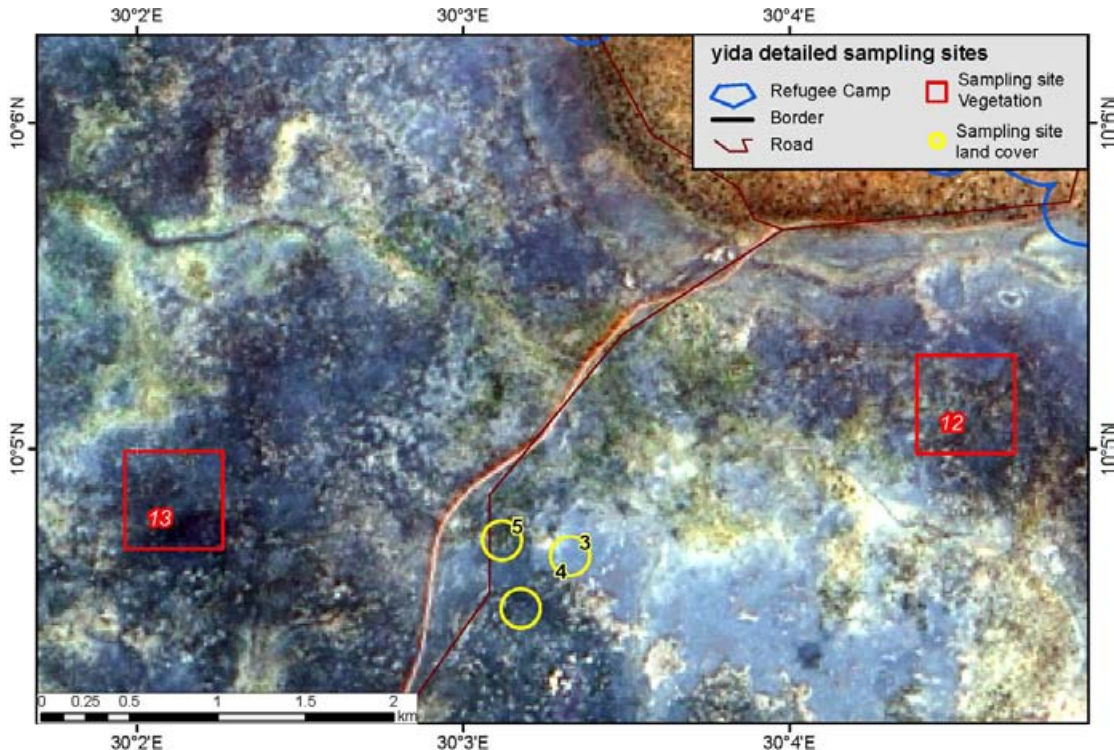
Fig. 11. Example of a potential vegetation and land cover survey site map in the vicinity of Yida refugee camp based on pansharpened Landsat 8 data.

2.5 Vegetation survey data

During the field campaign of Dr. Urs Bloesch and his team from 24 April to 12 May 2014 20 vegetation sites (16 in Maban, 4 in Pariang) and 17 land-cover sites (8 in Maban, 9 in Pariang) have been described as ground truthing sites and as a basis for a forest pre-inventory (Fig. 12 and Fig. 13) [*Bloesch*, 2014]. The detailed description of each survey site comprises among other parameters the tree species composition, estimated tree and shrub cover, land cover, vegetation type and tree heights and tree diameter at breast height. Each survey site was photographed in each cardinal direction with a GPS camera (Panasonic Lumix DMC-TZ10) and additionally marked with a handheld GPS (Garmin 62S). In total, more than 300 GPS photographs have been obtained to aid the tree identification and its assignment on satellite data. For further information on the field campaign and the recorded data, we refer to the "Forest mapping and pre-inventory report" [*Bloesch*, 2014].

We used the field campaign data to create a database in ArcGIS®, which included information on vegetation and land cover site locations, dominant tree species and associated tree/shrub cover. Depending on the reference satellite data (WorldView-2 or Landsat), we were able to assign the species to individual trees or to classify a region with predominant tree species. This database served as a basis to train tree species classification algorithms as described in section 3.1.1.
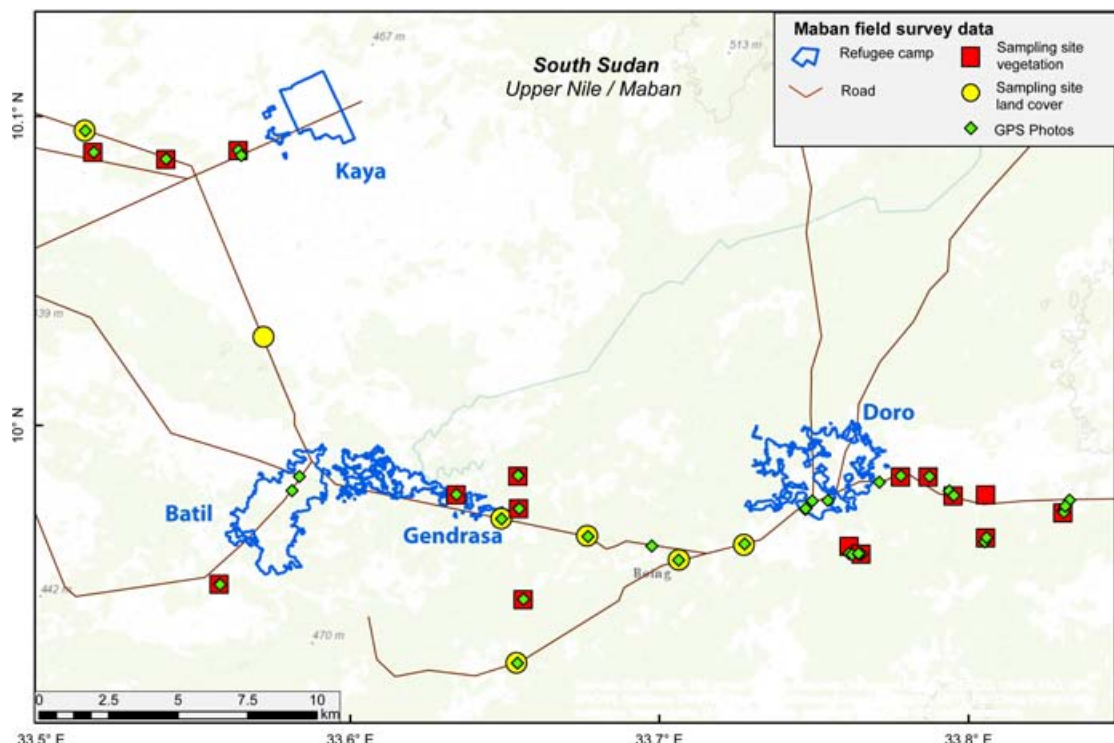
Fig. 12. Overview map of vegetation (red squares) and land cover (yellow circles) survey-sites and associated GPS photographs (green diamonds) in the vicinity of refugee camps in Maban.
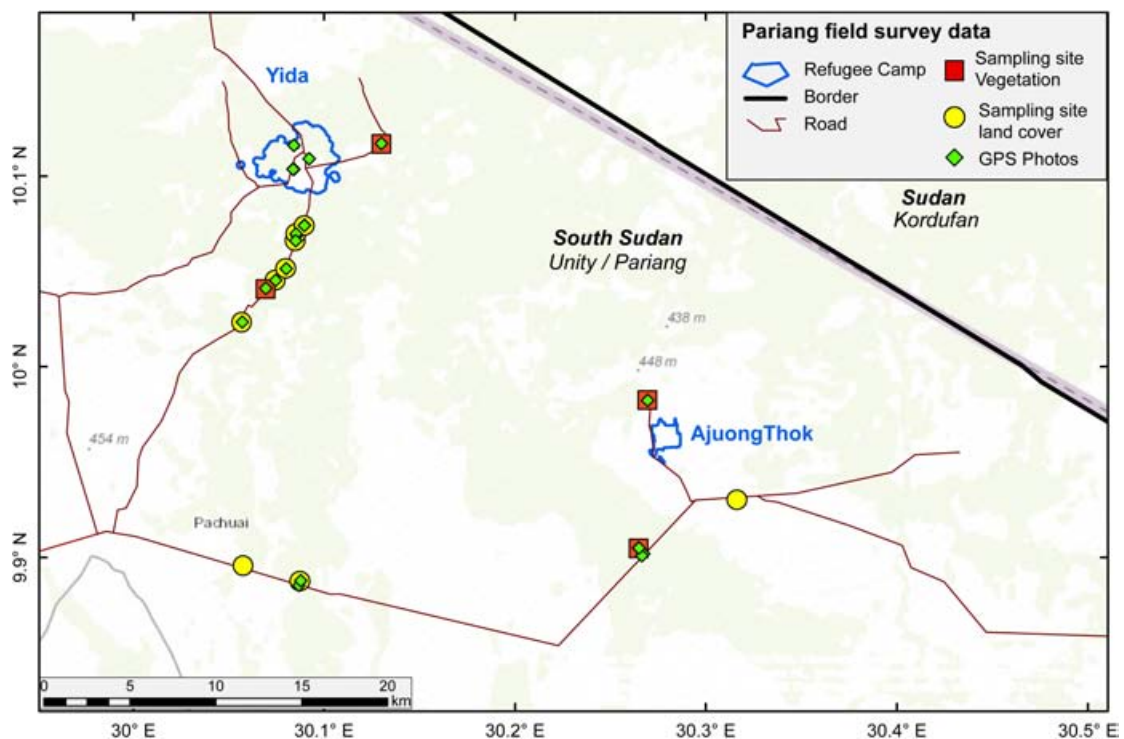

Fig. 13. Overview map of vegetation (red squares) and land cover (yellow circles) survey-sites and associated GPS photographs (green diamonds) in the vicinity of refugee camps in Pariang.

3. Forest monitoring data products

In this chapter, we describe the employed methodology as well as characteristics and limitations of each forest-mapping product.

3.1 Vegetation cover

In this section we describe our steps to generate a vegetation mask and vegetation surface cover map and compare the results from both remote sensing sensors.

3.1.1 Vegetation mask

Many ecosystems, including the grasslands, savannas and woodlands in South Sudan, contain next to green vegetation also dried up vegetation that is known as non-photosynthetic vegetation (NPV) [e.g., *Asner*, 1998]. In South Sudan this type of vegetation is simply dormant and photosynthetically inactive during the dry season that lasts approximately from November to April. Consequently, it absorbs less energy in the visible range of the electromagnetic spectrum and is thus less responsive to the NDVI as compared to photosynthetic active vegetation.

In our approach to detect all woody vegetation, we aim to differentiate between trees/shrubs and grassland as well as photosynthetically active and inactive trees.

Due to differences in availability and sensor characteristics between Landsat and WorldView-2 satellite data we follow different strategies to achieve this goal.

(A) WorldView-2 data

Our strategy for Worldview-2 data is twofold: First, we aim to detect green vegetation based on NDVI data. Second, we aim to detect dry vegetation or NPV based image classification algorithms.

Given that the available WorldView-2 data was obtained during the dry season (November/December & April), green vegetation encompasses predominantly trees and shrubs. This classification of green vegetation is based on a NDVI threshold, which we calibrate using the field survey tree/shrub cover estimates. Note that the WorldView-2 scenes from November 20th and December 6th may exhibit more photosynthetic active grassland as compared to the scenes from April. TRMM satellites rainfall data indicate the last pronounced rainfall in Maban on November 7th. Characteristics and availability of TRMM data is further explained in section 4.X.

For a general overview on the existing data, we firstly compared the field survey data on tree/shrub vegetation cover with WorldView-2 NDVI data. It should be noted that despite the one-year time lag between most WorldView-2 acquisitions from April 2013 and the field survey data from May 2014, both data cover approximately the same seasonal time with comparable phenological stages and tree/shrub foliage. Assuming similar rainfall patterns in both years, we would expect a slightly higher photosynthetic activity in May 2014 as compared to April 2013.

During the field campaign in May 2014 the canopy cover data for each survey site was estimated based on the tree/shrub-cover within the plot area. To compare these canopy cover estimates with WorldView-2 data, we first calculate the average NDVI within each plot area, which encompasses about 200 pixels per plot.

The comparison between the average WorldView-2 NDVI data from April 2013 and the field survey data of Maban from May 2014 (survey sites 1 to 13) yields a good

first-order agreement (Fig. 14). Given the different tree foliage conditions between the WorldView-2 data acquisition from November/December 2013 (survey sites 14 to 16) and the field survey in May 2014, we only included the WorldView-2 data from April (comparable season) into the subsequent analysis to ensure comparable vegetation conditions on the ground.
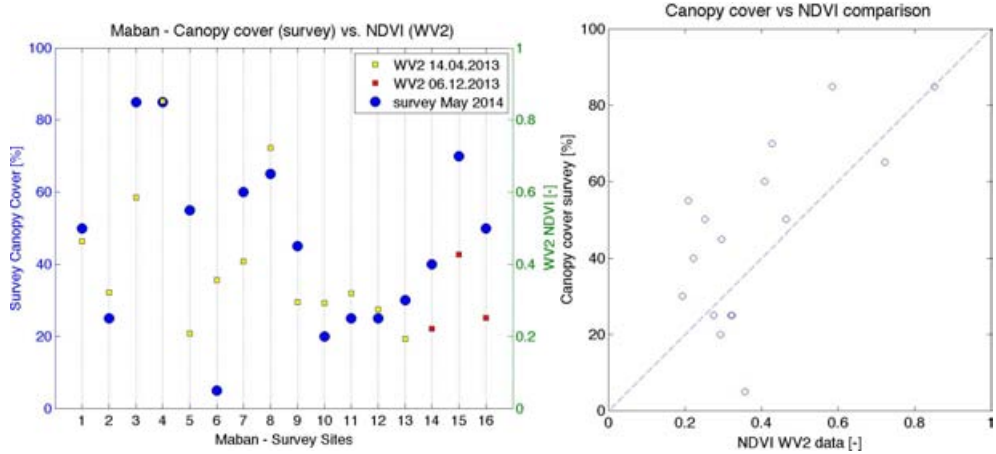
Fig. 14. (Left) Comparison of Maban field survey canopy cover estimates (blue circles) with WorldView-2 NDVI observations during the same pre-rain season in the previous year (yellow squares) and during the post-rain season (red squares) in 2014. (Right) Regression plot of pre-rain WorldView-2 NDVI observations and field survey canopy cover that highlights the good agreement between both data sets.

Deviations between both vegetation datasets may derive from different vegetation conditions between the years, slight misjudgments in the canopy cover estimates, geolocation uncertainties in the satellite data and BRDF effects derived from off-nadir satellite viewing angles.

The classification of a pixel as vegetation or non-vegetation is based on a defined NDVI threshold. To estimate the optimal NDVI threshold we quantified the root mean squared error between the canopy cover data derived from the WorldView-2 data and the survey data. The lowest deviation between both dataset is given for a NDVI threshold of 0.37 (Fig. 15).
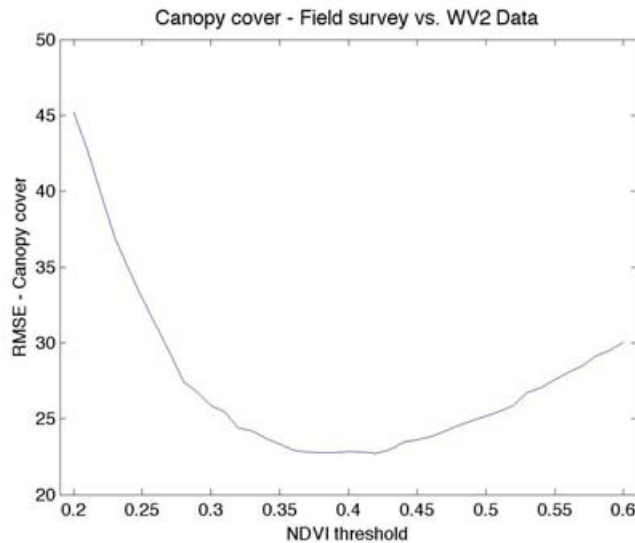
Fig. 15. Optimization of NDVI threshold, indicating the root mean square error (RMSE) between canopy cover of survey sites in Maban (sites 1-13) and canopy cover of WorldView-2 data with different NDVI thresholds.

Based on this NDVI threshold (0.37), we compared the canopy cover derived from WorldView-2 and the field survey data, which yield a weakly positive correlation ($r^2 = 0.18$) (Fig. 16).
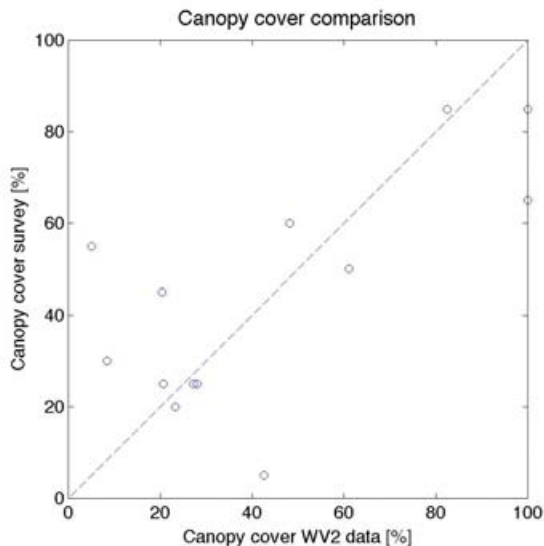
Fig. 16. Correlation between WorldView-2 derived canopy cover and estimated canopy cover from the field survey.

Based on this first approach, we detected all photosynthetic vegetation, which still includes extended grasslands at geomorphologic sinks that hold water for prolonged periods in the dry season. Furthermore, the NDVI does not depict non-photosynthetic vegetation. Therefore, we classified both seasonal WorldView-2 mosaics (November/December and April scenes) to identify these extended grassland regions and non-photosynthetic vegetation. This second approach is based on the Support Vector Machine (SVM) classification using ENVI® software. Based on this classification, we were able to further differentiate between swampy areas with extended grasslands, photosynthetic vegetation, non-photosynthetic vegetation and soils with varying degrees of burning severity. The SVM classifications of both

26

mosaics yielded consistently the highest score compared to the Spectral Angle Mapper (SAM) and Maximum Likelihood classifiers with an overall accuracy of >98% based on the training dataset. However, it should be noted the misclassifications can occurs particularly between non-photosynthetic vegetation and soils. Based on the classification results, we excluded the extended grasslands from the NDVI vegetation data and included the non-photosynthetic vegetation to it. Finally, we combined both seasonal WorldView-2 mosaics into one coherent woody vegetation mask map with the native 2 m spatial resolution (Fig. 17).
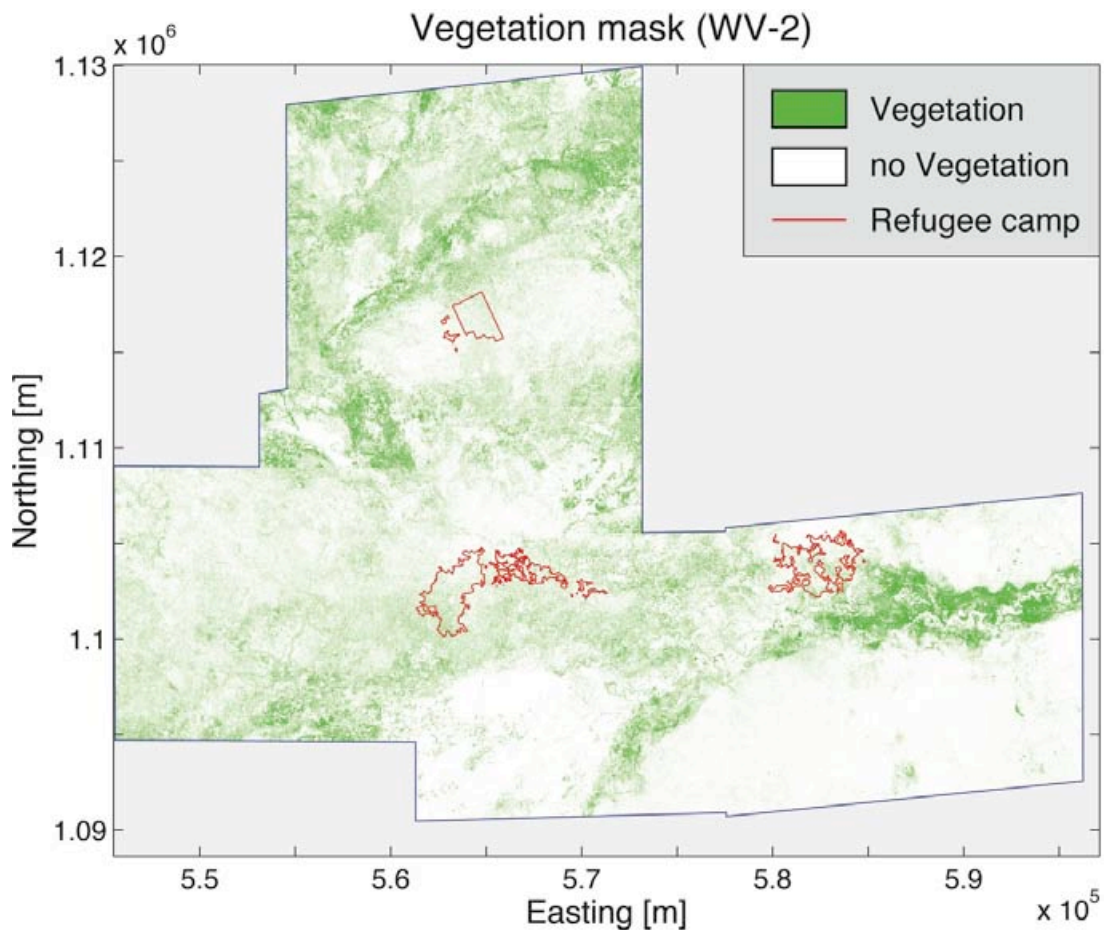
Fig. 17. Mosaicked vegetation mask based on WorldView-2 data in 2 m spatial resolution. Coordinates represent the UTM 36N projection.

(B) Landsat

Our strategy to detect woody vegetation based on Landsat data is relatively simple but based on expert knowledge about vegetation characteristics and additional TRMM satellite data indicating the onset of the dry season.

Due to the lower spatial resolution of Landsat data (30 m ground sampling distance) compared to WorldView-2 data (2m), Landsat pixels contain generally a mixture of vegetation, soil and other surface materials. This heterogeneity along with a limited spectral resolution makes a distinction between trees/shrubs and grasslands infeasible during the rainy season. However, as indicated by Dr. Urs Bloesch, there is a limited

time frame during four to six weeks after the last pronounced (>2mm) rainfall event, when grasslands (apart from topographic depressions) turned already from a photosynthetic to a non-photosynthetic state while trees are remain still photosyntetically active.

Taking advantage of these phenological differences, we used TRMM rainfall data to detect the start of the dry season and thus the timeframe for useful Landsat acquisitions (Fig. 18). The timing of these Landsat 7 acquisitions from 2000 to 2013 is illustrated in Fig. 5 and listed in Table A3-Table A8.
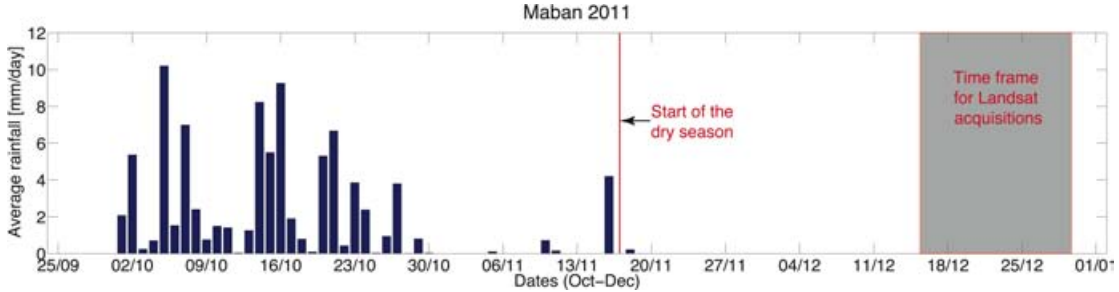
Fig. 18. Example of daily rainfall events in Maban during October to December 2011 as indicated by TRMM3B42 data. Last rainfall event >2mm marks the end of the rainy season and sets the time frame for Landsat acqisitions to distinguish between tree/shrub and grass cover.

To derive a vegetation mask based on Landsat data, we initially employed a similar NDVI threshold approach as described previously for the WorldView-2 data. However, we refined this approach as described in section 3.1.2. Nevertheless, we describe our first approach here, as it describes nicely some characteristics of Landsat data.

For a general overview on the Landsat data, we initially compared the Landsat 8-NDVI of the respective Maban survey sites at different times before during and after the field survey (Fig. 19). It should be noted that due to the coarse spatial resolution (30 m) there are generally one or two associated Landsat pixel centers within each survey site.
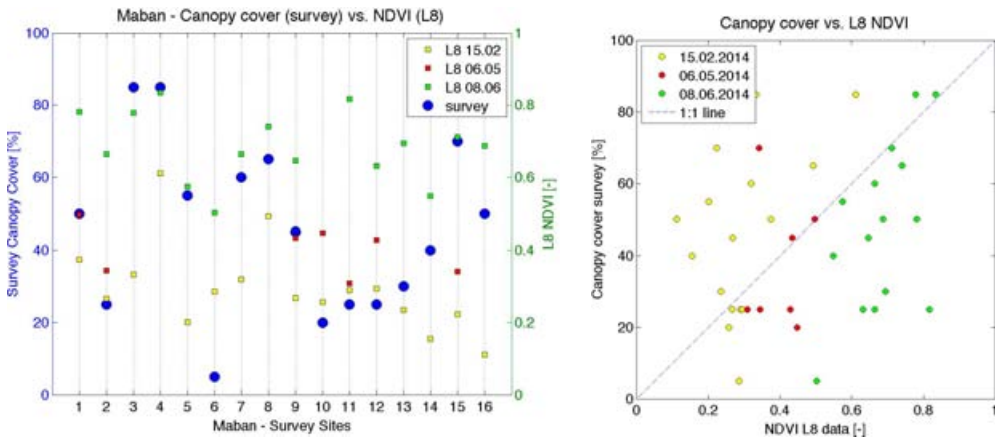
Fig. 19. (Left) Comparison of field survey canopy cover estimates (blue circles) with Landsat NDVI observations (colored squares) before (yellow), during (red), and after (green) the field campaign in 2014. (Right) Regression plot of data presented in the left panel that highlight the temporal variability of the Landsat NDVI data.

This direct comparison of Landsat and field survey data highlights the large temporal variability of the pixel-based NDVI and existing data gaps in Landsat data due to

28

cloud cover. Based on this non-existing correlation between Landsat NDVI and field survey canopy cover data, we establish a relation between Landsat NDVI data and WorldView-2 canopy cover of scene 13APR14083444-M1BS-500057177100_05_P001, which is characterized by large contrasts in vegetation classes ranging from grasslands to woodlands.

For this purpose, we rescaled WorldView-2 vegetation mask (2 m spatial resolution) of this scene to a Landsat compatible 30 m canopy cover dataset. The lowest deviation between both datasets is given for a NDVI threshold of 0.39 (Fig. 20).

This threshold could be used to derive a vegetation mask based on Landsat data. However, as described in section 3.1.2, we relate the NDVI directly to canopy cover to take advantage of its rich information content.
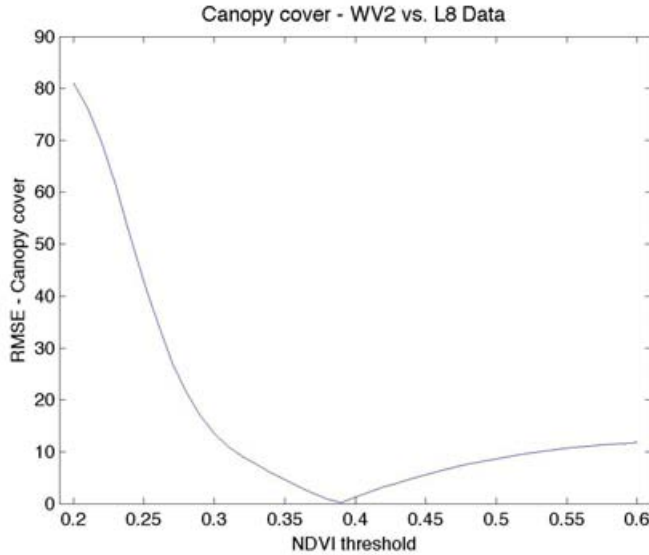
Fig. 20. Optimization of the NDVI threshold, indicating the root mean square error (RMSE) between a 30 m canopy cover of WorldView-2 scene (13APR14083444-M1BS-500057177100_05_P001) and complementary canopy cover of Landsat-8 data with different NDVI thresholds.

3.1.2 Vegetation cover

In this subsection, we first continue to describe our methodology to derive vegetation cover data based on Landsat acquisitions followed by the methodology for WorldView-2 data.

(A) Landsat

As mentioned in the previous section (3.1.1), we exploited sensor synergies between the different temporal and spatial scales of Landsat and WorldView-2 data by establishing a relation between WorldView-2 canopy cover data and Landsat NDVI data, as illustrated in Fig. 21 and Fig. 22.
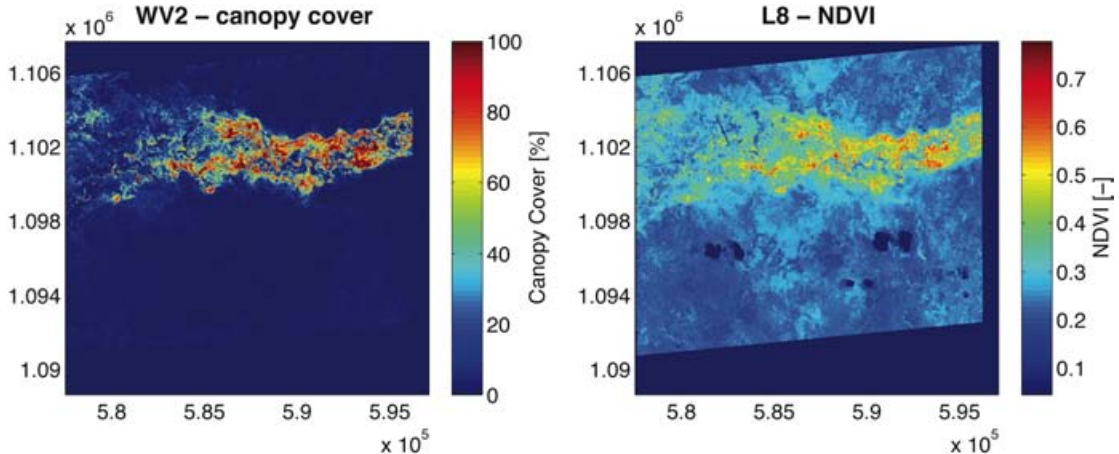
Fig. 21. Visual comparison of WorldView-2 canopy cover with Landsat 8 NDVI data. Left panel illustrates the canopy cover of WorldView-2 scene 13APR14083444-M1BS-500057177100_05_P001 from April 14th 2013 in a 30m spatial resolution based on the 2m vegetation mask. Right panel illustrates the spatially corresponding Landsat NDVI data from April 17th 2013 masked for clouds.

The regression between WorldView-2 canopy cover and Landsat NDVI reveals a linear relationship (Fig. 22), which we employ to convert Landsat NDVI data into canopy cover. Landsat NDVI data above 0.56 and below 0.26 that yield canopy cover values above 100% or below 0% are set to 100% or 0%, respectively.
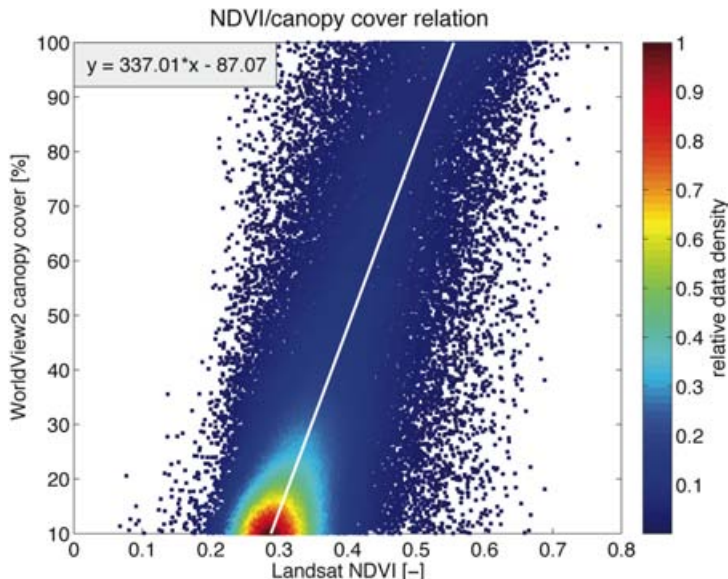
Fig. 22. Regression between WorldView-2 canopy cover with Landsat 8 NDVI data. Color-code indicates the relative data density.

To distinguish between grass- and tree/shrub cover, we utilized Landsat data acquired four to six weeks after the onset of the dry season. Based on the previously obtained NDVI-canopy cover-relationship we transformed Landsat NDVI measurements to canopy cover values. To account for data gaps inherent in the Landsat 7 data, we averaged the data stack of ten (Maban) to eleven (Pariang) acquisitions, which resulted in an average canopy cover dataset for both counties (Fig. 23 and Fig. 24)

In a final step we classified the canopy cover dataset according to the standard classification scheme into the following vegetation classes: (1) grasslands: 0-2%; (2)

Shrub/tree savanna: 2-30%; (3) Savanna woodland: 30-60%; and (4) Woodland: >60% (Fig. 23 and Fig. 25).
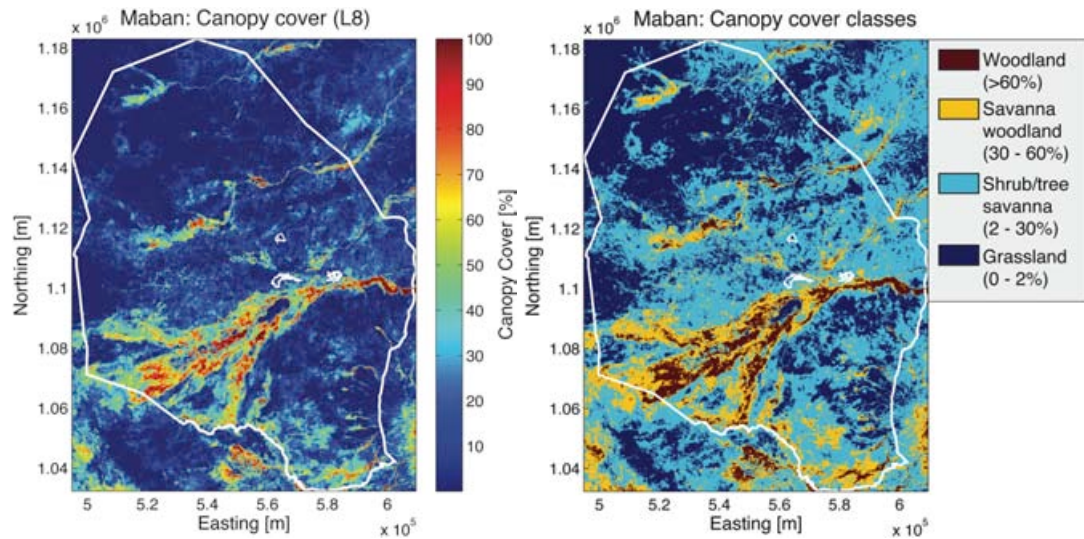
Fig. 23. Left panel: Canopy cover for Maban County. The County border is indicated by the white outline. Right panel: Vegetation classes according to the canopy cover classification scheme.
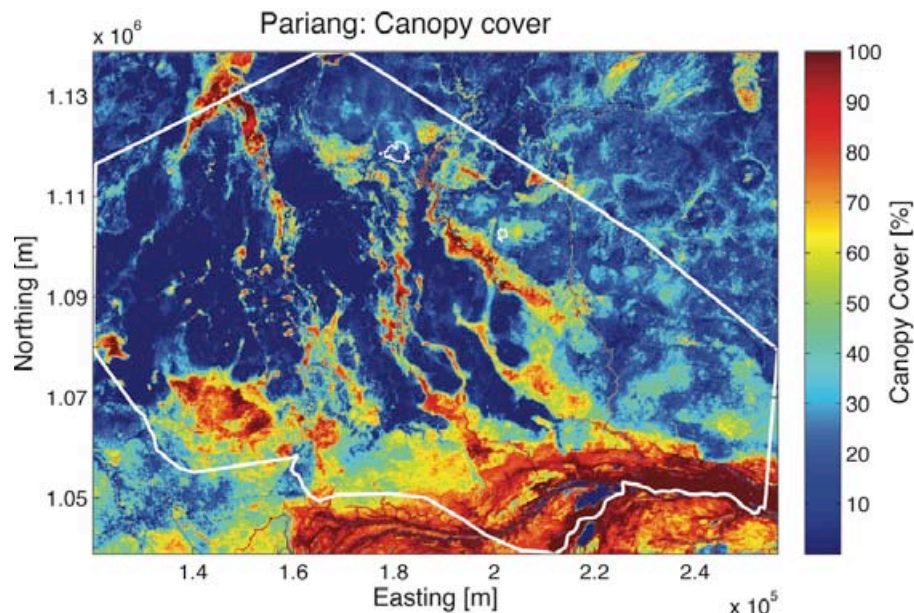
Fig. 24. Canopy cover for Pariang County. The County border is indicated by the white outline.
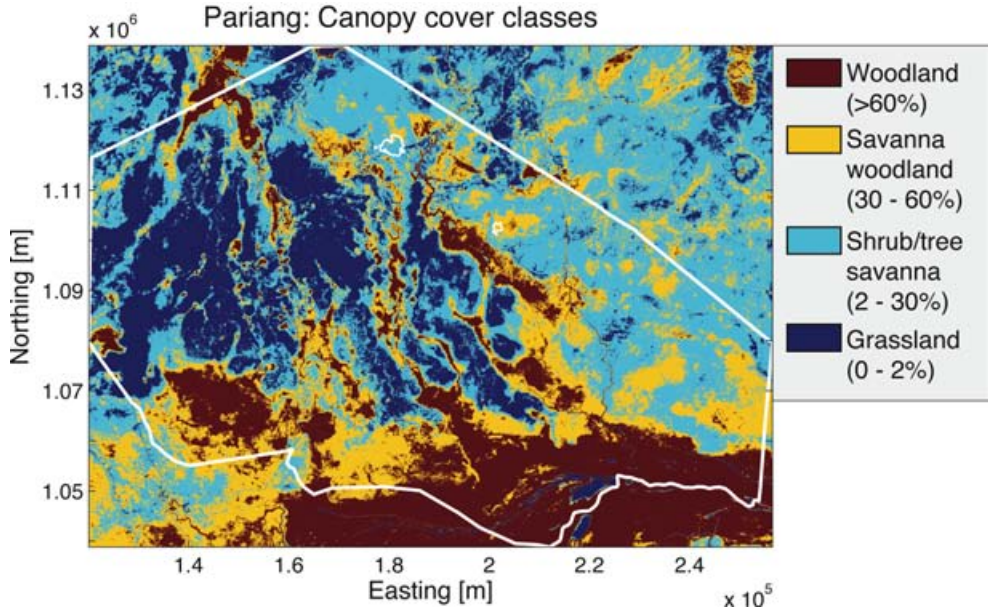
Fig. 25. Vegetation classes for Pariang according to the canopy cover classification scheme. The County is indicated by the white outline.

(B) WorldView-2

The canopy cover of WorldView-2 data is based on the vegetation mask data. This 2 m spatial resolution dataset is downscaled to 100 m (1pixel = 1ha) and thus integrates 2500 Boolean vegetation measurements per pixel. This canopy cover information is classified as previously described for Landsat data according to the presented vegetation class scheme (Fig. 26).
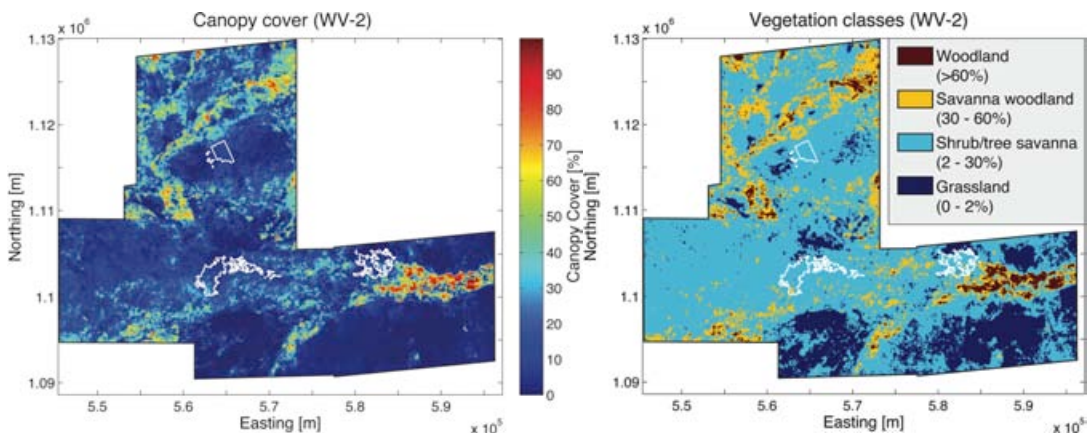
Fig. 26. Left panel: Canopy cover for Maban. The County is indicated by the white outline. Right panel: Vegetation classes according to the canopy cover classification scheme.

3.1.3 Vegetation cover comparison and validation

Given the two different dataset and methodologies to derive data on canopy cover and vegetation classes, we aim to compare both dataset and evaluate their performance by validating it with field data.

The visual comparison between Landsat and WorldView-2 data on vegetation classes indicates pronounced differences along the Yabus River and an overall lower

vegetation cover in the surrounding of the Kaya camp. Based on the field observation woodlands (Silak) are quite widespread around Kaya camp. As discussed previously the phenology and the particular foliage of Silak (very loose) may interfere the satellite images interpretation. However, general trends in areas with high and low vegetation cover are similar in both datasets (Fig. 27).
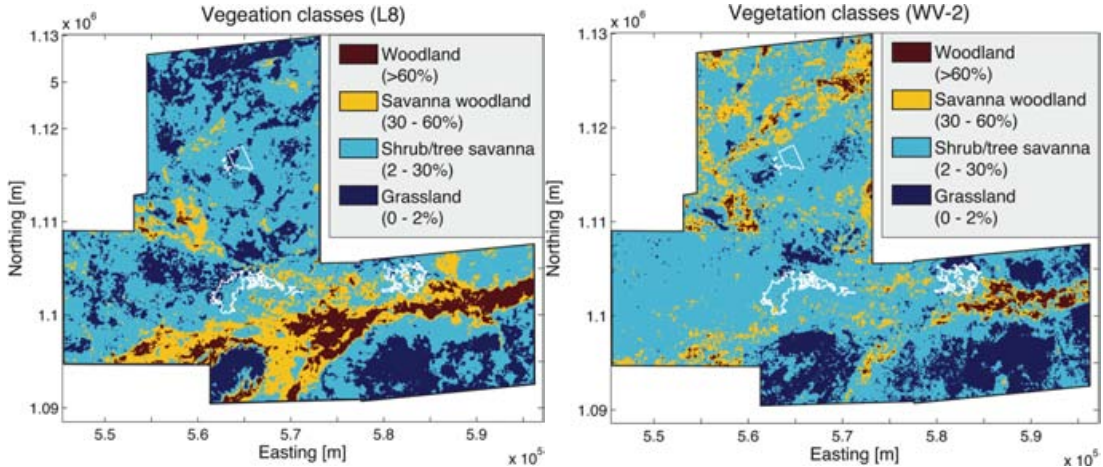
Fig. 27. Left panel: Vegetation classes of the WorldView-2 data extent in Maban based on Landsat data. Right panel: Vegetation classes based on WorldView-2 data.
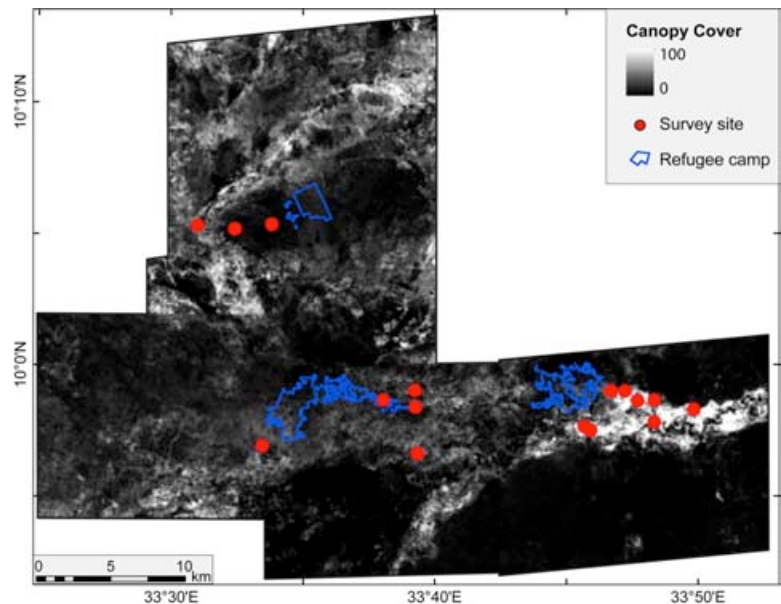
Fig. 28. Map of WorldView-2 canopy cover highlighting the vegetation survey locations (red circles) in divers canopy cover settings.

We validated both canopy cover datasets based on vegetation survey data (Fig. 28). Although the Landsat estimates depict the general trend in canopy cover, WorldView-2 estimates provide the slightly more reasonable results (Fig. 29). Based on the vegetation survey locations, Landsat and Worldview-2 data are highly correlated (Fig. 29).

33
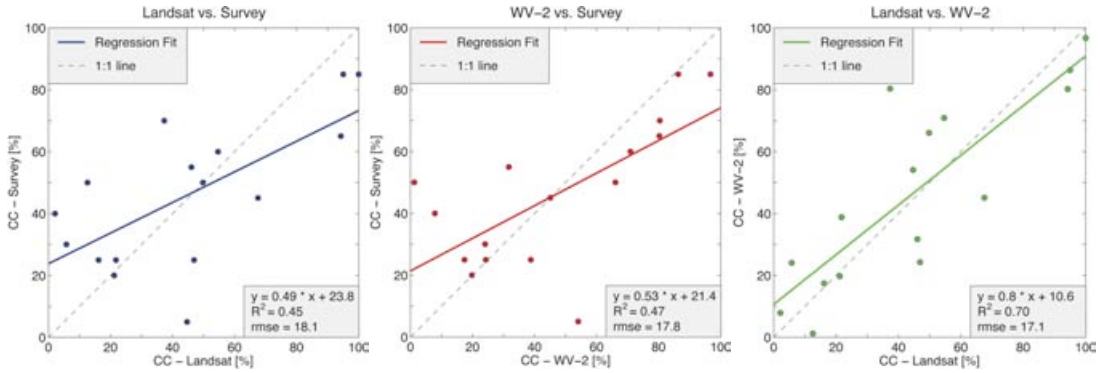
Fig. 29. Regression analysis on canopy cover data between the Landsat data, WorldView-2 data and vegetation survey data. Left panel: Linear relation between Landsat and vegetation survey data. Mid panel: Linear relation between WorldView-2 and vegetation survey data. Right panel: Linear relation between Landsat and WorldView-2 data.

It should be noted that extended areas in southern Pariang along the Bahr el Ghazal River are composed of evergreen grasslands. These wetlands receive sufficient water throughout the year to sustain different vegetation types as compared to the northern savanna region. Similar to these wetlands, there exist topographic depressions in Maban and Pariang, which hold water for extended periods into the dry season. These grasslands are photosynthetically active during the first months of the dry-season. Therefore, these grassland regions are characterized by high NDVI values in the Landsat imagery four to six weeks after the onset of the dry season. Consequently, our approach identifies these regions misleadingly as woodlands, which should be taken into account while interpreting the vegetation maps.

The onset of the dry-season is also characterized by pronounced fire activity as the vegetation dries up and allows for fire propagation. These burned areas exhibit a significantly reduced spectral reflectance in the visible and near infrared wavelength regions, which leads to a NDVI decrease that correlates to proportion of soil vegetation mixture per pixel. Therefore the canopy cover in such burnt areas may be captured in a lower degree as it actually is. Our approach to use Landsat data from several years may attenuate this effect, as the decadal average should have a reduced impact.

3.2 Tree Species

In this section we describe our methodology and results to differentiate between the locally dominant tree species within savanna woodlands and woodlands . According to the field survey report by Dr. Urs Bloesch the dominant tree species were identified as the Red acacia (*Acacia seyal*), the Desert date tree (*Balanites aegyptiaca*), and the Silak (*Anogeissus leiocarpus*), which form virtually monospecific stands [*Bloesch*, 2014]. In addition, the Doum palm (*Hyphaene thebaica*) occurs in Maban particularly along the Jabus River [*Bloesch*, 2014]. Other locally dominant tree species, which occur mainly in woodlands, like Guok (*Combretum* spp.) and Piok (*Terminalia* spp.), are not included in this analysis.

3.1.1 Classification approach

Based on the vegetation sites description [Annex F in *Bloesch*, 2014] along with GPS photos of the respective sites, we allocated each survey site in ArcGIS® with its dominant tree species. Using visual interpretation of available WorldView-2 imagery,

34

we defined conservative site-specific boundaries for each survey location to include a statically meaningful sampling size for Landsat imagery. This way we derived a "calibration dataset" for Maban and Pariang, which includes at least one survey site for each dominant tree species. It should be noted that the majority of survey sites (#16) are located in Maban and comparably less (#4) in Pariang (Fig. 12 and Fig. 13).

For the county of Maban we complemented the "calibration dataset" by an additional "validation dataset" (Fig. 30). We defined the location and extent of each validation dataset-site based on the visual interpretation of specific tree-species spectral and structural characteristics. For example, the Doum palm (*Hyphaene thebaica*) has a characteristically higher reflectance in the blue wavelength region, whereas the Desert date tree (*Balanites aegyptiaca*) typically occurs more isolated with an irregular tree-crown shape and often dominant in the vicinity of settlements. Furthermore, we used additional information on vegetation types from the land-cover sites description [Annex E in *Bloesch*, 2014] to verify our visual interpretation results.
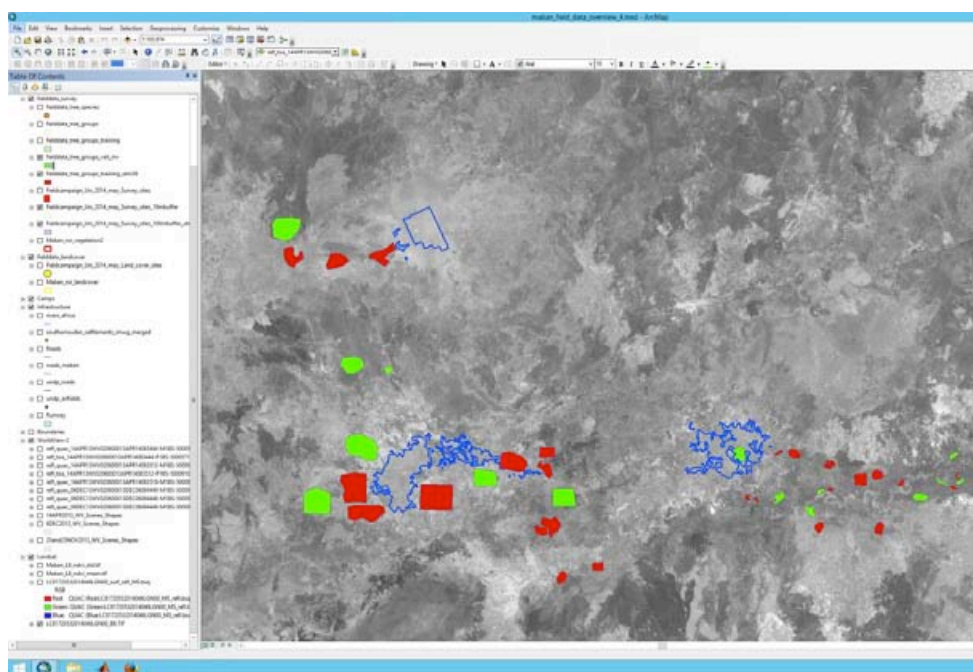
Fig. 30. Screenshot of ArcGIS® representing the calibration and validation datasets in Maban.

We used the calibration dataset to train the supervised classification algorithms and the validation dataset to validate its results. In general, supervised classifications are based on representative samples for each classification class. These calibration samples or "training sites" are used to identify the respective classes in the entire image based on their spectral signature.

For our classification purposes we tested the performance of three supervised classification algorithms:

Support Vector Machine (SVM) is a supervised classification method derived from statistical learning theory that often yields good classification results from complex and noisy data. It separates the classes with a decision surface that maximizes the margin between the classes. The surface is often called the optimal hyperplane, and the data points closest to the hyperplane are called support vectors. The support vectors are the critical elements of the training set.

35

Spectral Angle Mapper: (SAM) is a physically-based spectral classification that uses an n-D angle to match pixels to training data. This method determines the spectral similarity between two spectra by calculating the angle between the spectra and treating them as vectors in a space with dimensionality equal to the number of bands. This technique, when used on calibrated reflectance data, is relatively insensitive to illumination and albedo effects. SAM compares the angle between the training mean vector and each pixel vector in n-D space. Smaller angles represent closer matches to the reference spectrum. The pixels are classified to the class with the smallest angle.

Maximum Likelihood: (ML) Assumes that the statistics for each class in each band are normally distributed and calculates the probability that a given pixel belongs to a specific class. Each pixel is assigned to the class that has the highest probability (that is, the maximum likelihood).

The multi-temporal dataset used for the supervised tree species classifications consists of six (Maban) to eight (Pariang) Landsat-8 scenes, each scene including seven spectral "Operational Land Imager" bands. The opposing numbers of Landsat scenes stacked in one dataset indicate the maximum memory capacity of ENVI® to process the data. These scenes represent different times throughout the year to capture characteristic phenological vegetation conditions during the dry and rainy season. Subordinate to the distributed acquisition timing the scenes were selected by minimum cloud cover obscuring the ground conditions.

We evaluated the classification accuracy based on the *confusion matrix*, which shows the accuracy of a classification result by comparing it with ground truth information. In each confusion matrix an overall accuracy, producer and user accuracies, kappa coefficient, confusion matrix, and errors of commission and omission are reported.

The *overall accuracy* is calculated by summing the number of pixels classified correctly and dividing by the total number of pixels. The *kappa coefficient* (κ) is another measure of the accuracy of the classification ranging between 0 and 1.

Errors of commission represent pixels that belong to another class that are labeled as belonging to the class of interest.

Errors of omission represent pixels that belong to the ground truth class but the classification technique has failed to classify them into the proper class.

The *producer accuracy* is a measure indicating the probability that the classifier has labeled an image pixel into Class A given that the ground truth is Class A.

User accuracy is a measure indicating the probability that a pixel is Class A given that the classifier has labeled the pixel into Class A.

Among the three classifiers the SVM algorithm proved to be the most accurate one with the highest score in the overall accuracy. The confusion matrix of the SVM classification trained with the "calibration dataset" and validated with the "validation dataset" is given in the Appendix B. This classification approach for Maban yielded an overall accuracy of 62.6%.

For Pariang we could not implement the same approach as the data set on vegetation sites was comparably small, which results in overall accuracies of low explanatory power. Nevertheless, we used all available land cover and vegetation survey sites to create a training dataset that included seven regions for three tree species. The overall

accuracy among these training datasets is very high (99.3%), supporting the argument that the classification algorithm can spectrally distinguish individual tree classes.

The following figures illustrate the results of the classification (Fig. 31 Fig. 34).
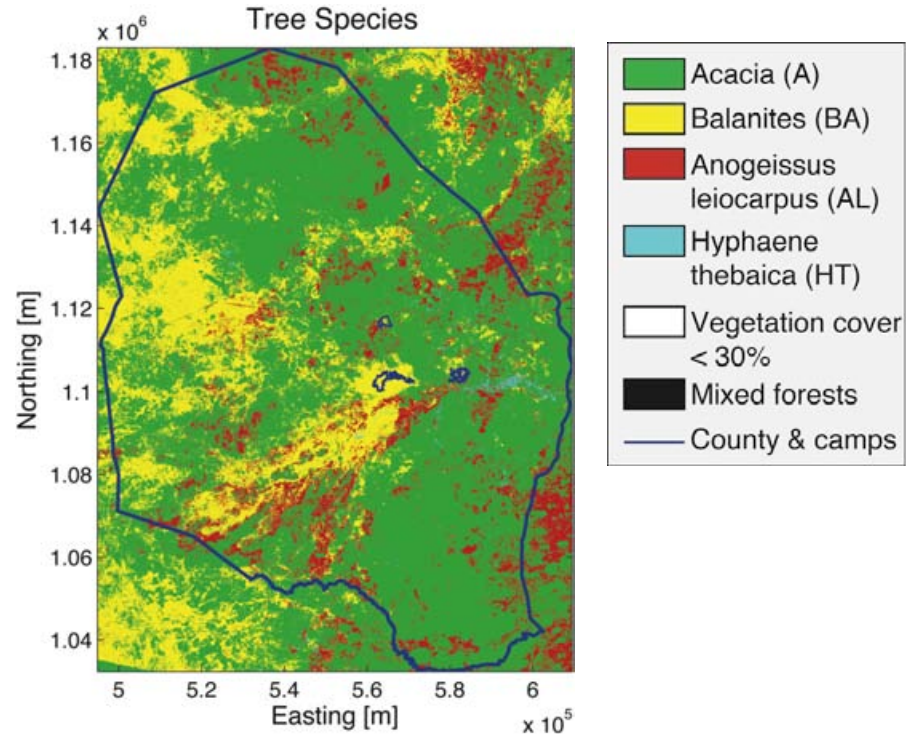
Fig. 31. SVM tree species classification result in Maban
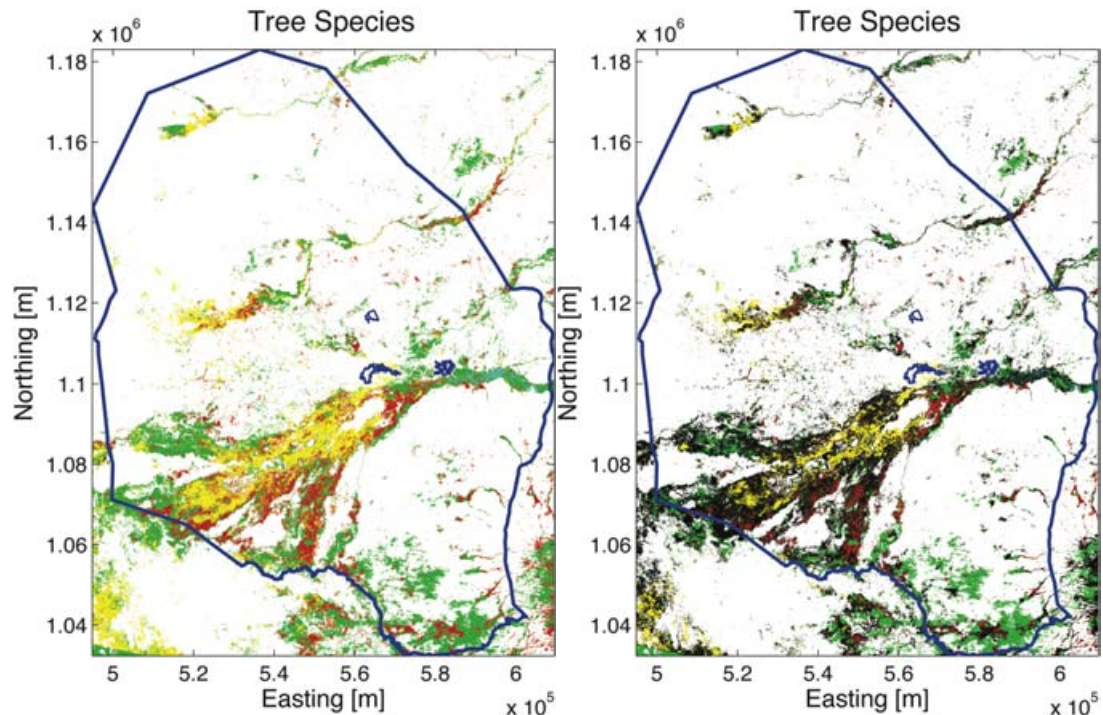
Fig. 32. (Left) SVM tree species classification result in Maban with vegetation masked below 30% canopy cover. (Right) Vegetation with less than 70% of pure stands labeled as mixed forest.

37
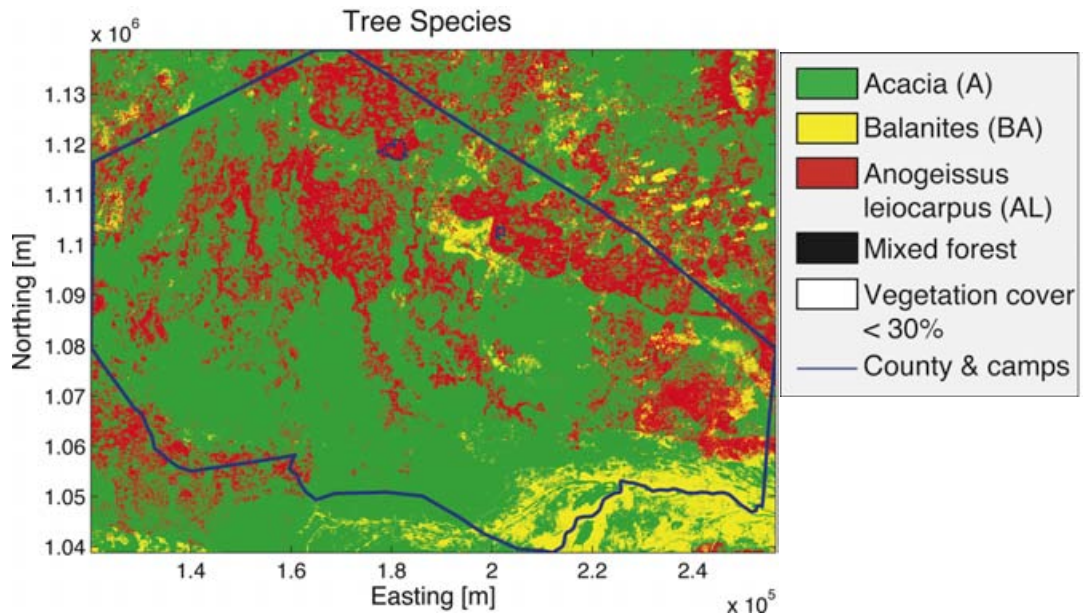
Fig. 33. SVM tree species classification result in Pariang
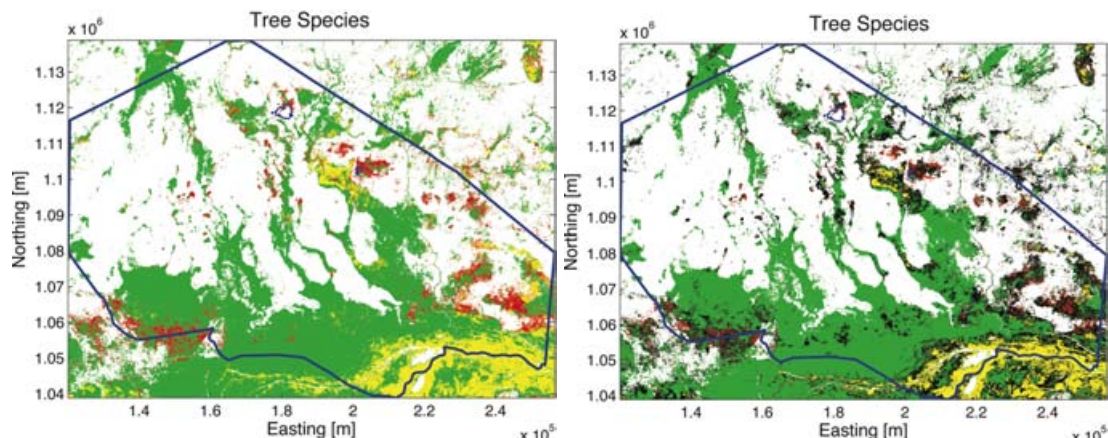
Fig. 34. Left: SVM tree species classification result in Pariang with vegetation masked below 30% canopy cover. Right: Vegetation with less than 70% of pure stands labeled as mixed forest.

For the tree species classification based on the WorldView-2 data we chose a similar approch. In contrast to the Landsat classification, our training-dataset is composed of individual tree spectra, which only includes canopy cover pixels rather than broader regions as illustrated for the Landsat data. In addition, we used the vegetations mask (section 3.1.1) to exlude soils and other land cover from the classification. Similar to the previous classification approach for the vegetation mask, we classified both temporal data clusters (Apr. vs. Nov./Dec.) seperately and mosaiced the final result (Fig. 35). Among the three classifiyers (i.e. ML, SAM, SVM) SVM performed the best.
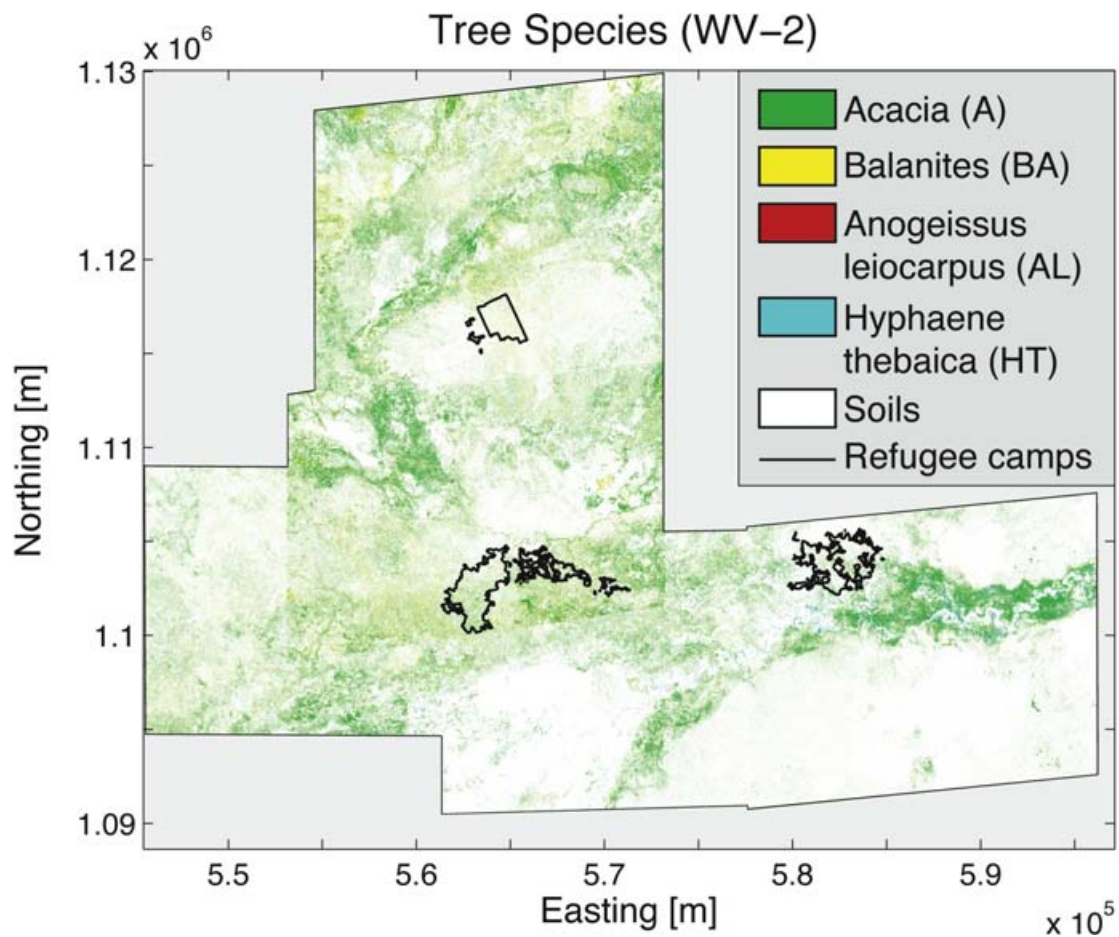
Fig. 35. Classification of tree species in WorldView-2 data

3.1.2 Classification uncertainties

The classification approach includes several uncertainties, which should be considered while interpreting the results.

First, we labeled our calibration/training dataset according the dominant tree species, which also incorporates other tree species present at varying degrees (0-50%) in the vegetation survey sites. Second, we extended the spatial extent of the survey sites based on visual interpretation of the available satellite imagery, which introduced a growing uncertainty of present tree species. Third, the survey sites are labeled according to their dominant tree species, irrespective of their canopy cover. As a result, varying degrees of mixed pixel (i.e. pixels including varying fractions of vegetation and soil) influence the spectral tree-species fingerprint. Fourth, randomly missing data due to cloud cover in some Landsat scenes introduces a bias in the classification, as certain seasonal information is missing. Fifths, burnt areas alter the spectral response of soils as they significantly decrease their spectral reflectance. Therefore, fire in areas with a low canopy cover (e.g. shrub/tree savannas) and high proportion of mixed pixel will have a more profound impact on the spectral reflectance as compared to high canopy cover areas (e.g. woodlands). This spectral variation due to fire can also influence classification results in areas with low canopy cover.

For the very high resolution WorldView-2 dataset, the main challenge is the heterogeneity within the canopy cover. Due to its high resolution, differences in

39

illuminated and shaded parts of a tree crown can result in different spectral classes, as the shaded parts are spectrally more similar among each other.

3.3   Land cover / Vegetation map

In this section we describe the procedure employed to generate the vegetation map of both counties, which combines information on vegetation classes and species as well as land cover.

Existing land cover dataset for South Sudan comprise the MODIS land cover product (MOD12Q1) produced at a spatial resolution of 500-m at annual time steps and the Africover dataset, which is digital georeferenced database on land cover produced from visual interpretation of Landsat satellite images between mid 90's and early 2000 (Fig. 36 and Fig. 37).
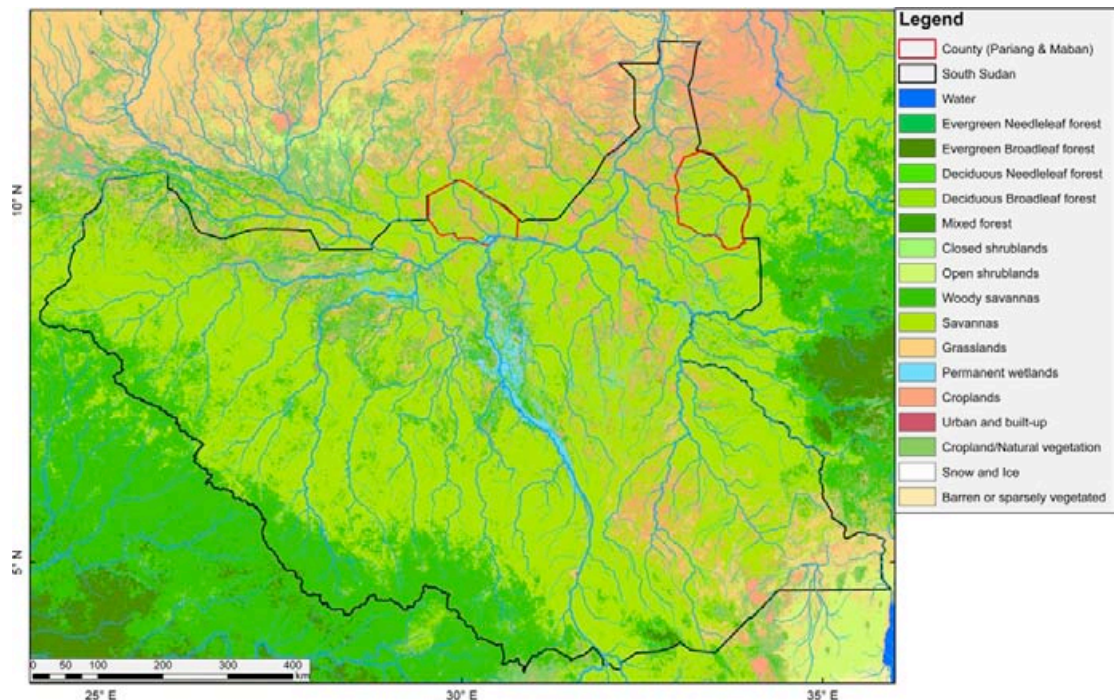
Fig. 36. MODIS land cover data from 2012 displayed with the USGS HydroSHEDS river network and overlain by administrative borders of South Sudan, Pariang and Maban.
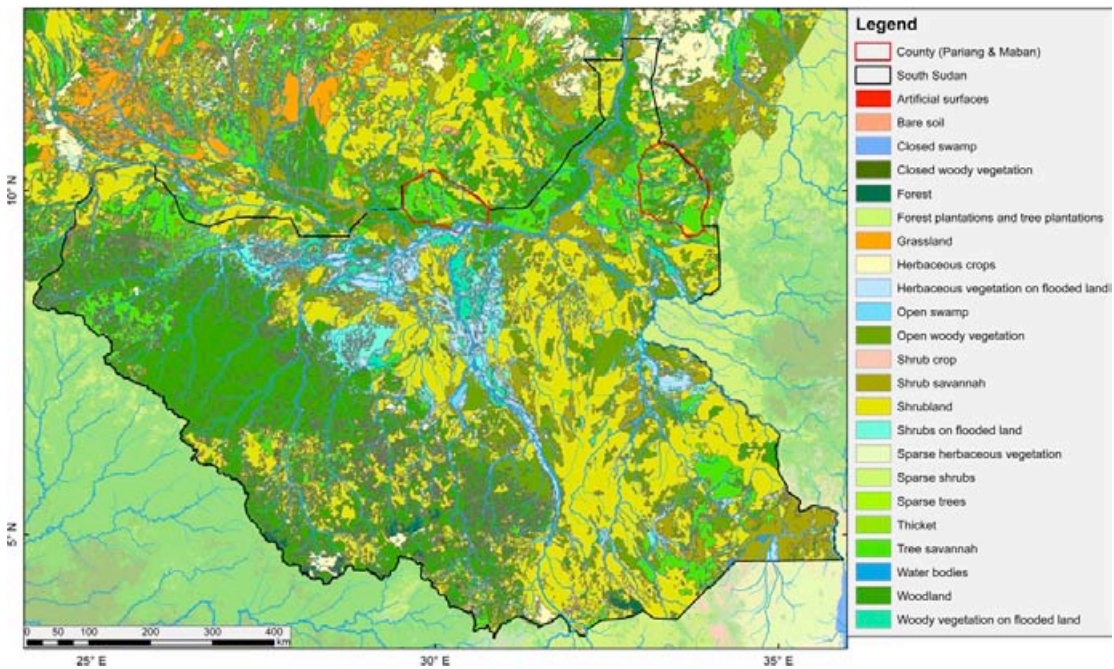
Fig. 37. Africover land cover data from 1995-2002 displayed with the USGS HydroSHEDS river network and overlain by administrative borders of South Sudan, Pariang and Maban.

Our approach to classify Landsat data revealed that different land cover types composed of soils (i.e. roads, airfields, agricultural areas, dry river beds, erosional features, various degrees of burnt soils) and artificial surfaces (i.e. roofing, tents) exhibit transitional spectral signatures that are hard to distinguish. Therefore, we extracted water bodies (i.e. lakes and rivers) as an additional land cover feature. Further information on burnt areas and its seasonal timing is given in chapter 4.

The basis of the vegetation map represents the combined information on the vegetation classes and vegetation species. Based on the canopy cover percentages, we distinguish between the four vegetation classes: (a) grassland 0-2%, (b) shrub/tree savanna 2-30%, (c) savanna woodland 30-60%, and (d) woodland >60%. The latter two classed are further subdivided by their tree species composition into the subclasses (i) Red Acacia (*Acacia seyal*), (ii) Silak (*Anogeissus leiocarpus*), (iii) Desert date tree (*Balanites aegyptiaca*), (iv) Doum palm (*Hyphaene thebaica*, not present in Pariang) and (v) mixed, which exhibits less than 70% monospecific stands. Furthermore, we distinguish riverine forests that mark systematically an assumed (?) 100 m wide belt to each side of watercourses with a canopy cover greater than 60%. Spatial data on watercourses and roads derive from *OpenStreetMap* (http://www.openstreetmap.org), whereas settlements and camps stem from *UNITAR* (http://www.unitar.org/unosat/sudan) (Fig. 38 and Fig. 39).

41
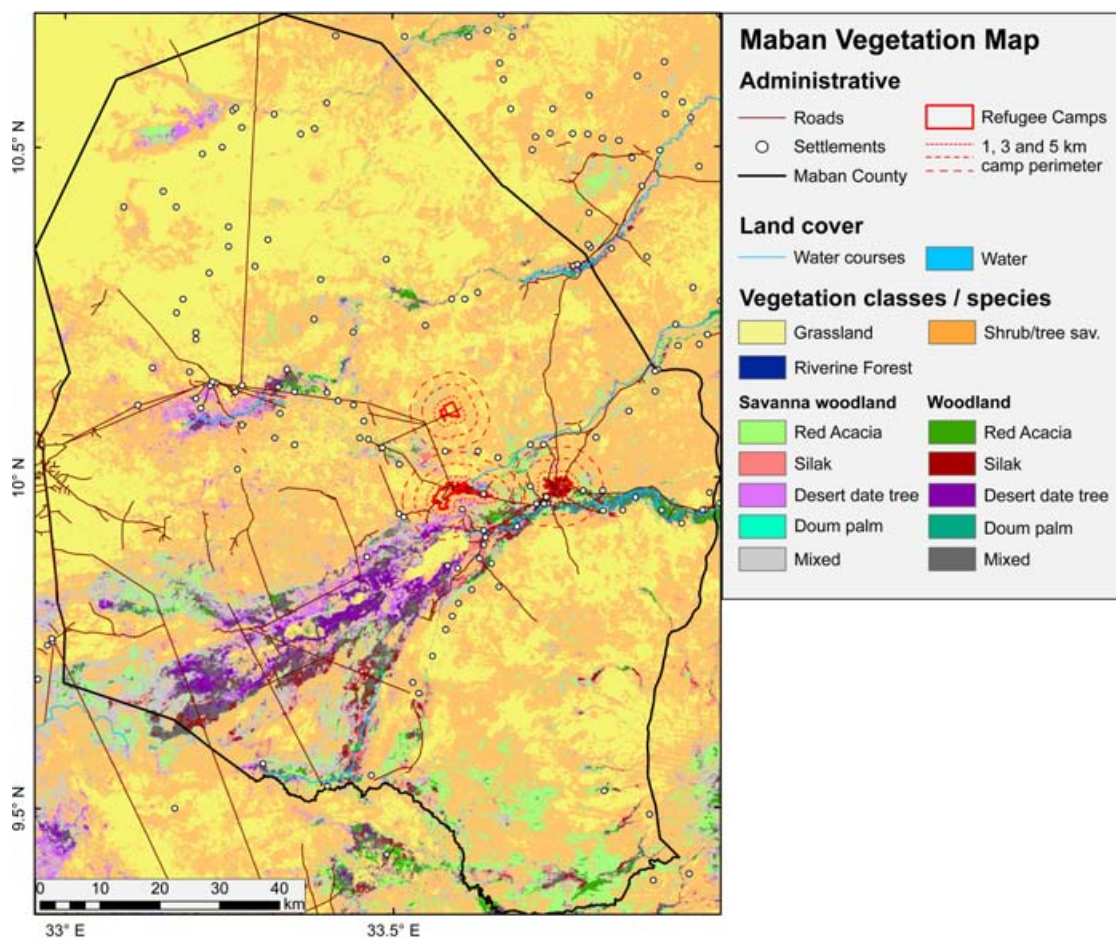
Fig. 38. Vegetation map of Maban.
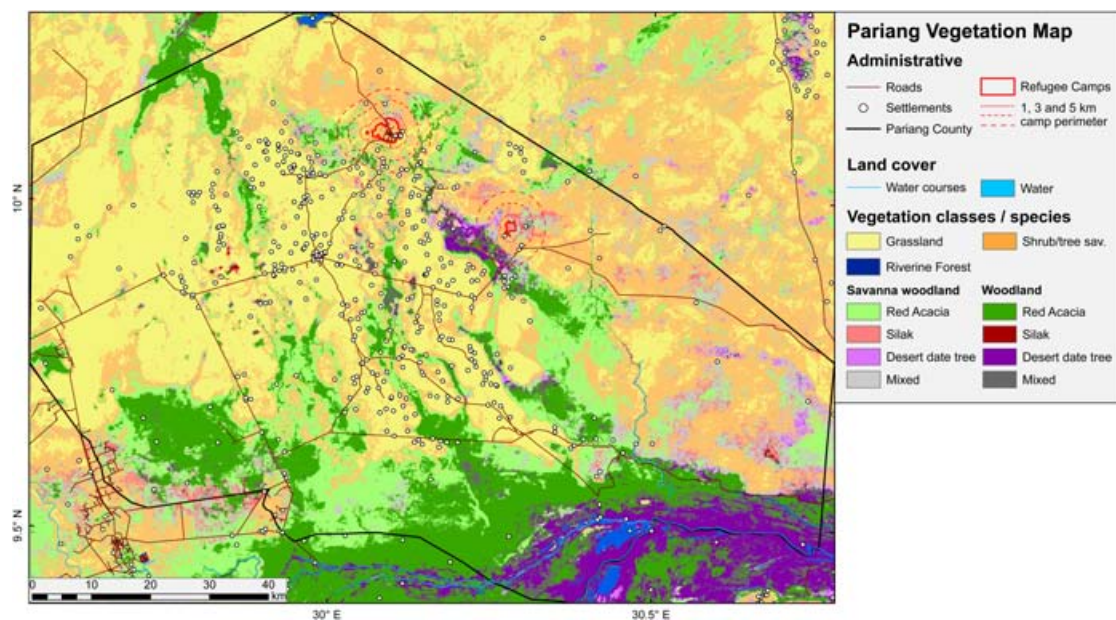
Fig. 39. Vegetation map of Pariang.

Based on the vegetation maps of both counties, we gathered statistical information on the spatial distribution of land cover classes and tree species subclasses (Table 5 and Table 6).

42

Table 5: Areal coverage of land cover classes and tree species in Maban.

County	Landcover class	Tree species	Area [km^2]	Percent [%]	Subpercent [%]	Canopy cover [mean]
Maban			11861.1	100.00		16.08
	Water		0.0	0.00		
	Grassland		4382.5	36.95		0.12
	Shrub/tree savanna		5187.6	43.74		13.63
	Savanna woodland		1640.0	13.83		42.37
		Red Acacia	563.5	4.75	34.36	40.65
		Desert date tree	213.9	1.80	13.04	44.86
		Silak	155.1	1.31	9.46	42.53
		Doum palm	1.4	0.01	0.09	44.65
		Mixed	706.0	5.95	43.05	42.96
	Woodland		626.0	5.28		76.50
		Red Acacia	90.8	0.77	14.50	75.36
		Desert date tree	144.0	1.21	23.01	74.27
		Silak	91.4	0.77	14.61	79.58
		Doum palm	5.3	0.05	0.85	91.60
		Mixed	294.4	2.48	47.03	76.70
	Riverine Forest		25.0	0.21		85.39

Table 6: Areal coverage of land cover classes and tree species in Maban.

County	Landcover class	Tree species	Area [km^2]	Percent [%]	Subpercent [%]	Canopy cover [mean]
Pariang			8925.6	100.00		30.73
	Water		50.0	0.56		
	Grassland		2890.5	32.38		1.70
	Shrub/tree savanna		2159.2	24.19		19.70
	Savanna woodland		2044.7	22.91		44.15
		Red Acacia	1334.4	14.95	65.26	45.04
		Desert date tree	44.8	0.50	2.19	39.13
		Silak	170.9	1.91	8.36	45.19
		Mixed	494.6	5.54	24.19	41.84
	Woodland		1771.5	19.85		76.60
		Red Acacia	1240.0	13.89	70.00	76.47
		Desert date tree	254.7	2.85	14.38	71.69
		Silak	12.4	0.14	0.70	93.28
		Mixed	264.3	2.96	14.92	81.20
	Riverine Forest		9.7	0.11		92.85

Once more, it should be noted that overall canopy cover in Pariang is likely to be lower due to the misclassification of wetlands (evergreen grasslands) along the Bahr el Ghazal River as forests.

3.4 Vegetation dynamics

In this section we describe the methodology to assess vegetation changes that occurred after the refugees arrived in South Sudan (July 2011 onwards). This assessment is based on multi-temporal analysis of Landsat data and comprises two approaches.

Approach 1: We detect "vegetation changes" based on NDVI differences from data that cluster around the years 2002, 2008 and 2013 (Fig. 5). These temporal data cluster comprise 5 to 6 Landsat scenes at varying times during the year that cover different phenological vegetation states. Therefore, this approach encompasses all kind of vegetation changes, including variations in grassland, shrub and tree cover.

Approach 2: We detect "forest changes" based on NDVI differences from data acquired at the onset of the dry season during the years 2000 to 2013 (Fig. 5). Due to this acquisition timing the grass layer is mostly photosynthetically inactive while mainly trees and shrubs are depicted by the NDVI.

Both approaches are hampered by challenges, such as annually varying vegetation (precipitation) characteristics, data gaps by cloud cover, and varying surface characteristics due to different fire histories. Our approach to overcome these challenges is based on (a) incorporating data from multiple years, (b) selecting comparable datasets from different years, and (c) leveling data to account for annual variations. For both approaches, we used multiple datasets (Approach 1: 18; Approach 2: 19), which we averaged over multiple years/seasons to compensate for data gaps such caused by cloud cover or severely burnt areas (section 2.2.3). For approach #2 we selected six scenes per time cluster that were obtained during a similar time of the year with a comparable scene-average NDVI. To account for annual variations in vegetation cover, we leveled scene-average differences to located "hotspots" of vegetation change (Fig. 40 and Fig. 41).
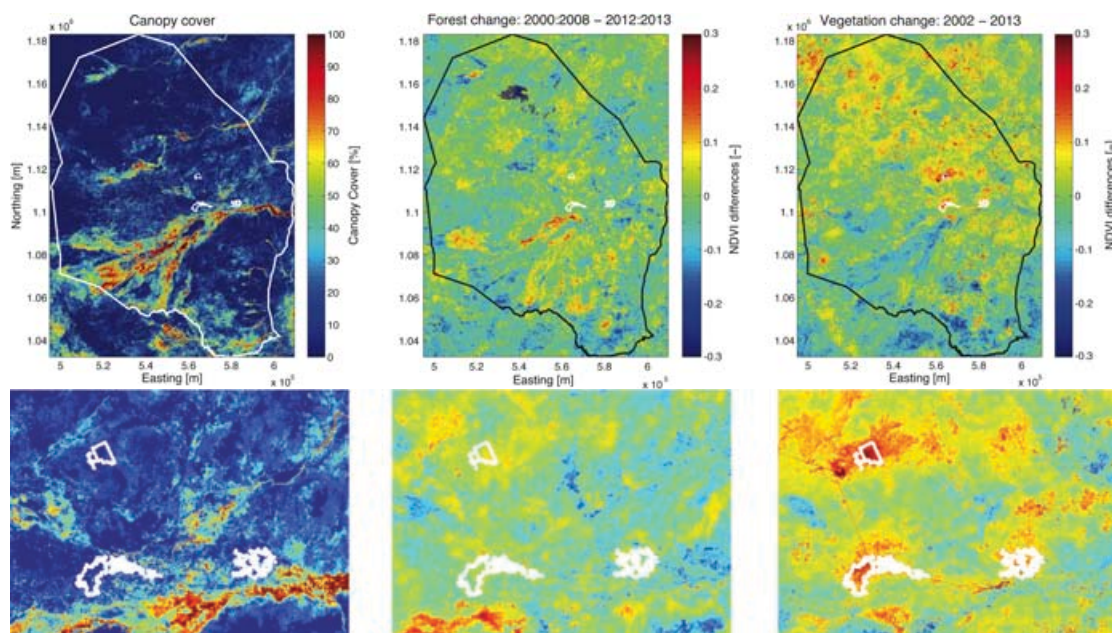
Fig. 40. (Upper left) Canopy cover of Maban. County border and refugee camps indicated by thick and thin white outlines, respectively. (Upper middle) "Forest change" (approach 2) compares changes in tree/shrub density between the time periods 2000-

2008 and 2012-2013. (Upper right) "Vegetation change" (approach 1) compares changes in vegetation density between the temporal data cluster of 2002 and 2013. Lower images highlight close ups of the refugee camps.
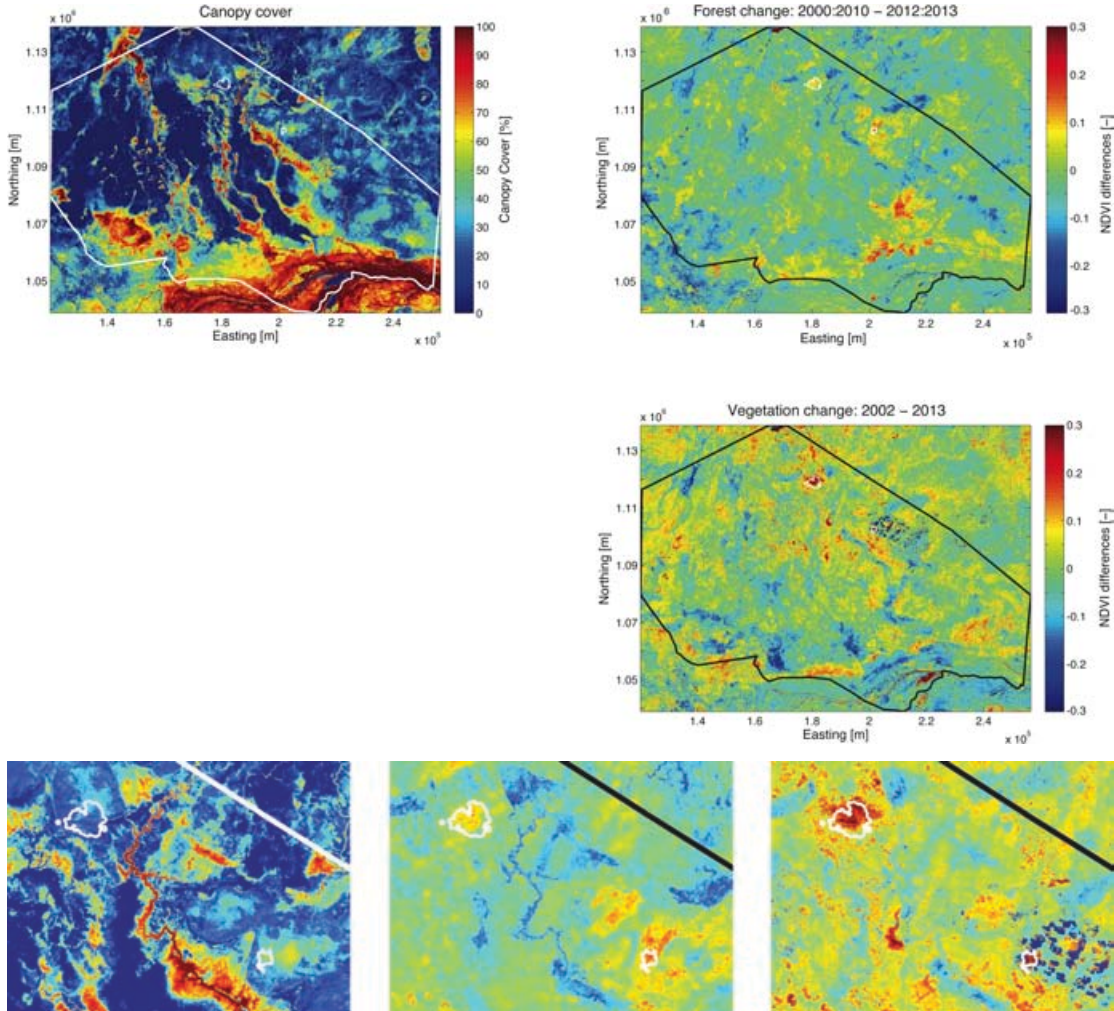
Fig. 41. (Upper left) Canopy cover of Pariang. County border and refugee camps indicated by thick and thin white outlines, respectively. (Upper right) "Forest change" (approach 2) compares changes in tree/shrub density between the time periods 2000-2010 and 2012-2013. (Lower right) "Vegetation change" (approach 1) compares changes in vegetation density between the temporal data cluster of 2002 and 2013. Lower images highlight close ups of the refugee camps.

The "vegetation change" product (approach 1) indicates pronounced NDVI changes in the areas within and surrounding the refugee camps. These vegetation losses are presumably driven by reductions in tree cover and grassland due to animal grazing and increased surface exposure of roads, tents and other roofing materials.

The "forest change" product (approach 2) indicates less pronounced NDVI changes in the refugee camp areas with the exception of the AjuongThok Camp in Pariang. Potentially, some refugee camps might have had a low forest cover in the first place and some tree species like to Desert date tree (*Balanites aegyptiaca*) are spared from tree cutting for cultural reasons.

Table 7: Overview on relative changes in NDVI and Canopy cover for both approaches (Forest method and Vegetation method) to detect vegetation change. Positive changes

indicate reductions in NDVI and Canopy Cover while negative changes represent increases.

Refugee Camp	Forest method		Vegetation method			
	2000:2010 - 2012:2013		2002-2008		2002-2013	
	Relative changes		Relative changes		Relative changes	
	NDVI	Canopy cover (%)	NDVI	Canopy cover (%)	NDVI	Canopy cover (%)
Adjoungthok	0.15	50.60	-0.04	-12.49	0.24	81.17
Adjoungthok 3km	0.08	26.94	-0.02	-5.65	0.04	14.74
Yida	0.07	25.09	0.00	-1.40	0.20	66.30
Yida 3km	0.02	5.74	0.01	3.32	0.09	29.77
Batil-Gendrassa	0.03	9.89	-0.02	-8.11	0.09	29.94
Batil-Gendrassa 3km	0.03	11.67	-0.02	-7.37	0.05	18.08
Doro	0.01	3.01	-0.01	-4.30	0.07	22.29
Doro 3km	0.00	-0.32	0.00	-1.23	0.04	12.62
Kaya	0.06	19.36	0.01	3.42	0.17	55.92
Kaya 3km	0.05	15.82	0.01	4.77	0.11	38.47

To quantify changes in the surrounding of and within the refugee camps, we calculated the relative changes in NDVI and related those to changes in canopy cover based on the NDVI-canopy cover relation given in Fig. 22. It is notable that the vegetation changes generally decrease with increasing distance from the refugee camps and that the changes occurred after the arrival of the refugee in 2011. The canopy cover was remarkably stable within and in the surrounding of the camps/settlement over the decade prior to the arrival of the refugees.

4.   Fire regime in South Sudan

4.1 Data acquisition

MODIS Burnt Area Product

For the analysis of burnt areas in South Sudan, we used the GeoTIFF version of the MODIS MCD45 product (collection 5.1) by University of Maryland (http://modis-fire.umd.edu/Burned_Area_Products.html). This version is a Level 3 gridded 500m monthly product in Plate-Carrée projection, which combines MODIS-TERRA and MODIS-AQUA land surface reflectance data from the year 2000 onwards.

Each product tile contains the following components:

- Per-pixel burning information
  - the approximate day of burning (1-366) or 0 (no burning detected)
  - codes to indicate no decision due to persistent missing, bad quality or cloudy data.
  - QA information.
- Mandatory and product-specific metadata properties and processing path information.

The MODIS burned area algorithm maps the approximate day of burning using multitemporal land surface reflectance data based on a method described by *Roy et al.* [2002; 2005]. The identification of the date of burning is constrained by the frequency and occurrence of missing observations and to reflect this, the algorithm is run to report the burn date with an 8-day precision [*Roy and Boschetti*, 2009].

We downloaded the MODIS burned area via ftp from the website http://modis-fire.umd.edu/ after obtaining a username and password from the user online form: http://modis-fire.umd.edu/form.html.

TRMM 3B42 product:

A number of climate rainfall products are produced from the passive microwave (TMI) and precipitation radar (PR) sensors on board the Tropical Rainfall Measuring Mission (TRMM) satellite, which was launched in November of 1997. We used a daily satellite-derived rainfall record, based on the TRMM product 3B42 (version 7), which has a spatial resolution of 0.25° x 0.25° (~30 km x 30 km) and a temporal resolution of 3 hours. This data set combines microwave and infrared rain-rate estimates from sensors onboard several low-earth orbit and one geosynchronous satellite, which are rescaled to monthly rain-gauge data [*Huffman et al.*, 2007].

We downloaded the global dataset from the following earth science data interface: http://mirador.gsfc.nasa.gov/.

Africover

Africover was a UN project, which collected and collated geographical information on Africa (e.g. land cover) using satellites. The FAO released the full resolution land cover databases of the AFRICOVER project countries: Burundi, DRC, Egypt, Eritrea, Kenya, Rwanda, Somalia, Sudan (at that time including the now independent South Sudan), Tanzania and Uganda. These multipurpose vector datasets were produced

from visual interpretation of LANDSAT TM satellite images (spectral bands 4,3,2) between mid 90's and early 2000 [*Kalensky*, 1998; *Torbick et al.*, 2006]. Information and data can be displayed/downloaded through the FAO's geo-catalogue:

http://www.fao.org/geonetwork/srv/en/main.search?title=africover%20landcover

Within the area of South Sudan, the following land cover types are distinguished: Artificial surfaces, Bare soil, Closed woody vegetation, Forest, Grassland, Herbaceous crops, Herbaceous vegetation on flooded land, Open swamp, Open woody vegetation, Shrub savannah, Shrubland, Shrubs on flooded land, Sparse shrubs, Sparse trees, Thicket, Tree savannah, Water bodies, Woodland, Woody vegetation on flooded land.

4.2 Data analysis

In this section, we will analyze spatiotemporal characteristics of and links between burned areas, rainfall and land cover. On a spatial scale, we will analyze the area of South Sudan at three levels:

(a) National: South Sudan = 3.0°-13.0°N, 25.0°-36.0°E;

(b) State: Upper Nile = 7.5°-12.5°N, 30.5°-34.5°E;

                   Unity = 7.0°-10.5°N, 28.5°-31.0°E;

(c) County: Pariang = 9.8°-10.3°N, 29.9°-30.4°E;

                   Maban = 9.7°-10.3°N, 33.3°-33.9°E;

Within these areas we will assess the average annual fire frequency and the typical seasonal timing of fires. Furthermore, we will analyze temporal trends of burned areas over the last decade. On a temporal scale, we analyze MODIS burned area data from April 2000 to April 2014 (with June 2001 missing) at three levels: (a) annual basis, (b) post-rain (Aug-Dec, so-called early dry season fires) and pre-rain (Jan-Jul, so-called late dry season fires) basis, and (c) monthly/daily basis.

Concerning the TRMM rainfall data, we analyze the spatial rainfall distribution in South Sudan and temporal variation over the past decade on the national, state and county level. In combination with the burnt area data we investigate the relationships between burnt areas, rainfall amounts and periods. Furthermore, we quantified which land cover classes are affected by fires to which degree.

4.2.1 Spatiotemporal analysis of burnt areas

In the spatial domain, we illustrate for each region the mean annual fire frequency, which represents the average occurrence of fires per year over the timespan 2000-2014 (Fig. 42, Fig. 44, Fig. 48). Maps on the spatial distribution of fires during the pre- (Jan.-Jul.) and post- (Aug.-Dec.) rain season are given in Appendix C.

In the temporal domain, we analyze the average daily distribution of fires during the year (Fig. 42, Fig. 45, Fig. 49). The monthly distribution of fires highlights the strong seasonality of fires in this region (Fig. 43, Fig. 46, Fig. 50). Few to no fires occur during the rainy season, which contrasts pronounced areal fires after the onset of the dry season to the next rainy season. Therefore, we analyze annual variation between fire cycles (or "fire years") from August to July, which encompasses all fire occurrences during the dry season (Fig. 43, Fig. 47, Fig. 51). Furthermore, we provide

tables with monthly percentages of burnt areas from 2000 to 2014 in each region (Table 8, Table 12).

South Sudan

The average annual area burnt in South Sudan amounts to 52.8%. The temporal fire distribution reveals a pattern of early dry season fires (Oct.-Nov.) in relatively dry northern regions towards late dry season fires (Mar.-May) in wetlands and rarely burnt areas. Areas that are burnt less often also tend to get burnt very late or very early in the dry season.
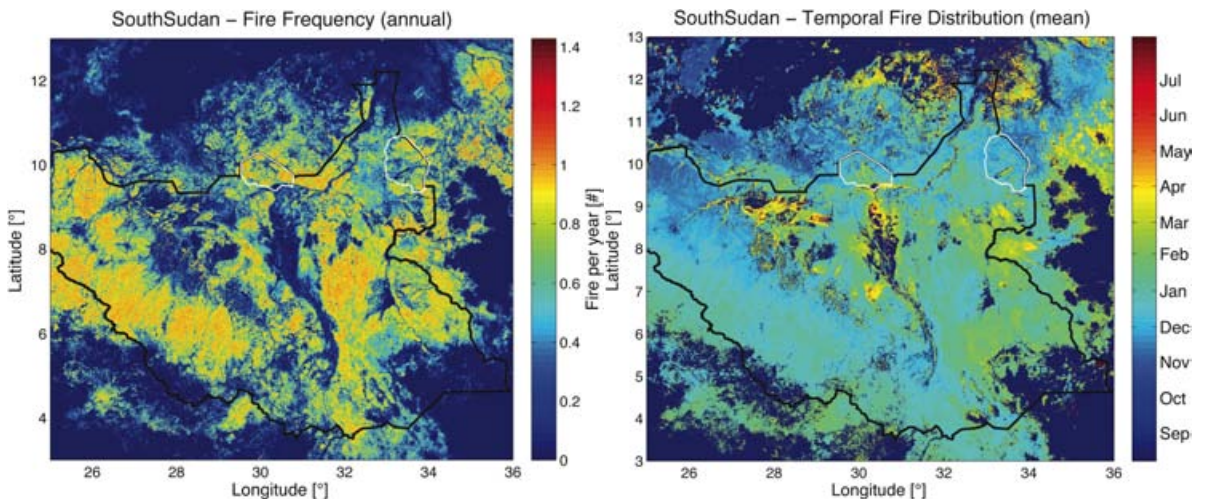
Fig. 42. (Left) Mean annual fire frequency in South Sudan, illustrating the average number of fires per year. (Right) Mean annual temporal fire distribution in South Sudan, illustrating the average timing of fires during the year. Black outline indicates the border of South Sudan. White outlines indicate the Counties of Pariang and Maban.
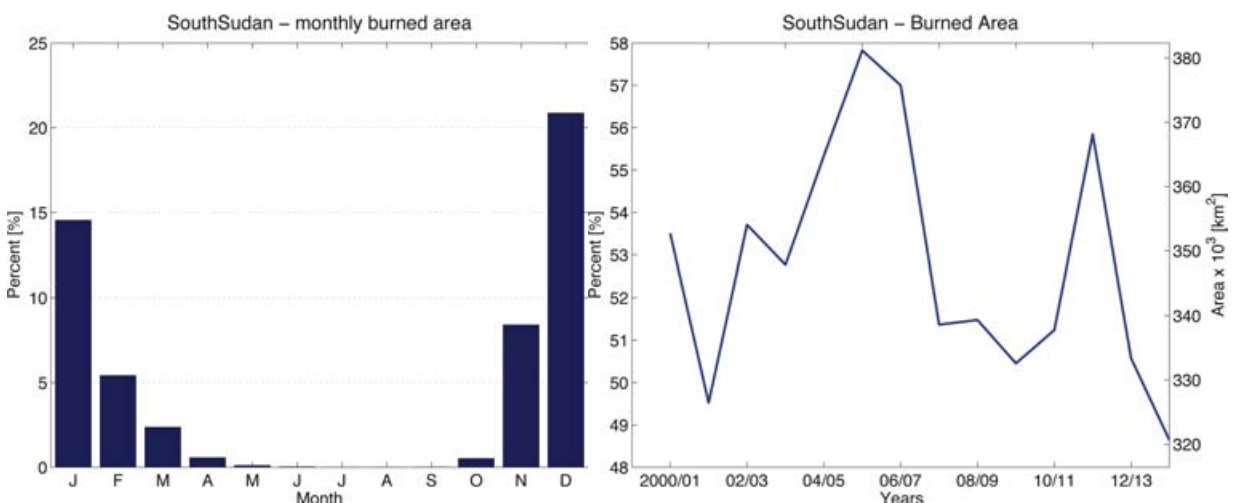
Fig. 43. (Left) Mean monthly percentage of burnt area of South Sudan. (Right) Annual variations of burned area and percentage in South Sudan from 2000 to 2014 during the annual period from August to July.

Table 8: Monthly percentage of burnt areas in South Sudan.

Years	Jan	Feb	Mar	Apr	May	Jun	Jul	Aug	Sep	Oct	Nov	Dec	Total
2000	NaN	NaN	NaN	0.7	0.1	0.0	0.0	0.0	0.0	1.6	8.3	24.5	NaN
2001	13.2	4.0	1.4	0.4	0.2	NaN	0.0	0.0	0.0	0.7	5.2	18.3	43.3
2002	14.9	8.3	1.7	0.3	0.2	0.1	0.0	0.0	0.1	0.4	9.0	23.0	57.8

2003	14.8	4.3	1.5	0.6	0.2	0.0	0.0	0.0	0.0	0.4	7.7	23.0	52.5
2004	12.3	6.0	2.5	0.4	0.2	0.0	0.0	0.0	0.0	0.8	7.9	24.1	54.4
2005	15.4	3.8	2.6	0.7	0.1	0.0	0.0	0.0	0.0	0.8	13.4	26.5	63.2
2006	9.6	4.2	2.3	1.0	0.0	0.0	0.0	0.0	0.0	0.2	9.2	17.9	44.4
2007	18.5	6.9	3.6	0.7	0.1	0.0	0.0	0.0	0.0	0.5	6.2	21.6	58.1
2008	13.7	6.1	3.1	0.1	0.0	0.0	0.0	0.0	0.0	0.7	8.7	19.3	51.7
2009	14.9	4.5	2.8	0.2	0.2	0.2	0.0	0.0	0.0	0.3	14.2	20.3	57.7
2010	10.9	2.7	1.4	0.5	0.0	0.0	0.0	0.0	0.0	0.1	5.3	17.8	38.8
2011	16.8	7.0	3.1	0.9	0.1	0.0	0.0	0.0	0.0	0.1	7.8	21.0	56.9
2012	16.1	6.8	3.2	0.8	0.0	0.0	0.0	0.0	0.0	0.4	8.6	17.8	53.8
2013	14.6	6.2	1.9	0.9	0.0	0.0	0.0	0.0	0.0	0.5	6.2	17.0	47.5
2014	17.8	5.1	1.8	0.1	NaN	NaN	NaN	NaN	NaN	NaN	NaN	NaN	NaN

Upper Nile & Unity

The average annual area burnt in Upper Nile and Unity amounts to 52.6% and 51.7%, respectively.
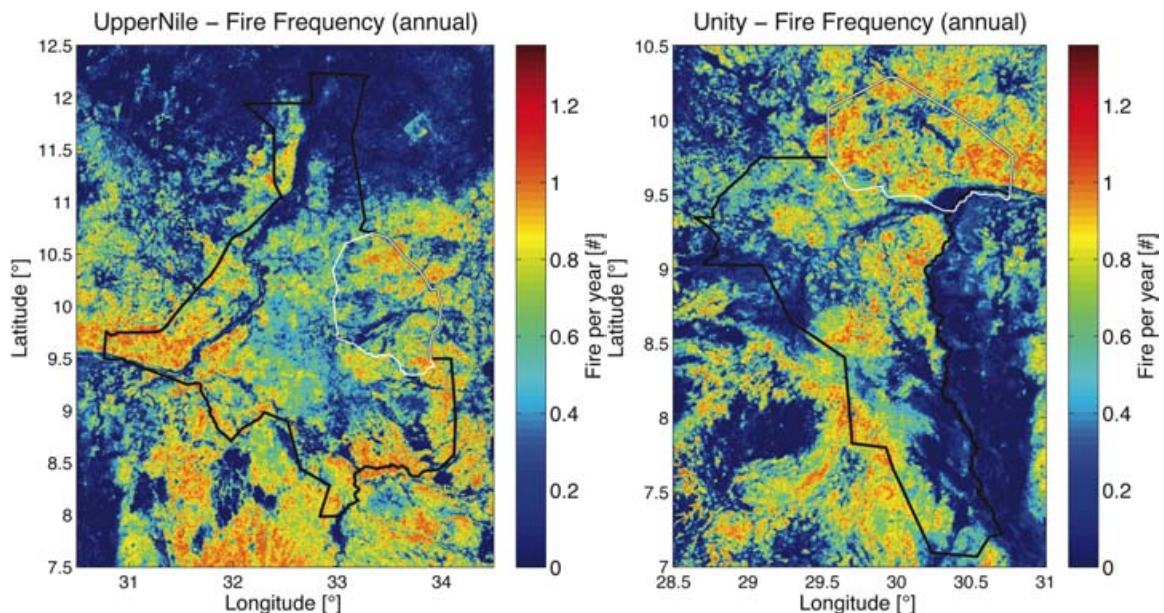
Fig. 44. Mean annual fire frequency in Upper Nile (left) and Unity (right), illustrating the average number of fires per year. Black outline indicates the border of the States, while white outlines indicate the Counties of Pariang and Maban.
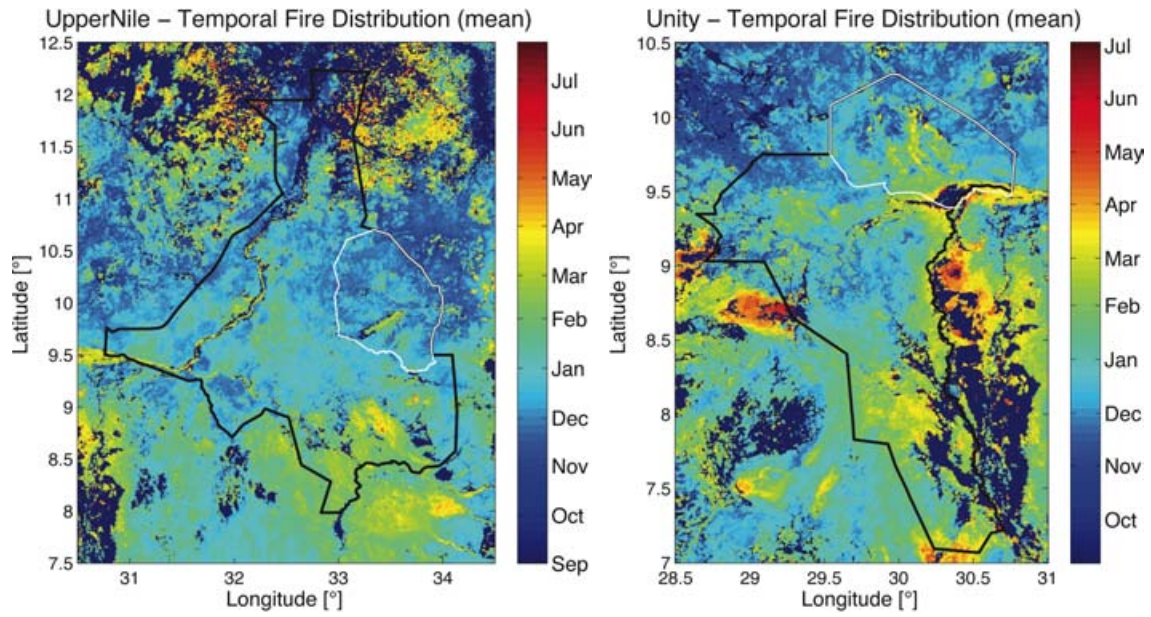
Fig. 45. Mean annual temporal fire distribution in Upper Nile (left) and Unity (right), illustrating the average timing of fires during the year. Black outline indicates the border of the States, while white outlines indicate the Counties of Pariang and Maban.
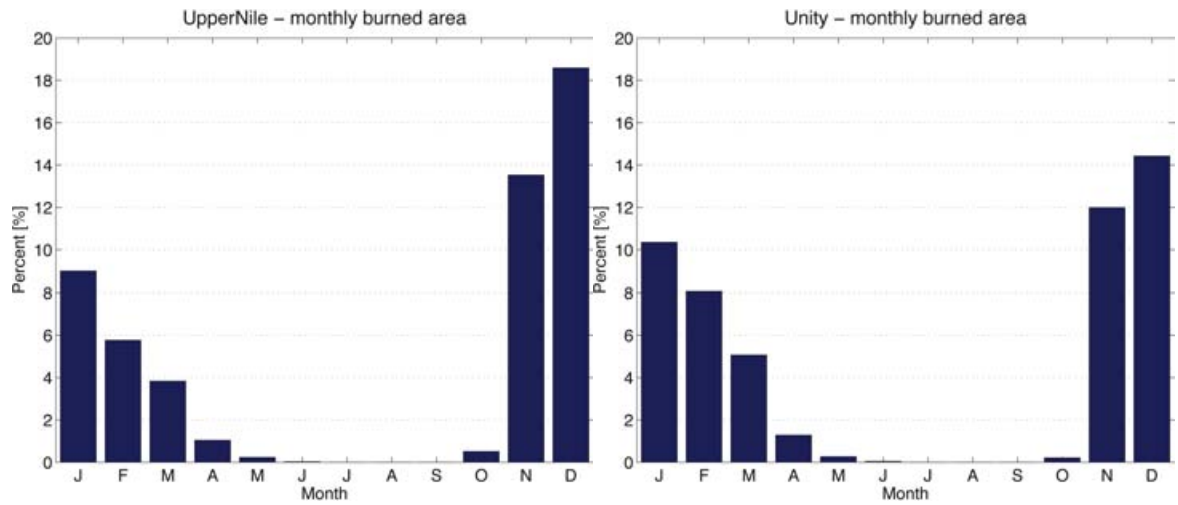
Fig. 46. Mean monthly percentage of burnt area in Upper Nile (left) and Unity (right).
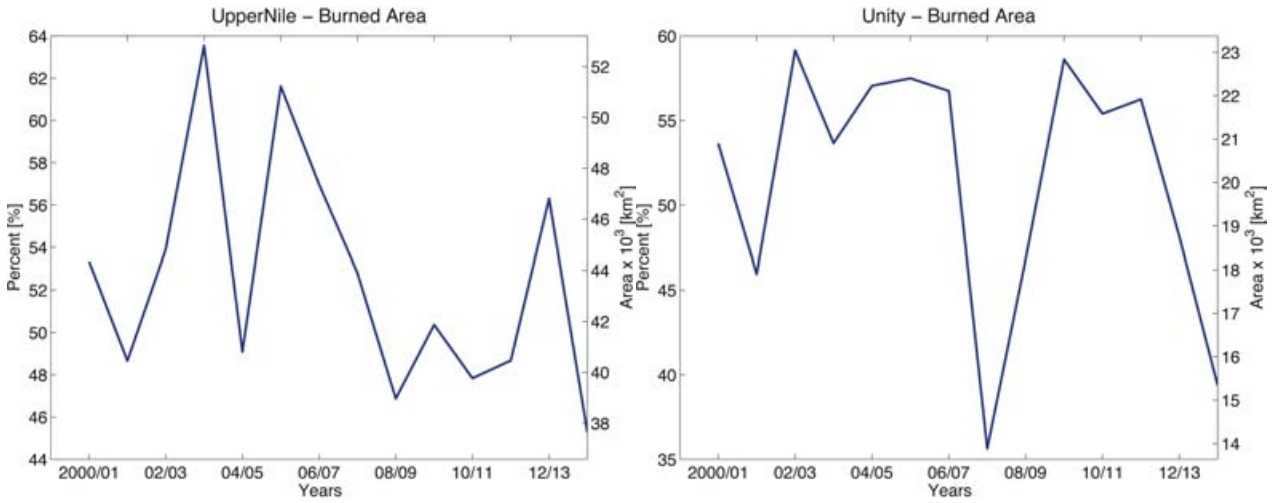
Fig. 47. Annual variations of burned area and percentage in Upper Nile (left) and Unity (right) from 2000 to 2014 during the annual period from August to July.

Table 9: Monthly percentage of burnt areas in Upper Nile.

Years	Jan	Feb	Mar	Apr	May	Jun	Jul	Aug	Sep	Oct	Nov	Dec	Total
2000	NaN	NaN	NaN	1.4	0.3	0.0	0.0	0.0	0.0	0.7	10.8	22.5	NaN
2001	9.7	6.1	2.5	0.7	0.3	NaN	0.0	0.0	0.0	0.5	6.1	15.8	41.8
2002	13.7	7.5	3.5	1.1	0.4	0.0	0.0	0.0	0.0	0.1	14.3	23.8	64.6
2003	9.0	3.9	1.7	0.8	0.2	0.0	0.0	0.0	0.0	0.3	17.9	23.7	57.4
2004	11.9	5.9	3.0	0.7	0.3	0.0	0.0	0.0	0.0	0.2	11.0	17.1	50.2
2005	8.6	5.4	4.6	2.0	0.2	0.0	0.0	0.0	0.0	0.7	20.3	20.2	61.9
2006	8.0	6.8	4.2	1.3	0.0	0.0	0.0	0.0	0.0	0.3	15.2	20.8	56.6
2007	8.2	5.9	5.2	1.1	0.4	0.0	0.0	0.0	0.0	0.2	11.2	16.3	48.4
2008	11.7	7.0	6.1	0.2	0.1	0.0	0.0	0.0	0.0	1.0	13.6	13.3	53.1
2009	8.1	4.0	5.5	0.5	0.7	0.3	0.0	0.0	0.0	1.0	22.1	15.4	57.4
2010	7.0	2.7	1.5	0.6	0.0	0.0	0.0	0.0	0.0	0.1	6.8	19.5	38.3
2011	8.4	7.5	3.8	1.6	0.1	0.0	0.0	0.0	0.0	0.2	13.6	15.6	50.8
2012	7.4	7.5	3.7	0.7	0.1	0.0	0.0	0.0	0.0	1.3	16.9	21.3	58.8
2013	5.4	4.6	4.1	2.5	0.2	0.0	0.0	0.0	0.0	0.6	9.7	14.9	42.0
2014	9.5	5.8	4.3	0.6	NaN	NaN	NaN	NaN	NaN	NaN	NaN	NaN	NaN

Table 10: Monthly percentage of burnt areas in Unity.

Years	Jan	Feb	Mar	Apr	May	Jun	Jul	Aug	Sep	Oct	Nov	Dec	Total
2000	NaN	NaN	NaN	1.5	0.1	0.0	0.0	0.0	0.0	0.8	11.7	16.9	NaN
2001	12.0	7.9	2.5	1.4	0.3	NaN	0.0	0.0	0.0	0.1	10.7	13.4	48.4
2002	10.8	7.0	2.8	0.9	0.2	0.0	0.0	0.0	0.0	0.0	18.7	20.5	61.0
2003	10.3	5.4	2.8	0.8	0.6	0.0	0.0	0.0	0.0	0.7	15.1	16.2	51.9
2004	6.9	8.1	5.5	0.6	0.5	0.0	0.0	0.0	0.0	0.1	14.4	18.4	54.7
2005	11.4	6.0	5.4	0.9	0.4	0.0	0.0	0.0	0.0	0.2	18.0	14.0	56.2
2006	8.6	7.8	6.1	2.9	0.0	0.0	0.0	0.0	0.0	0.1	12.9	11.4	49.8
2007	9.9	11.9	8.3	2.0	0.2	0.0	0.0	0.0	0.0	0.1	3.1	9.9	45.4
2008	6.5	8.4	7.4	0.1	0.2	0.0	0.0	0.0	0.0	0.4	12.6	11.9	47.5
2009	9.9	5.8	4.3	0.8	0.8	0.4	0.0	0.0	0.0	0.1	17.4	17.4	56.8
2010	13.4	6.4	2.8	1.1	0.0	0.0	0.0	0.0	0.0	0.0	5.0	17.1	45.8

52

2011	11.8	11.1	7.9	2.3	0.2	0.0	0.0	0.0	0.0	0.0	11.2	12.4	57.0
2012	13.0	9.9	7.9	1.7	0.1	0.0	0.0	0.0	0.0	0.3	11.3	12.5	56.7
2013	10.2	7.4	4.3	2.0	0.1	0.1	0.0	0.0	0.0	0.1	5.8	10.1	40.0
2014	10.3	10.0	2.9	0.2	NaN	NaN	NaN	NaN	NaN	NaN	NaN	NaN	NaN

Maban & Pariang

The average annual area burnt in Maban and Pariang amounts to 57.9% and 67.0%, respectively.
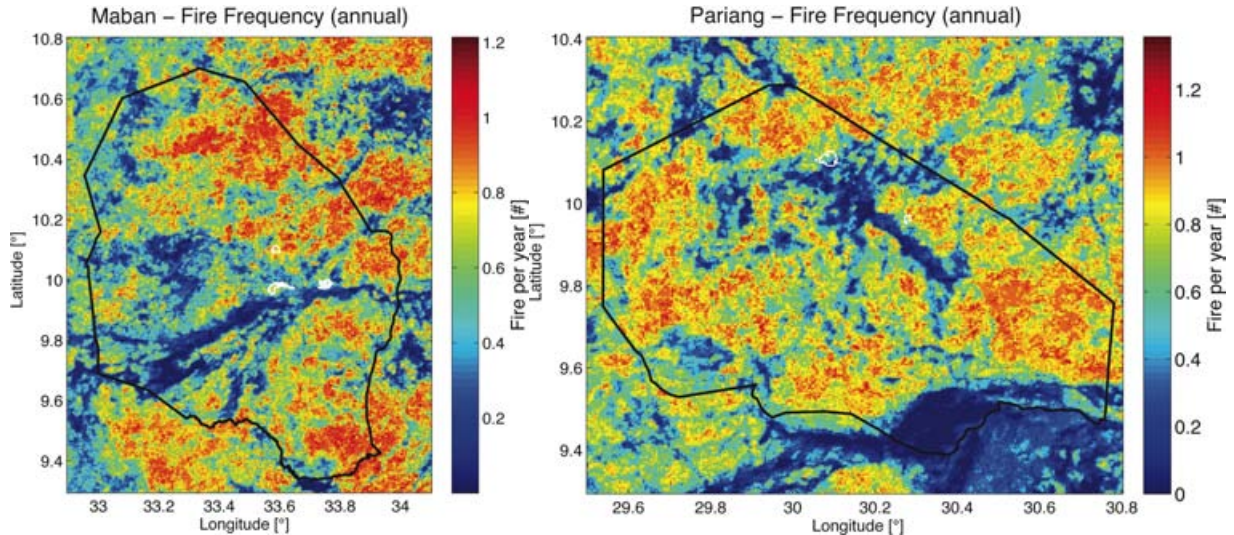
Fig. 48. Mean annual fire frequency in Maban (left) and Pariang (right), illustrating the average number of fires per year. Black outlines indicate the County borders, while white outlines represent refugee camps.
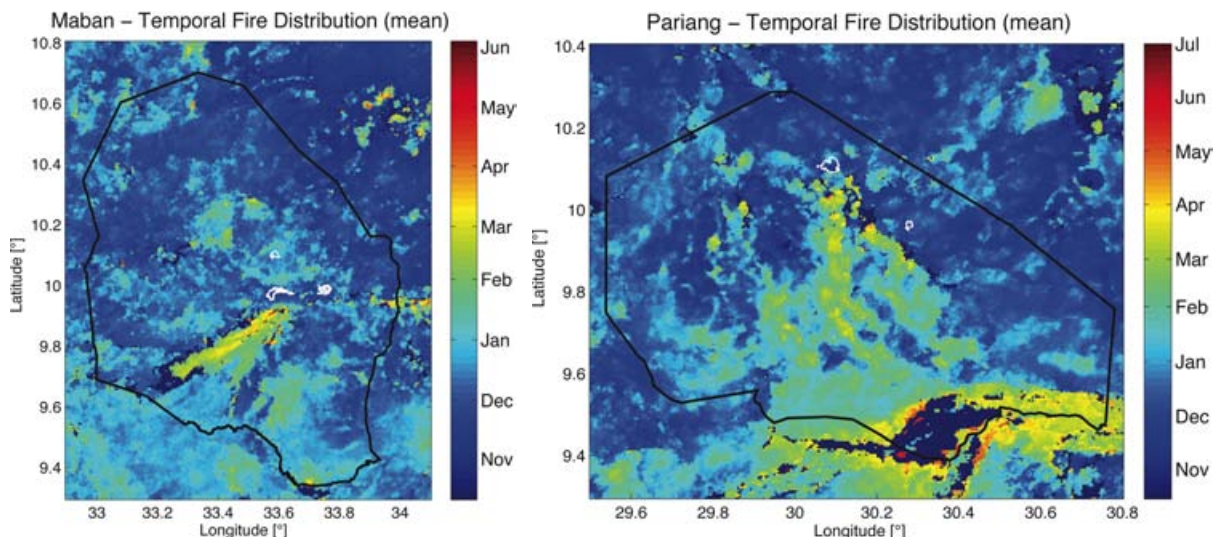

Fig. 49. Mean annual temporal fire distribution in Maban (left) and Pariang (right), illustrating the average timing of fires during the year. Black outlines indicate the County borders, while white outlines represent refugee camps.
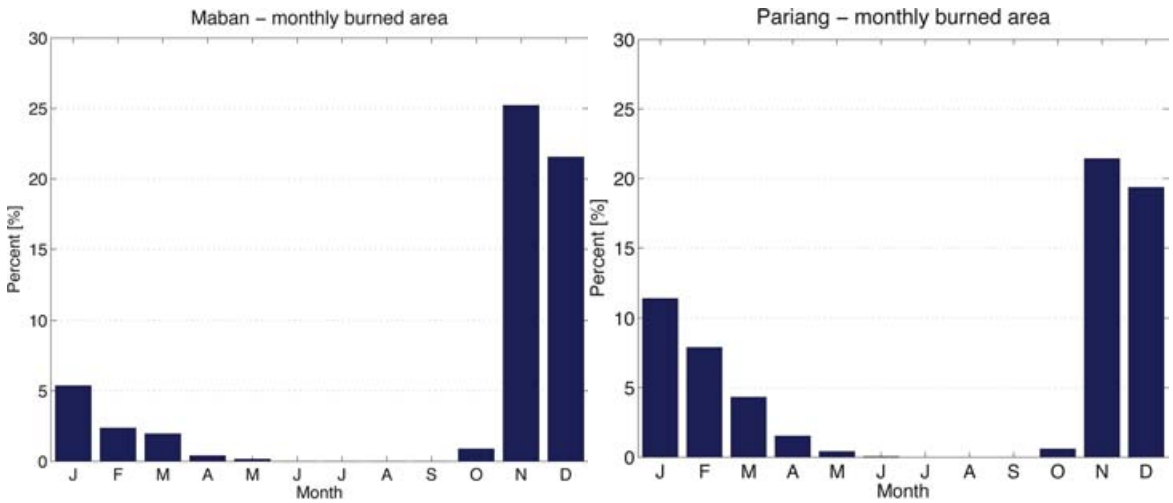
Fig. 50. Mean monthly percentage of burnt area in Maban (left) and Pariang (right).
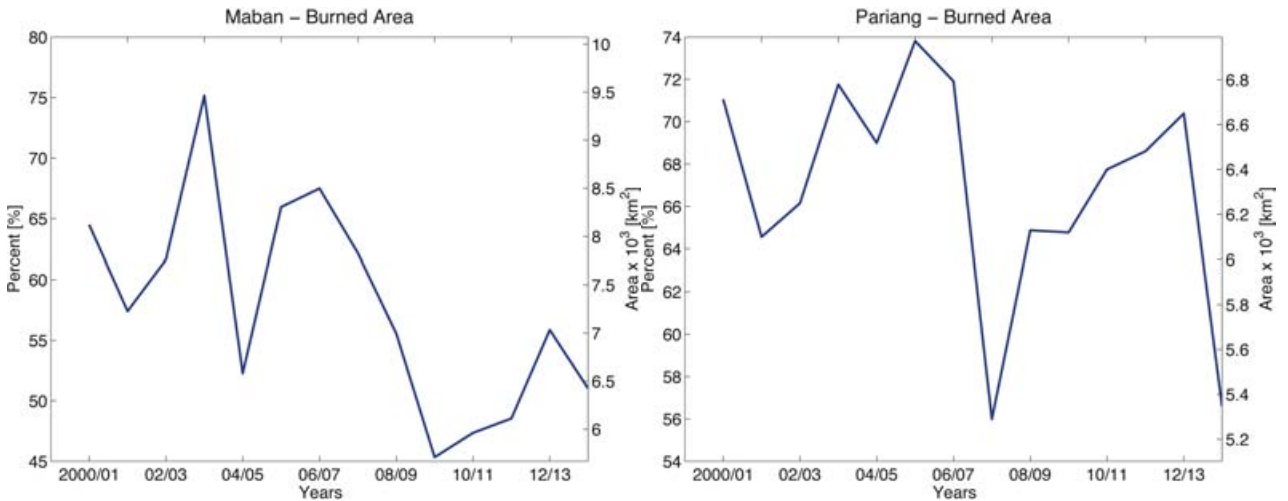
Fig. 51. Annual variations of burned area and percentage in Maban (left) and Pariang (right), from 2000 to 2014 during the annual period from August to July.

Table 11: Monthly percentage of burnt areas in Maban.

Years	Jan	Feb	Mar	Apr	May	Jun	Jul	Aug	Sep	Oct	Nov	Dec	Total
2000	NaN	NaN	NaN	0.6	0.4	0.0	0.0	0.0	0.0	0.2	23.2	27.7	NaN
2001	6.1	4.2	2.5	0.4	0.2	NaN	0.0	0.0	0.0	0.0	13.4	26.6	53.3
2002	10.5	4.3	2.0	0.4	0.2	0.0	0.0	0.0	0.0	0.2	21.9	27.8	67.3
2003	7.3	2.6	1.6	0.1	0.1	0.0	0.0	0.0	0.0	0.6	40.9	28.6	81.9
2004	2.7	1.5	0.3	0.2	0.3	0.0	0.0	0.0	0.0	0.6	23.5	18.1	47.2
2005	4.3	3.3	1.5	0.6	0.2	0.0	0.0	0.0	0.0	0.3	33.5	24.2	68.0
2006	4.3	1.6	1.8	0.3	0.0	0.0	0.0	0.0	0.0	1.2	31.9	21.9	63.0
2007	5.9	2.8	2.9	0.6	0.2	0.0	0.0	0.0	0.0	0.1	23.1	26.5	62.1
2008	10.2	1.6	0.6	0.0	0.1	0.0	0.0	0.0	0.0	2.9	30.8	15.1	61.3
2009	3.2	1.0	2.5	0.1	0.1	0.0	0.0	0.0	0.0	1.4	28.9	9.7	46.7
2010	3.1	1.4	0.4	0.5	0.0	0.0	0.0	0.0	0.0	0.5	14.5	23.2	43.6
2011	4.9	2.9	1.1	0.2	0.0	0.0	0.0	0.0	0.0	0.9	18.3	15.3	43.7
2012	5.6	2.2	5.2	0.8	0.2	0.0	0.0	0.0	0.0	0.8	27.1	19.6	61.5
2013	3.1	1.5	2.6	0.8	0.3	0.0	0.0	0.0	0.0	2.5	22.1	17.2	50.2
2014	4.0	2.3	2.4	0.4	NaN	NaN	NaN	NaN	NaN	NaN	NaN	NaN	NaN

54

Table 12: Monthly percentage of burnt areas in Pariang.

Years	Jan	Feb	Mar	Apr	May	Jun	Jul	Aug	Sep	Oct	Nov	Dec	Total
2000	NaN	NaN	NaN	1.9	0.1	0.0	0.0	0.0	0.0	2.9	22.4	18.0	NaN
2001	14.6	8.7	2.5	1.6	0.4	NaN	0.0	0.0	0.0	0.3	18.8	18.8	65.7
2002	11.6	7.5	4.4	2.6	0.5	0.0	0.0	0.0	0.0	0.0	23.0	21.9	71.5
2003	10.0	7.1	2.7	0.8	0.7	0.0	0.0	0.0	0.0	1.5	26.4	24.3	73.5
2004	7.2	7.6	4.0	0.5	0.3	0.0	0.0	0.0	0.0	0.3	31.1	20.4	71.5
2005	8.6	3.3	4.2	0.6	0.4	0.0	0.0	0.0	0.0	0.4	33.8	18.3	69.7
2006	8.8	6.8	3.6	2.0	0.0	0.0	0.0	0.0	0.0	0.3	21.0	21.9	64.3
2007	12.1	10.7	4.2	1.5	0.3	0.0	0.0	0.0	0.0	0.0	10.1	20.3	59.1
2008	10.9	6.1	7.5	0.4	0.8	0.0	0.0	0.0	0.0	1.1	19.2	18.5	64.4
2009	12.5	7.4	3.4	1.1	1.5	0.2	0.0	0.0	0.0	0.3	27.8	15.3	69.5
2010	9.7	6.1	3.2	2.2	0.0	0.0	0.0	0.0	0.0	0.0	10.4	23.6	55.3
2011	13.4	10.8	5.8	2.9	0.7	0.1	0.0	0.0	0.0	0.1	23.3	13.5	70.6
2012	13.0	10.4	6.5	1.8	0.0	0.0	0.0	0.0	0.0	1.1	24.1	16.4	73.3
2013	15.4	5.6	5.1	2.5	0.1	0.1	0.0	0.0	0.0	0.0	8.4	19.9	57.0
2014	12.2	12.2	3.4	0.5	NaN	NaN	NaN	NaN	NaN	NaN	NaN	NaN	NaN

4.2.2   Spatiotemporal rainfall analysis

In the spatial domain, we illustrate for South Sudan the mean annual rainfall pattern, which represents the average rainfall during the timespan 1998-2014 (Fig. 52). Due to the coarse resolution of the TRMM 3B42 data (~30 km per pixel) we constrain the map representation to the national scale.

In the temporal domain, we analyze the average monthly rainfall distribution during the year as well as the annual variations of rainfall between 2000 and 2013 on the national, state and county level (Fig. 52 - Fig. 57).

South Sudan
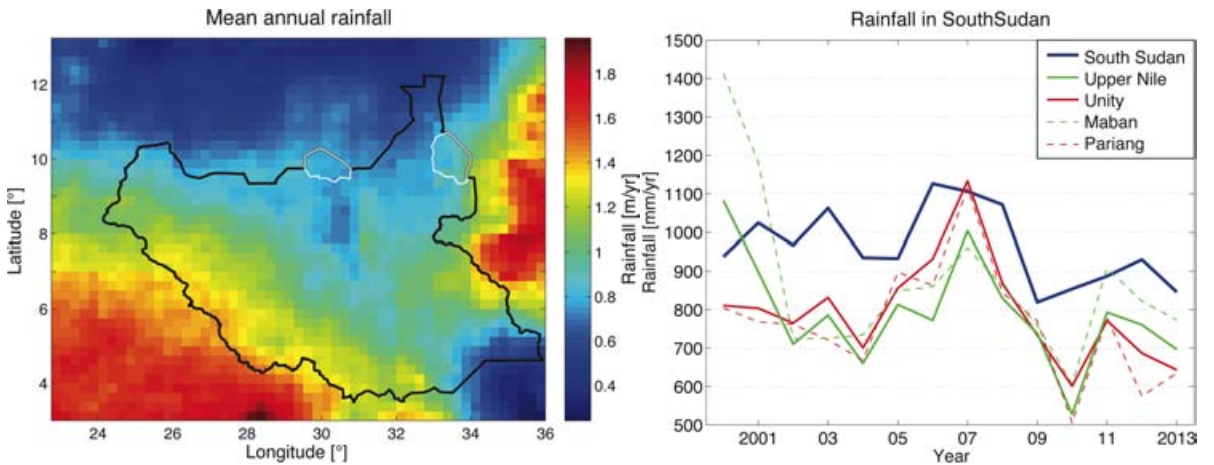
Fig. 52. (Left) Spatial distribution of rainfall mean annual rainfall amounts based on TRMM 3B42 data. (Right) Annual variations in rainfall amounts across South Sudan and the investigated subregions.

Notably, there is a pronounced rainfall depression of the Sudd wetland (northern central South Sudan), which may be associated with the microclimate of this region that is characterized by very high evaporation rates [*Mohamed and Savenije*, 2014]. Otherwise, rainfall magnitudes increase with increasing topography and decrease towards higher latitudes (Fig. 52). Annual rainfall in South Sudan over the time period 2000-2013 varies on average by 100 mm with annual mean of 964 mm (Fig. 52).

Furthermore, we illustrate the spatial distribution of the average peak rainfall event (Fig. 53). In other word, this map represents the time of the year, when highest rainfall magnitudes are most likely to occur. We calculated this temporal distribution based on a pixelwise weighted geometric average of rainfall magnitude time series with respect to their associated time of the year (Julian days). This map illustrates that peak rainfall events in the northern parts of the country occur on average one month later as compared to the southeastern parts of the country (Fig. 53). Annual rainfall in South Sudan has a pronounced seasonality with high rainfall magnitudes during June August and September with contrast little to no rainfall during December, January and February (Fig. 53).
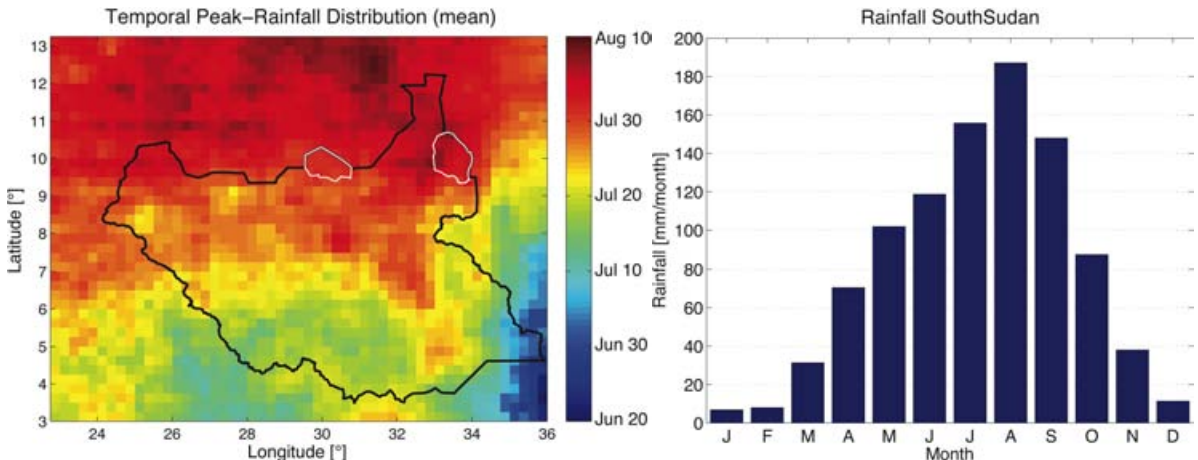
Fig. 53. (Left) Temporal distribution of peak rainfall amounts in South Sudan. (Right) Mean monthly rainfall amounts in South Sudan (1998-2014).

Upper Nile & Unity

In the states Upper Nile and Unity the monthly rainfall occurrences are temporally more confined to the rainfall season (May – October) as compared to larger regions, which integrate more rainfall events (Fig. 54). Average rainfall in Upper Nile with a mean annual magnitude of 791 ± 139 mm/yr is comparable to Unity with 796 ± 133 mm/yr.
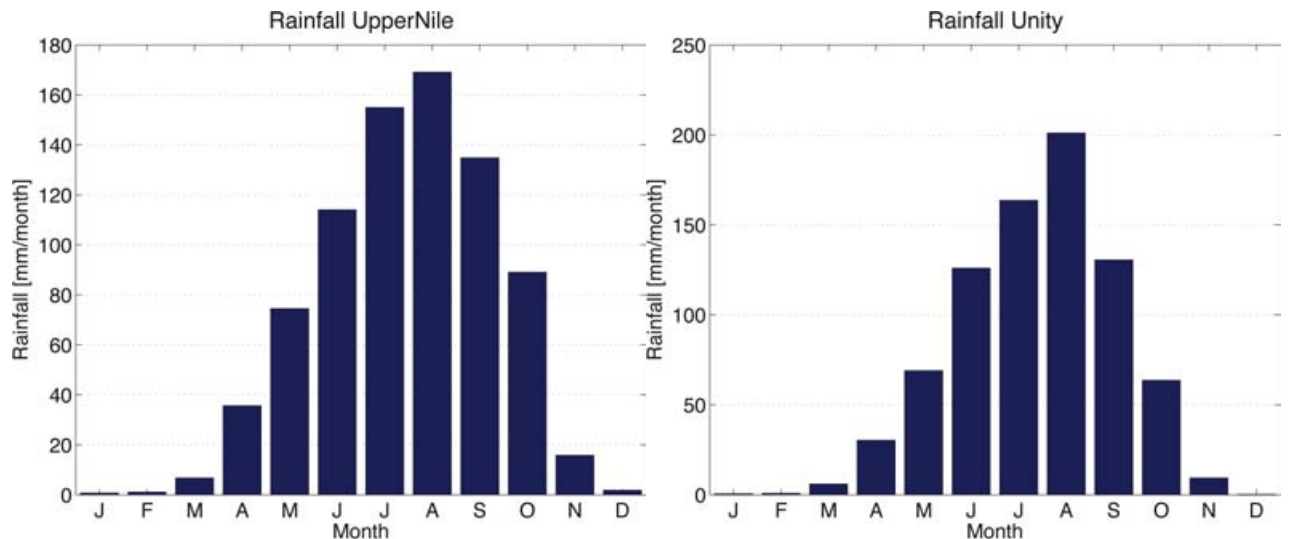
Fig. 54. Mean monthly rainfall amounts in Upper Nile (left) and Unity (right) States (1998-2014). Please, note the different rainfall magnitudes on both charts.

The temporal rainfall variations in both states are comparable with the exception of extremely high rainfall magnitudes in the Upper Nile state in 2000 (Fig. 55).
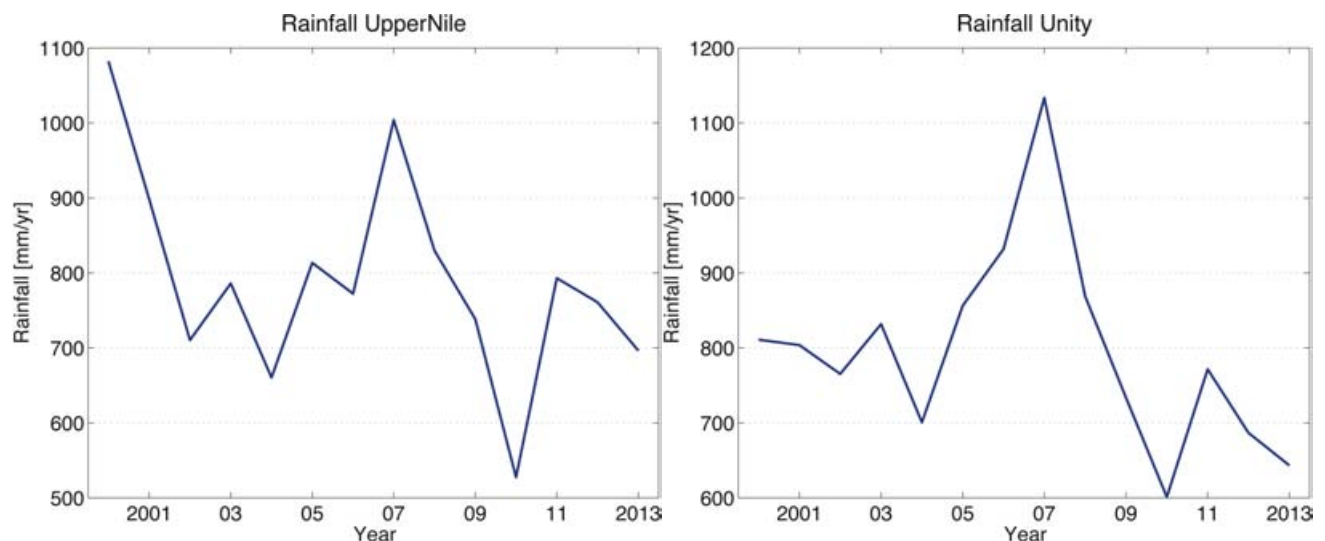
Fig. 55. Annual variations in rainfall amounts in Upper Nile (left) and Unity (right) States (1998-2014).

Maban & Pariang

Average rainfall in Maban with a mean annual magnitude of 870 ± 206 mm/yr is significantly higher as in Pariang with 765 ± 149 mm/yr (Fig. 56). These differences result from more rainfall during the build-up and retreat phase of the monsoon.

The annual rainfall variability varies in Maban between 600 mm/yr and 1400 mm/yr and in Pariang between 500 mm/yr and 1100 mm/yr, which highlights the large difference in water availability humans and ecosystems have to cope with.
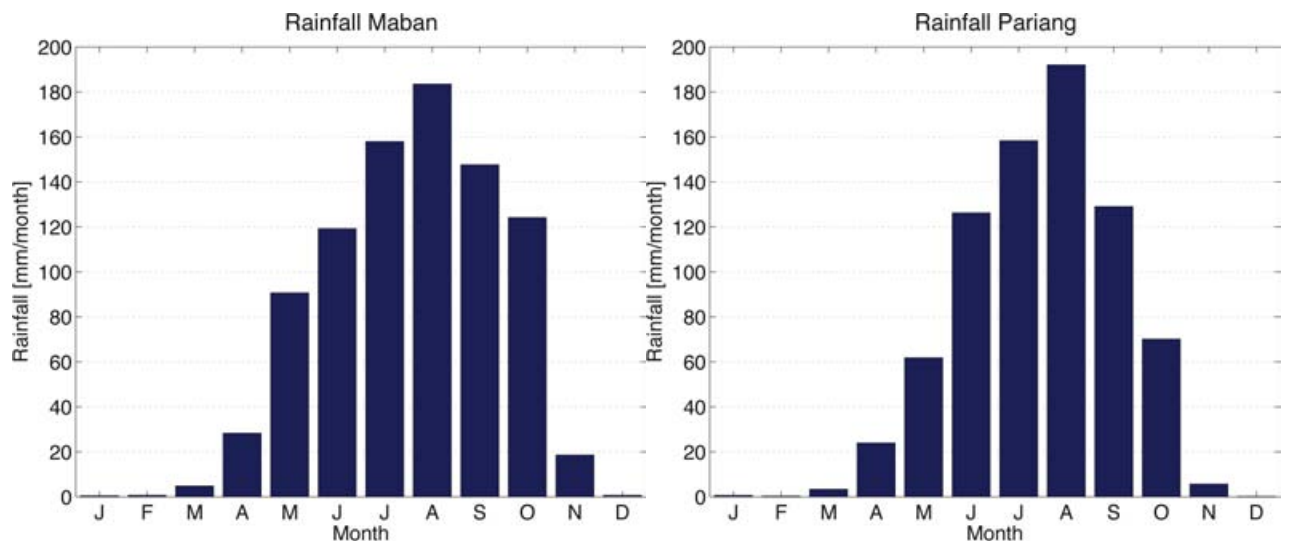
Fig. 56. Mean monthly rainfall amounts in Maban (left) and Pariang (right) County (1998-2014).
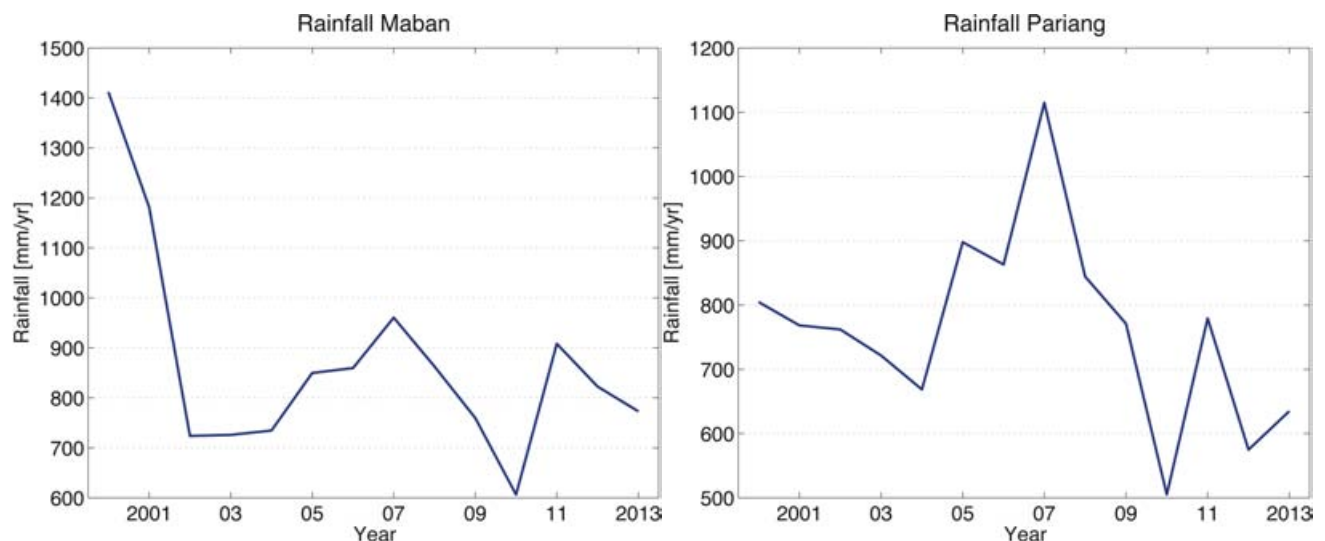
Fig. 57. Annual variations in rainfall amounts in Maban (left) and Pariang (right) County (2000-2013).

The following table provides annual information on the rainfall and dry-season duration, their respective rainfall amounts and the time of the Landsat acquisition periods (Table 13,

Year	First rainfall	Last rainfall	Rainfall season		Dry season		Total	Landsat acquisition period	
			Duration	Amount	Duration	Amount	Amount		
			[d]	[mm]	[d]	[mm]	[mm]		
1998	26-Apr	11-Nov	200	920.7	159	8.9	938.7	11-Dec	31-Dec
1999	19-Apr	23-Nov	219	935.4	132	12.9	942.1	23-Dec	12-Jan
2000	3-Apr	13-Nov	225	1281.3	142	27.7	1286.9	13-Dec	2-Jan
2001	4-Apr	2-Nov	213	1094.2	174	25.0	1103.5	2-Dec	22-Dec
2002	25-Apr	8-Nov	198	693.6	193	32.4	700.4	8-Dec	28-Dec
2003	20-May	10-Nov	175	716.6	148	11.7	737.2	10-Dec	30-Dec
2004	6-Apr	30-Oct	208	709.9	174	26.1	717.6	29-Nov	19-Dec

58

2005	22-Apr	23-Nov	216	835.0	159	11.5	838.5	23-Dec	12-Jar
2006	1-May	30-Oct	183	818.2	148	27.1	826.7	29-Nov	19-Dec
2007	27-Mar	12-Nov	231	935.1	147	7.1	941.5	12-Dec	1-Jar
2008	7-Apr	22-Oct	199	827.0	169	17.4	830.6	21-Nov	11-Dec
2009	9-Apr	1-Nov	207	725.6	183	13.7	731.1	1-Dec	21-Dec
2010	3-May	15-Nov	197	551.9	157	16.5	556.4	15-Dec	4-Jar
2011	21-Apr	16-Nov	210	894.7	148	7.8	897.4	16-Dec	5-Jar
2012	12-Apr	6-Nov	209	784.0	176	6.4	785.6	6-Dec	26-Dec
2013	1-May	7-Nov	191	715.6			720.9	7-Dec	27-Dec

Table 14). The dry season is assigned to the year in which it begins. We determined the onset and ending of the rainfall season, based on the County specific rainfall time series (e.g. Fig. 18). Our selection criteria for the onset and ending encompassed rainfall events larger than 2 mm with neighboring events (>2 mm) within ten days.

Table 13: Onset and ending of the rainfall and dry seasons with their respective rainfall amounts in Maban.

Year	First rainfall	Last rainfall	Rainfall season		Dry season		Total	Landsat acquisition period	
			Duration	Amount	Duration	Amount	Amount		
			[d]	[mm]	[d]	[mm]	[mm]		
1998	26-Apr	11-Nov	200	920.7	159	8.9	938.7	11-Dec	31-Dec
1999	19-Apr	23-Nov	219	935.4	132	12.9	942.1	23-Dec	12-Jar
2000	3-Apr	13-Nov	225	1281.3	142	27.7	1286.9	13-Dec	2-Jar
2001	4-Apr	2-Nov	213	1094.2	174	25.0	1103.5	2-Dec	22-Dec
2002	25-Apr	8-Nov	198	693.6	193	32.4	700.4	8-Dec	28-Dec
2003	20-May	10-Nov	175	716.6	148	11.7	737.2	10-Dec	30-Dec
2004	6-Apr	30-Oct	208	709.9	174	26.1	717.6	29-Nov	19-Dec
2005	22-Apr	23-Nov	216	835.0	159	11.5	838.5	23-Dec	12-Jar
2006	1-May	30-Oct	183	818.2	148	27.1	826.7	29-Nov	19-Dec
2007	27-Mar	12-Nov	231	935.1	147	7.1	941.5	12-Dec	1-Jar
2008	7-Apr	22-Oct	199	827.0	169	17.4	830.6	21-Nov	11-Dec
2009	9-Apr	1-Nov	207	725.6	183	13.7	731.1	1-Dec	21-Dec
2010	3-May	15-Nov	197	551.9	157	16.5	556.4	15-Dec	4-Jar
2011	21-Apr	16-Nov	210	894.7	148	7.8	897.4	16-Dec	5-Jar
2012	12-Apr	6-Nov	209	784.0	176	6.4	785.6	6-Dec	26-Dec
2013	1-May	7-Nov	191	715.6			720.9	7-Dec	27-Dec

Table 14: Onset and ending of the rainfall and dry seasons with their respective rainfall amounts in Pariang.

Year	First rainfall	Last rainfall	Rainfall season		Dry season		Total	Landsat acquisition period
			Duration	Amount	Duration	Amount	Amount	

			[d]	[mm]	[d]	[mm]	[mm]		
1998	17-Mar	27-Oct	225	818.0	172	9.3	820.9	26-Nov	16-Dec
1999	17-Apr	20-Oct	187	878.8	171	26.0	888.0	19-Nov	9-Dec
2000	8-Apr	23-Oct	199	779.9	163	33.9	790.7	22-Nov	12-Dec
2001	4-Apr	27-Oct	207	790.0	200	35.1	793.4	26-Nov	16-Dec
2002	15-May	12-Nov	182	753.2	193	20.5	775.7	12-Dec	1-Jan
2003	24-May	10-Nov	171	701.8	147	7.3	710.9	10-Dec	30-Dec
2004	5-Apr	27-Oct	206	676.8	177	24.0	680.5	26-Nov	16-Dec
2005	22-Apr	28-Oct	190	849.6	186	17.2	851.2	27-Nov	17-Dec
2006	2-May	31-Oct	183	808.2	159	5.9	811.9	30-Nov	20-Dec
2007	8-Apr	10-Nov	217	1113.8	148	8.1	1116.2	10-Dec	30-Dec
2008	6-Apr	22-Oct	200	813.9	171	12.4	816.3	21-Nov	11-Dec
2009	11-Apr	2-Nov	206	734.5	170	16.1	741.6	2-Dec	22-Dec
2010	21-Apr	14-Nov	208	496.3	167	6.1	507.3	14-Dec	3-Jan
2011	30-Apr	23-Oct	177	782.6	172	7.2	784.5	22-Nov	12-Dec
2012	12-Apr	5-Nov	208	594.3	179	16.8	596.1	5-Dec	25-Dec
2013	3-May	24-Oct	175	624.4			627.4	23-Nov	13-Dec

4.2.3 Spatiotemporal analysis on burnt area vs. rainfall

In this subsection, we explore links between rainfall characteristics (seasonal rainfall magnitudes and duration) and burnt areas in Maban and Pariang. Our analysis focuses on these counties only to avoid spatial averaging effects, which would affect larger areas on the state and national level.

First, we explore the relation between rainfall (Jan.-Dec.) and burnt areas (Aug.-Jul.) (Fig. 58). As revealed in the previous sections (4.2.1 and 4.2.2), rainfall is predominantly confined to the rainfall season, whereas burning starts in the subsequent dry season. We assign the fire season to the year in which it begins.
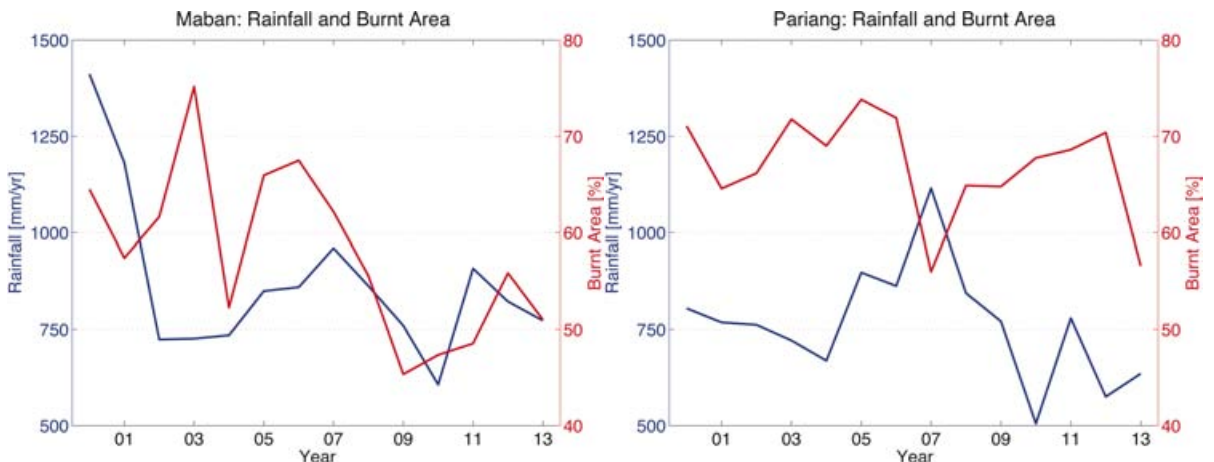
Fig. 58. Annual variations of rainfall and burnt areas in Maban (left) and Pariang (right) from 2000 to 2013.

Based on annual variation (Fig. 58) and regression analysis (Fig. 59) there is no significant trend between annual rainfall magnitudes and burnt areas. Rainfall magnitudes seem to have no first-order impact on the amount of burnt areas in the

subsequent dry season. Presumably rainfall may contribute to the fire hazard by increasing the amount of available biomass (grasses) and prohibit fire spread increasing soil moisture.
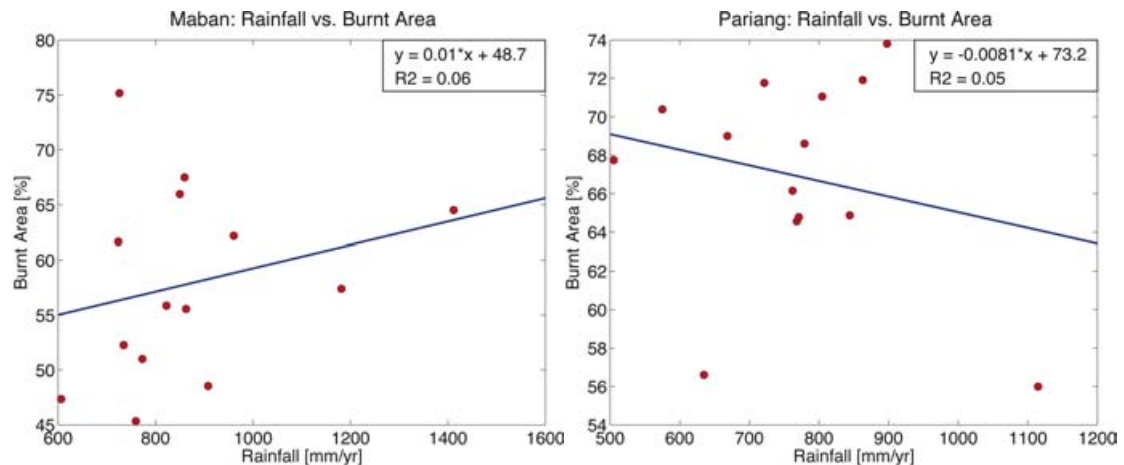
Fig. 59. Regression analysis of annual variations between rainfall and burnt areas in Maban (left) and Pariang (right).

This hypothesis is further supported by the analysis of dry-season rainfall and burnt areas, which similarly reveals no significant relations.
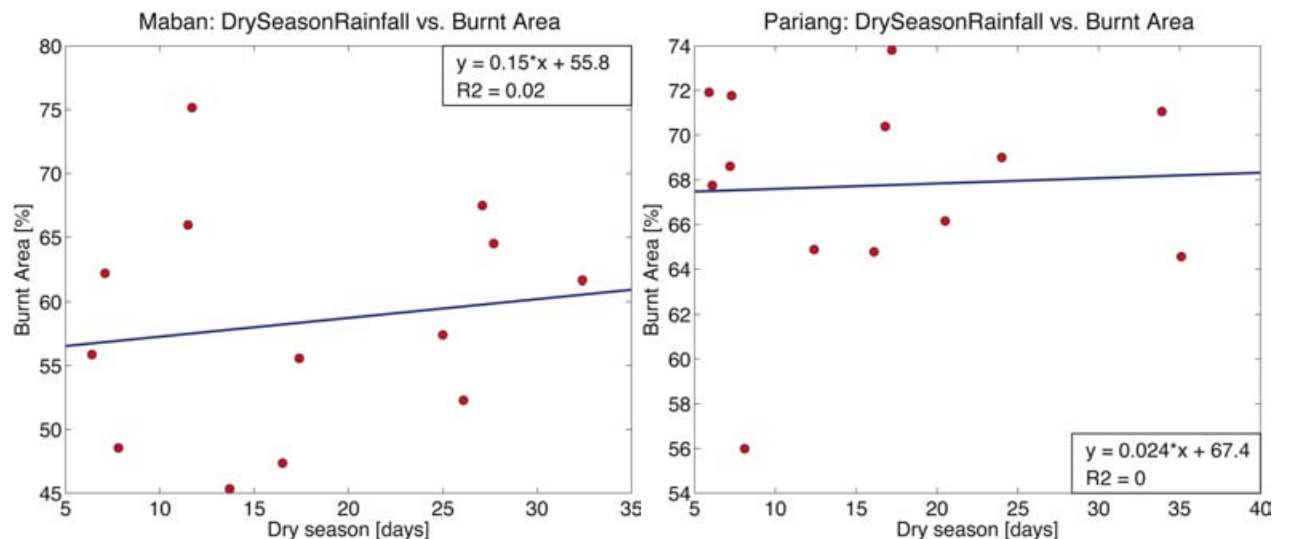
Fig. 60. Regression analysis of annual variations between dry-season rainfall and burnt areas in Maban (left) and Pariang (right).

Further regression analysis between the dry and rainfall season duration and the burnt areas also reveal no significant relationship (Fig. 61 and Fig. 62).
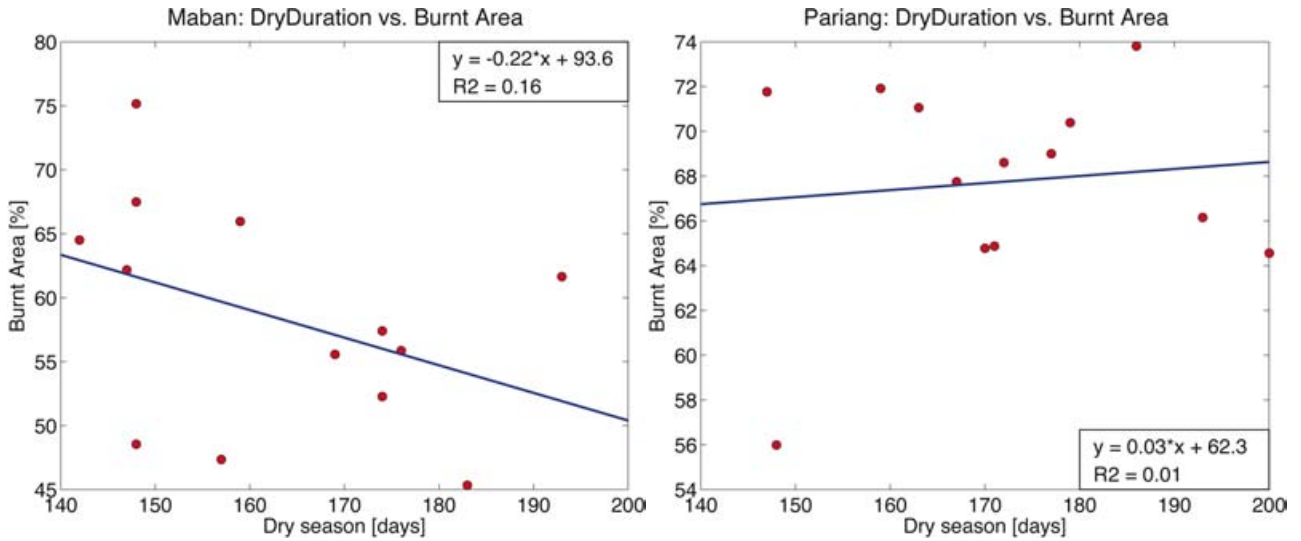
Fig. 61. Regression analysis of annual variations between dry-season duration and burnt areas in Maban (left) and Pariang (right).
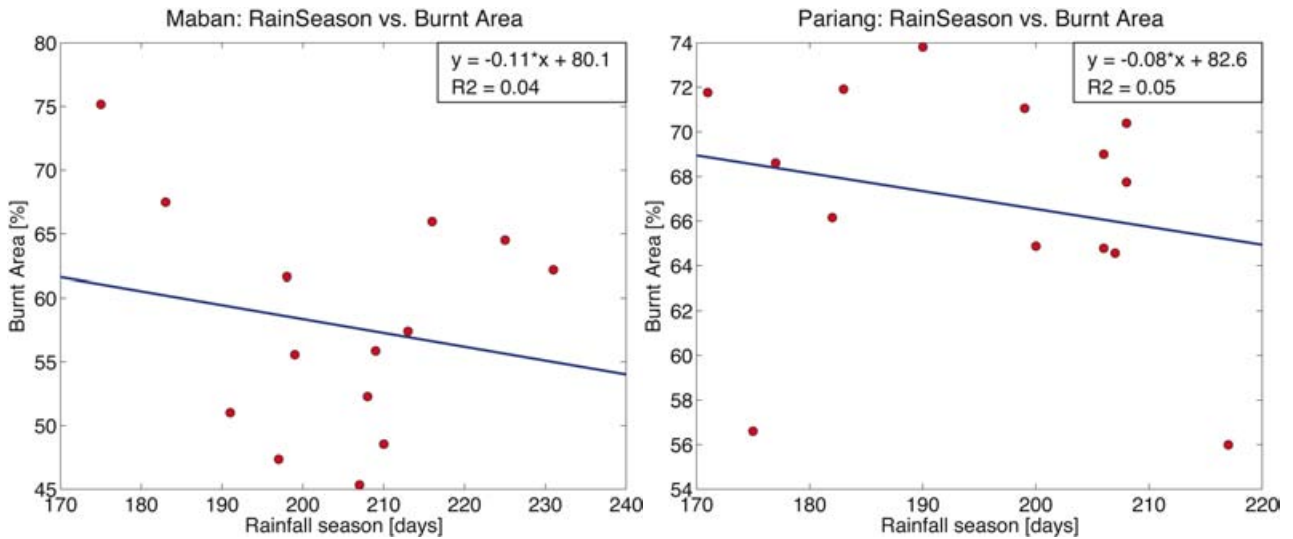
Fig. 62. Regression analysis of annual variations between rainfall season duration and burnt areas in Maban (left) and Pariang (right).

Apart of the above multi-month analysis we also investigated the relation of burnt areas and rainfall/no rainfall days during the onset of the dry season (Oct.-Nov.) (Fig. 63). However, this temporally confined analysis also revealed no conclusive relationship.
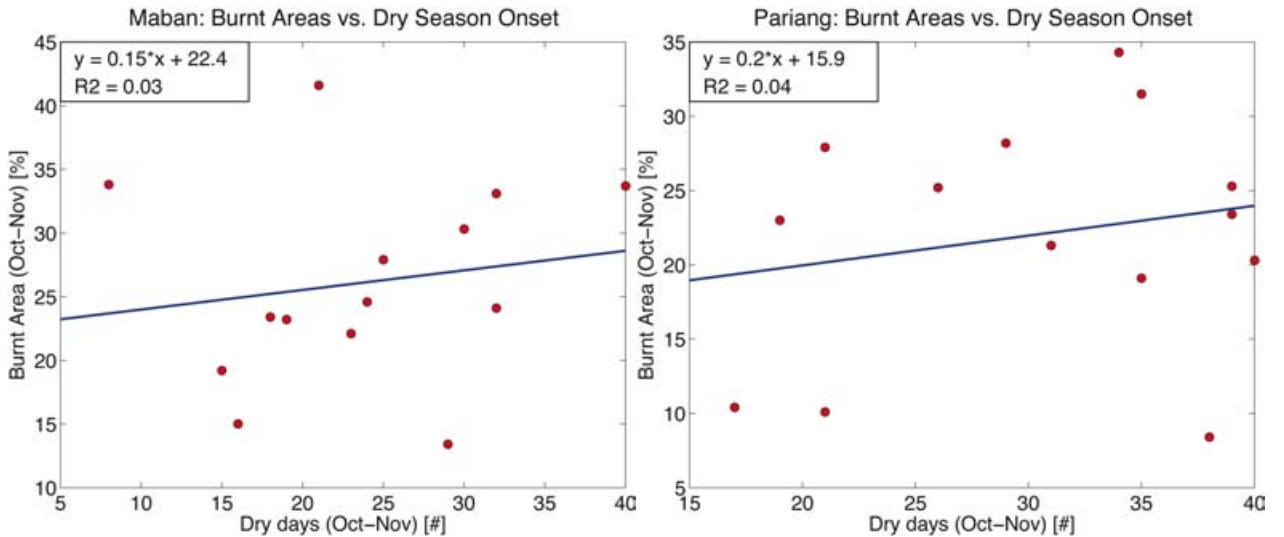
Fig. 63. Regression analysis of variations between dry days in the period October to November and the burnt areas in Maban (left) and Pariang (right) during that period.

As no single factor (seasonal duration and rainfall magnitude) seems to have a first order impact on the annual amount of burnt areas, we also analyzed their combined effect in multiple linear regression analysis. However, the R2 statistic (0.29, 0.23) as well as the F statistic (1.21, 0.91) and its p value (0.35, 0.47) indicate no significant relation for Maban and Pariang, respectively.

These non-existing relationships let us conclude that rainfall is not a first-order driving factor to explain annual variations of rainfall. Potentially, more direct variables, like soil moisture or wind speed, may yield better relationships. Although fire activities clearly start after the onset of the dry period, we cannot find a close relation between the amount of burnt area and the number of burning days at the beginning of the dry season (Oct. – Nov.). These non-existing relations may suggest that the human influence in fire regime patterns is rather random and hard to be explained by rainfall magnitudes and distributions only.
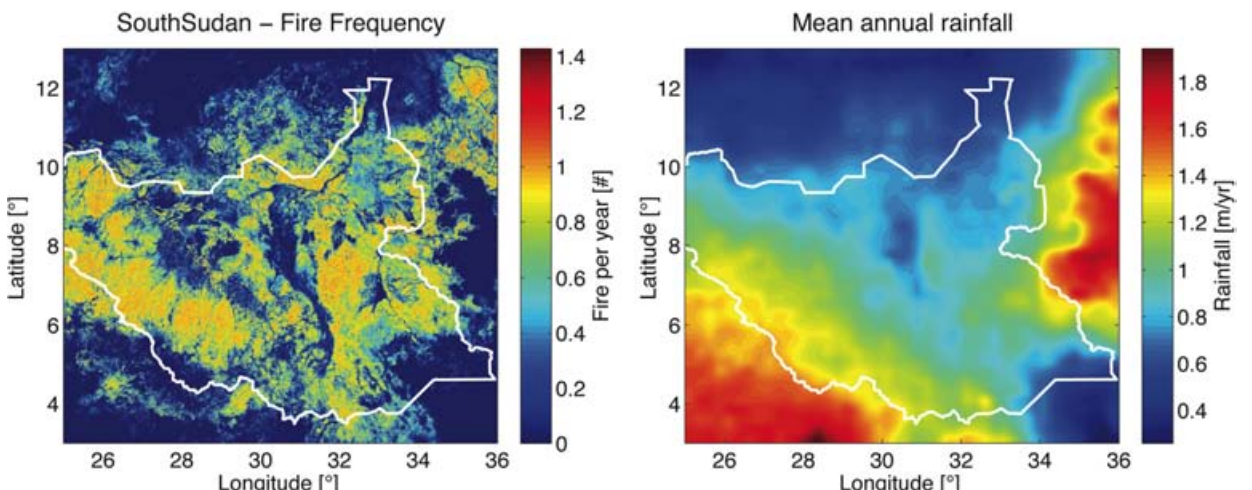
Fig. 64. Visual comparison of fire frequencies (left) and mean annual rainfall (right) in South Sudan.

In a spatial analysis of rainfall magnitudes and fire occurrences, we find a first order relationship between both variables (Fig. 64). Areas of pronounced rainfall in the bordering regions of South Sudan appear to be too wet to support fire propagation,

63

whereas areas with too little rainfall do not accumulate enough biomass (grasses) for extended fires. The direct comparison of spatial rainfall distribution and fire occurrences indicates an optimal rainfall magnitude range that supports fire spread between 0.6 to 1.4 m/yr (Fig. 65).
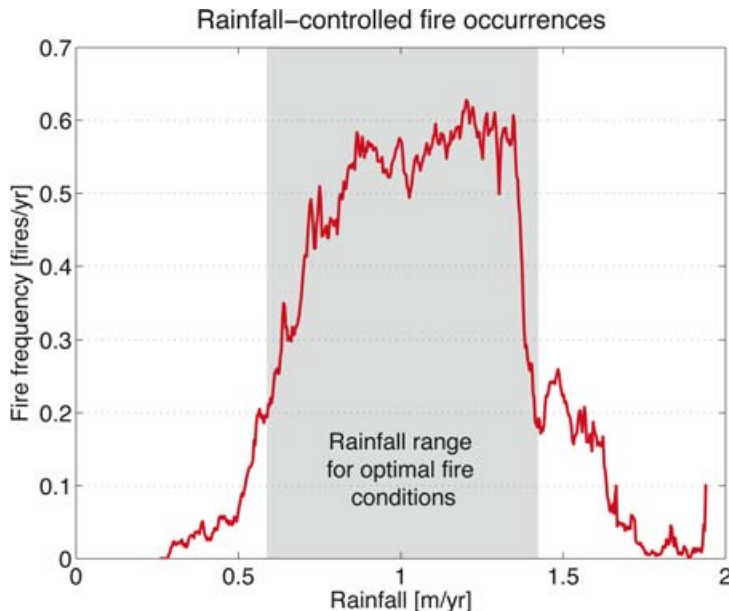
Fig. 65. Relation of fire frequencies in dependence of mean annual rainfall.

4.2.4   Spatial analysis on burnt area vs. land cover

In this subsection, we explore links between landcover (africover dataset) and burnt areas in South Sudan, Maban and Pariang.

South Sudan
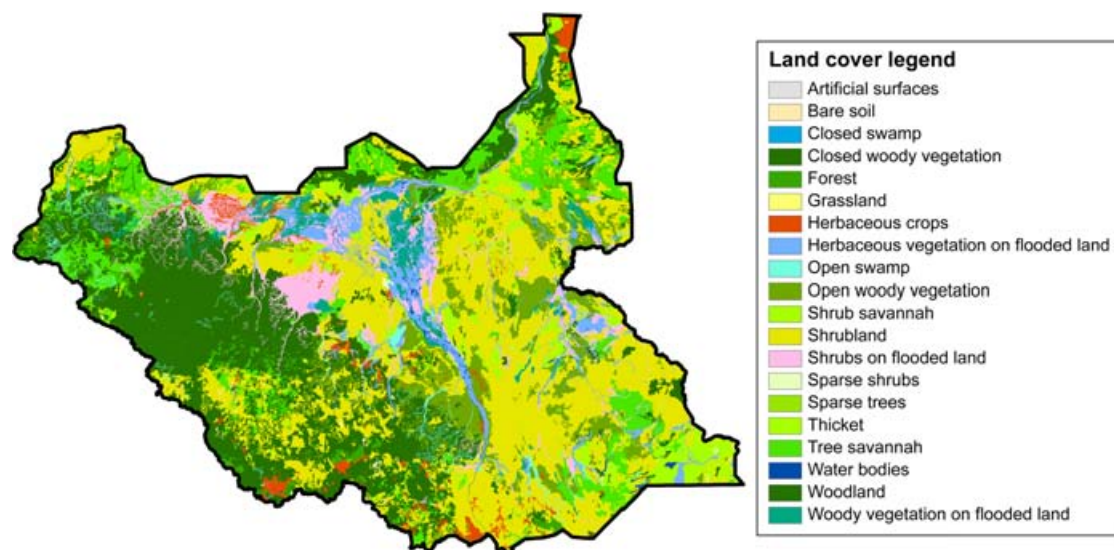
Fig. 66. Land cover in South Sudan based on the "africover" dataset.

On the national scale it becomes apparent that wetlands are much less often affected by fires, as compared to more common land cover classes like tree and shrub savanna and woodlands. If wetlands are affected by fire, these fires occur late in the dry season

(Fig. 66, Fig. 67). A similar pattern can be observed for watercourses. Furthermore, fires frequently affect the widespread land cover types, like shrublands and woodlands, which account for about 60% areal coverage.
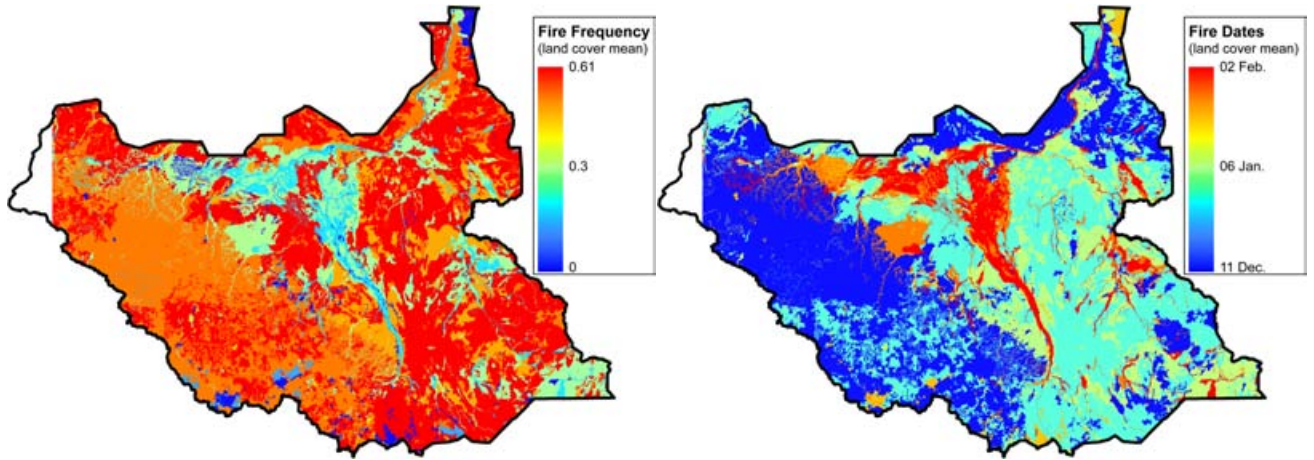
Fig. 67. (Left) Mean annual fire frequency of the respective land cover classes in South Sudan, representing the average number of fires per year and class. (Right) Mean annual temporal fire distribution of the respective land cover classes in South Sudan, representing the average timing of fires during the year of each class.

The fire frequency in various types of land cover is quite heterogeneous indicated by the high standard deviation of about 0.3 in the larger widespread classes. The same effect can be observed for the temporal fire distribution. Nevertheless, some general trends can be observed: (a) urban and frequently flooded land cover types are hardly affected by fires; (b) the frequently burnt areas (frequency > 0.5 fire per year) account for almost 80% of the total area; (c) fires tend to occur more often in densely vegetated regions as compared to less dense vegetation region, with the exception of forests (Table 15). Dense forests presumably lack the grass layer that supports fire spread.

Table 15: Statistics (mean, standard deviation (std) and occurrence) on fire frequency and temporal distribution of fire (Fire Julian Day) by land cover class in South Sudan. Note that differences in areal coverage in both analyses (fire frequency & temporal distribution) are due to different distributions of "no data" values.

Land cover	Fire Frequency		Area	Area	Fire Julian Day		Area	Area
	MEAN	STD	%	km^2	MEAN	STD	%	km^2
Tree savannah	0.61	0.32	10.2	66927	355	25.6	10.6	61259
Shrubland	0.61	0.30	33.9	223143	5	23.1	35.9	206791
Woodland	0.55	0.33	26.3	173296	355	21.2	27.3	156984
Open woody vegetation	0.52	0.33	7.7	50481	10	24.8	7.8	45095
Closed woody vegetation	0.49	0.28	0.1	443	355	20.2	0.1	433
Thicket	0.46	0.29	0.1	344	15	26.5	0.1	329
Sparse trees	0.46	0.28	0.0	294	345	27.3	0.0	280
Grassland	0.39	0.39	0.1	585	356	38.2	0.1	397
Open swamp	0.39	0.30	0.8	5290	11	35.2	0.8	4401

Shrubs on flooded land	0.39	0.31	4.9	32534	23	35.7	4.6	26223
Shrub savannah	0.38	0.35	5.8	37872	10	33.8	4.6	26261
Woody vegetation on flooded land	0.37	0.31	2.3	14980	33	39.8	2.1	12295
Bare soil	0.36	0.33	0.1	754	356	22.3	0.1	601
Herbaceous vegetation on flooded land	0.30	0.30	4.8	31802	29	37.5	4.2	24015
Sparse shrubs	0.28	0.30	0.1	600	21	44.7	0.1	367
Forest	0.27	0.34	0.6	4251	4	14.3	0.4	2059
Herbaceous crops	0.17	0.23	1.9	12732	19	40.4	1.3	7459
Artificial surfaces	0.04	0.12	0.0	99	353	34.7	0.0	22
Water bodies	0.04	0.10	0.2	1607	33	41.3	0.1	418
Closed swamp	0.00	0.03	0.0	35	14	4.8	0.0	1

Maban
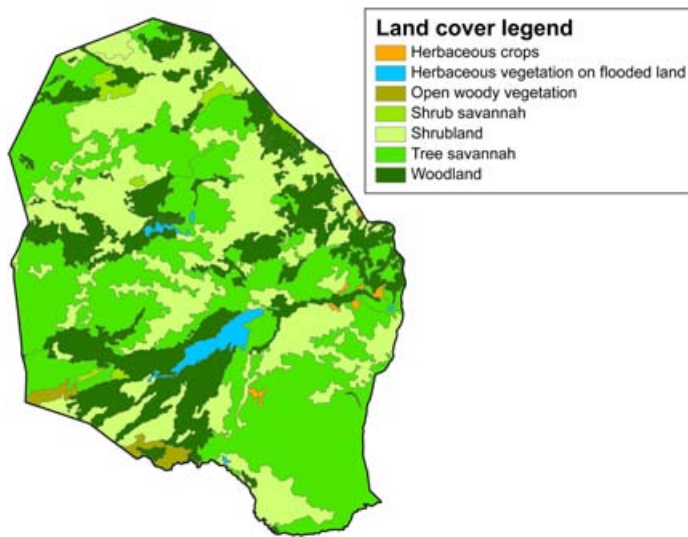
Fig. 68. Land cover in Maban based on the "africover" dataset.

Similar to Pariang, wetlands in Maban are much less affected by fires, which may occur late in the dry season (Fig. 68, Fig. 69).
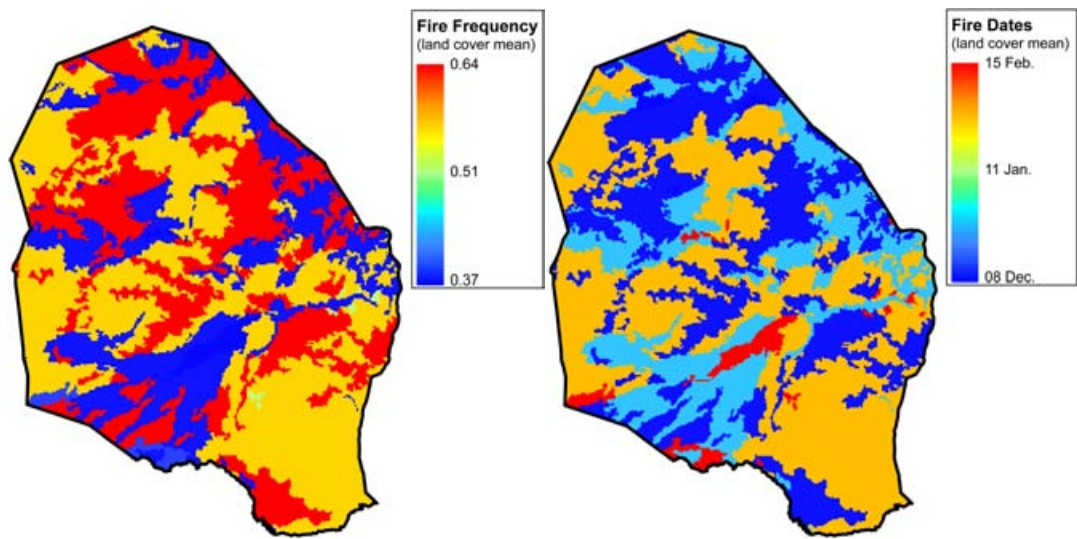
Fig. 69. (Left) Mean annual fire frequency of the respective land cover classes in Maban, representing the average number of fires per year and class. (Right) Mean annual temporal fire distribution of the respective land cover classes in Maban, representing the average timing of fires during the year of each class.

Repeatedly, shrubland and shrub/tree savanna classes are most affected by fires, which along with woodlands account for more than 90% of the area in Maban (Fig. 70, Table 16).

Table 16: Statistics (mean, standard deviation (std) and occurrence) on fire frequency and temporal distribution of fire (Fire Julian Day) by land cover class in Maban. Note that differences in areal coverage in both analyses (fire frequency & temporal distribution) are due to different distributions of "no data" values.

Land cover	Fire Frequency		Area	Area	Fire Julian Day		Area	Area
	MEAN	STD	%	km^2	MEAN	STD	%	km^2
Shrub savannah	0.64	0.27	1.2	157	342.4	14.4	1.2	154
Shrubland	0.62	0.23	31.9	4047	343.5	17.7	32.2	4009
Tree savannah	0.59	0.24	42.0	5325	350.3	18.5	42.6	5295
Herbaceous crops	0.57	0.18	0.3	40	355.1	17.2	0.3	40
Open woody vegetation	0.52	0.22	1.0	132	352.4	10.5	1.1	132
Woodland	0.51	0.29	22.1	2797	345.8	23.8	21.1	2624
Herbaceous vegetation on flooded land	0.39	0.24	1.5	186	46.3	22.5	1.4	180
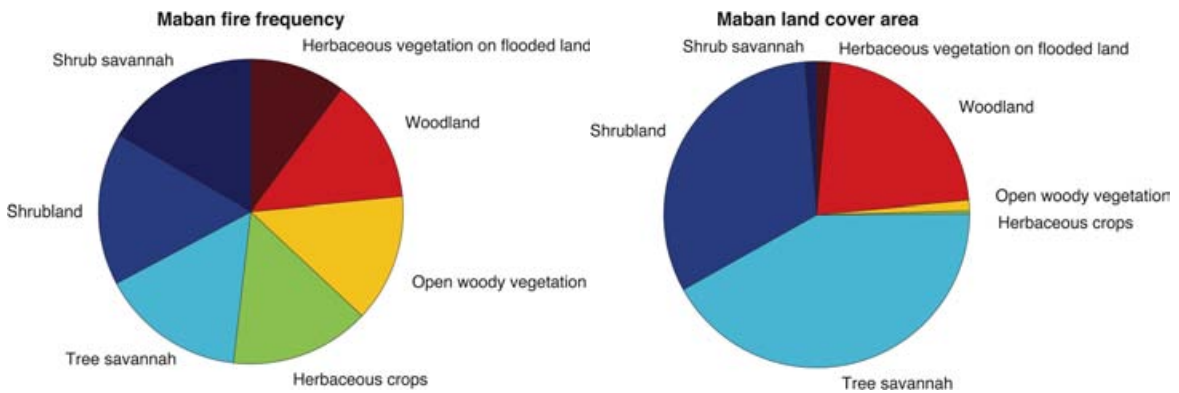
Fig. 70. Pie chart representing the fire frequency (left) and areal partitioning (right) of land cover classes in Maban.

Pariang
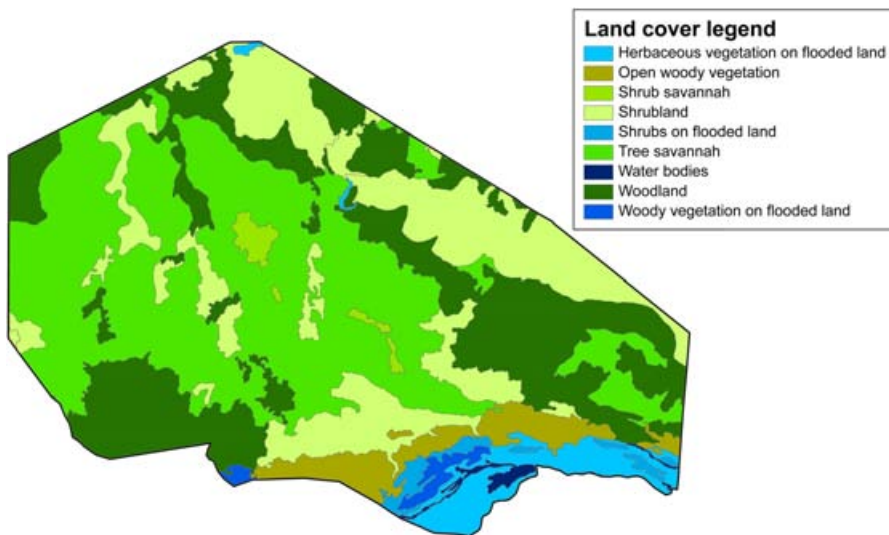
Fig. 71. Land cover in Pariang based on the "africover" dataset.

More apparent than on the national scale, we can observe in Pariang that wetlands are much less affected by fires, which eventually may occur late in the dry season (Fig. 71 and Fig. 72).

Most fires occur in shrublands and tree savannas. Similarly woodlands area heavily affected. All three classes account for more that 80% of the County area (Fig. 73 and Table 17).

Table 17: Statistics (mean, standard deviation (std) and occurrence) on fire frequency and temporal distribution of fire (Fire Julian Day) by land cover class in Pariang. Note that differences in areal coverage in both analyses (fire frequency & temporal distribution) are due to different distributions of "no data" values.

Land cover	Fire Frequency		Area	Area	Fire Julian Day		Area	Area
	MEAN	STD	%	km²	MEAN	STD	%	km²
Shrubland	0.76	0.21	21.8	2070	359.5	30.5	22.6	2061
Tree savannah	0.72	0.24	39.7	3772	363.6	28.0	41.1	3749
Open woody vegetation	0.66	0.22	4.5	429	25.1	25.4	4.7	426
Woodland	0.66	0.30	26.3	2498	357.4	24.1	26.6	2432
Shrub savannah	0.55	0.24	1.0	94	336.9	22.1	1.0	92
Shrubs on flooded land	0.28	0.23	1.2	113	73.8	19.9	0.9	84
Herbaceous vegetation on flooded land	0.16	0.18	4.2	398	67.5	25.4	2.7	246
Woody vegetation on flooded land	0.14	0.24	0.9	85	44.3	34.3	0.3	28
Water bodies	0.04	0.11	0.6	55	44.2	34.0	0.1	13
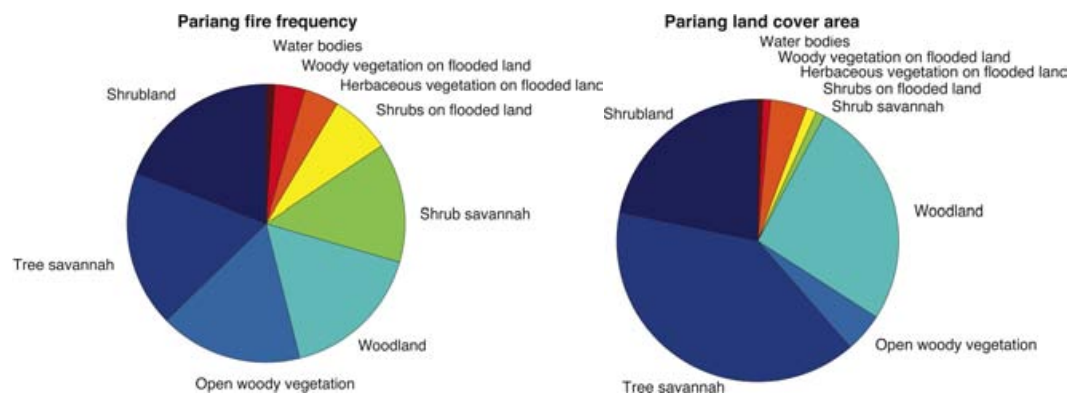
**Fig. 73. Pie chart representing the fire frequency (left) and areal partitioning (right) of land cover classes in Pariang.**

# 5. Conclusions and Recommendations

With respect to the "*forest monitoring*" project, we achieved our aims to extract various data products on vegetation cover and tree species to generate a vegetation map for the Counties of Maban and Pariang in South Sudan. Furthermore, we quantified vegetation changes in both counties with a focus on refugee camps to illustrate changes in canopy cover that are related to the arrival of refugees in 2011. During this project, we developed sophisticated methodologies for the generation of each data product. These methodologies combine remote sensing and ground truthing data, utilize different remote sensing approaches (e.g. spectral reflectance indices, data classification), exploit sensor synergies (i.e. Landsat, WorldView-2) and build upon local expert knowledge. The profound expertise on complex local vegetation conditions by Dr. Urs Bloesch was indispensible for data interpretation. Despite multiple challenges, like (i) profound landscape alteration by fires, (ii) extreme cloud cover conditions during the rainy season (iii) very high-resolution data availability, and consequently (iv) the need for multiple Landsat datasets with time-intensive pre- and post-processing needs, the outcome and quality of the results is remarkable. In retrospect, we gained valuable operating experience for potential future projects alike this.

For the vegetation cover products, we used different adapted approaches for WorldView-2 and Landsat data to generate vegetation masks and vegetation surface cover products. Based on WorldView-2 data, we first detected green vegetation based on a field data optimized NDVI threshold. Second, we identified dry vegetation based on the most efficient SVM image classification algorithm. We downscaled this high-resolution vegetation mask to yield canopy cover information on the hectare scale. The vegetation mask for both counties is based on specific timing of Landsat acquisitions after the onset of the dry season, detected by TRMM 3B42 satellite information, in order to distinguish between dried up grasslands and shrub/tree vegetation. Exploiting the linear relation between Landsat NDVI and WorldView-2 canopy cover, we converted the NDVI of selected Landsat acquisitions to canopy cover data on a 30 m and 100 m spatial scale. The comparison and validation of both vegetation cover products with ground observations yield reasonable results with R^2 values about 0.45 to 0.5. It should be noted that extended wetlands along major rivers are misclassified as woodlands based on this approach.

For the tree species products, we distinguished between the Red acacia (Acacia seyal), the Desert date tree (Balanites aegyptiaca), the Doum palm (Hyphaene thebaica, only in Maban), and the Silak (Anogeissus leiocarpus), which form virtually monospecific vegetation units. The classification in Maban is based on an extended calibration and validation dataset, to train and validate the supervised classification approach that yielded an overall accuracy of 62.6%. The lower ground data and WorldView-2 data availability in Pariang facilitated simply a supervised classification approach without validation. Classification of WorldView-2 data is based on

pixelwise tree species spectra, rather than regional spectra as used for the Landsat data classification.

For the vegetation map products, we combine the vegetation classes and vegetation species. Based on the canopy cover percentages, we distinguish between grassland, shrub/tree savanna, savanna woodland, and woodland vegetation classes. The latter two classes are further divided into subclasses by their tree species composition. Furthermore, we distinguish riverine forests that mark a densely vegetated 100 m wide belt to each side of watercourses and mixed savanna woodlands and mixed woodlands that exhibit less than 70% of a pure stand (?). Spatial data on watercourses, roads, settlements and refugee camps derive from *OpenStreetMap* and *UNITAR.*

For the vegetation dynamics products, we used two approaches to assess (i) vegetation changes using all-season NDVI data and compared selected annual data clusters and (ii) forest changes using the selected annual Landsat data at the onset of the dry season to exclude grasslands from shrub/tree vegetation. Both approaches indicate vegetation reductions within and in the surroundings of refugee camps, which generally decrease with increasing distance from the refugee camps.

The analysis of the fire regime indicated that substantial areas of South Sudan (52.8%), Upper Nile (52.6%), Unity (51.7%), Maban (57.9%), and Pariang (67.0%) get burnt on average each year. We analyzed the spatial and temporal distribution of fires and investigated potential relationships with rainfall characteristics (seasonal rainfall magnitudes and duration). Multiple linear regression analysis did not reveal significant links between both variables in Maban and Pariang, supporting the argument of a random human influence or fire spread. However, optimal fire spread conditions appear to be limited to climatic zones with annual rainfall ranging between 0.6 and 1.4 m/yr. The subsequent analysis of burnt areas in relation with land cover types revealed that (a) urban and frequently flooded land cover types are hardly affected by fires, (b) the frequently burnt areas (frequency > 0.5 fire per year) account for almost 80% of the total area; (c) fires tend to occur more often in densely vegetated regions as compared to less dense vegetated regions, with the exception of forests.

Some recommendations to optimize the workflow for potential future projects on forest monitoring and fire regime analysis in South Sudan include:

Forest monitoring

- Multi-seasonal very-high-resolution WorldView-2 imagery of seamless cloud-free acquisitions at the beginning and end of the dry season (Dec., Apr.) provides best means to spectrally distinguish between different tree species.
- In addition to supervised classification, further object-based classification approaches should be included for tree species identification with very high-resolution imagery.

- Multi-annual very-high-resolution WorldView-2 imagery acquisitions at the beginning of the dry season before and after the refugee influx should be used to detect vegetation changes within and around refugee camps.
- Multiple (20-30) training and validation sites (accurately located by a differential GPS) should be surveyed at the same seasonal time (or same time) as the satellite imagery acquisitions.
- More time should be allocated to refine the supervised classification approach and to analyze sources of misclassifications and uncertainties.
- Upcoming multispectral Sentinel-2 data (end of 2015) may provide better means to spectrally distinguish between shrub/tree savannas and grasslands on the County to State level.

Fire regime

- Complementary to rainfall, data analysis of soil moisture (recent SMOS or upcoming SMAP satellite mission), weather variability (wind speed) and human activates (e.g., civil wars, nomad migrations) might be helpful to explain annual variations in fire extent. Further analysis on the impact of rainfall magnitudes on available biomass (grasses) should provide additional information on potential causal rainfall-fire relations.

References

Asner, G. P. (1998), Biophysical and biochemical sources of variability in canopy reflectance, *Remote sensing of environment*, *64*(3), 234-253.

Bloesch, U. (2014), Forest mapping and pre-inventory of the Sudanese refugee hosting areas in Maban and Pariang counties, South Sudan (24 April – 12 May 2014)*Rep.*, 1-34 pp, UNHCR/SDC, Berne.

Bloesch, U., A. Schneider, and C. Lino (2013), Towards an environmental strategy for Sudanese refugee hosting areas in Upper Nile and Unity States, South Sudan*Rep.*, 1-46 pp, UNHCR/SDC, Berne.

ENVI (2014), Calibrating Images Tutorial, online resource, last webpage visit in December 2014: http://www.exelisvis.com/docs/CalibratingImagesTutorial.html.

Huffman, G. J., R. F. Adler, D. T. Bolvin, G. Gu, E. J. Nelkin, K. P. Bowman, Y. Hong, E. F. Stocker, and D. B. Wolff (2007), The TRMM Multisatellite Precipitation Analysis (TMPA): Quasi-Global, Multiyear, Combined-Sensor Precipitation Estimates at Fine Scales, *Journal of Hydrometeorology*, *8*(1), 38-38.

Kalensky, Z. D. (1998), AFRICOVER Land Cover Database and Map of Africa, *Canadian journal of remote sensing*, *24*(3), 292-297.

Mohamed, Y., and H. H. G. Savenije (2014), Impact of climate variability on the hydrology of the Sudd wetland: Signals derived from long term (1900-2000) water balance computations, *Wetl Ecol Manag*, *22*(2), 191-198.

Myneni, R. B., F. G. Hall, P. J. Sellers, and A. L. Marshak (1995), The interpretation of spectral vegetation indexes, *Geoscience and Remote Sensing, IEEE Transactions on*, *33*(2), 481-486. doi:10.1109/36.377948.

Roy, D. P., and L. Boschetti (2009), Southern Africa validation of the MODIS, L3JRC, and GlobCarbon burned-area products, *IEEE transactions on geoscience and remote sensing*, *47*(4), 1032-1044.

Roy, D. P., P. E. Lewis, and C. O. Justice (2002), Burned area mapping using multi-temporal moderate spatial resolution data-a bi-directional reflectance model-based expectation approach, *Remote sensing of environment*, *83*(1-2), 263-286.

Roy, D. P., Y. Jin, P. E. Lewis, and C. O. Justice (2005), Prototyping a global algorithm for systematic fire-affected area mapping using MODIS time series data, *Remote sensing of environment*, *97*(2), 137-162.

Tiller, S., and S. Healy (2013), Have we lost the ability to respond to refugee crises? The Maban response., *Humanitarian Exchange*(57), 17-20.

Torbick, N., D. Lusch, J. Qi, N. Moore, J. Olson, and J. Ge (2006), Developing land use/land cover parameterization for climate-land modelling in East Africa, *International journal of remote sensing*, *27*(19), 4227-4244.

Updike, T., and C. Comp (2010), "Radiometric Use of WorldView-2 Imagery," *Rep.*, DigitalGlobe

Zhu, X., D. Liu, and J. Chen (2012), A new geostatistical approach for filling gaps in Landsat ETM+ SLC-off images, *Remote Sensing of Environment*, *124*(0), 49-60.

Appendix

A) Landsat data

Table A1: Landsat-8 scenes used for data analysis in Maban County.

Nb.	Landsat Scene ID	Date			Cloud cover	Survey data	NDVI
		Y	*M*	*D*	*(%)*	*(%)*	*(mean)*
1	LC817205320313107LGN01	2013	4	17	6.1	99.3	0.24
2	LC81720532013139LGN01	2013	5	19	64.3	22.7	0.35
3	LC81720532013155LGN00	2013	6	4	63.1	37.6	0.25
4	LC81720532013171LGN00	2013	6	20	16.6	69.5	0.46
5	LC81720532013219LGN00	2013	8	7	53.1	89.5	0.70
6	LC81720532013251LGN00	2013	9	8	15.5	77.3	0.80
7	LC81720532013299LGN00	2013	10	26	54.0	14.5	0.59
8	LC81720532013315LGN00	2013	11	11	11.3	87.2	0.47
9	LC81720532013331LGN00	2013	11	27	10.4	100.0	0.43
10	LC81720532013347LGN00	2013	12	13	2.6	100.0	0.21
11	LC81720532013363LGN00	2013	12	29	0.0	100.0	0.18
12	LC81720532014046LGN00	2014	2	15	0.0	100.0	0.17
13	LC81720532014078LGN00	2014	3	19	62.7	0.0	0.25
14	LC81720532014126LGN00	2014	5	6	81.5	0.0	0.35
15	LC81720532014158LGN00	2014	6	7	15.5	77.9	0.50
16	LC81720532014190LGN00	2014	7	09	82.9	0.0	0.50

Table A2: Landsat-8 scenes used for data analysis in Pariang County.

Nb.	Landsat Scene ID	Date			Cloud cover	Survey data	NDVI
		Y	*M*	*D*	*(%)*	*(%)*	*(mean)*
1	LC81740532013121LGN01	2013	5	1	0.5	100.0	0.26
2	LC81740532013137LGN01	2013	5	17	6.8	96.0	0.38
3	LC81740532013169LGN00	2013	6	18	81.3	36.2	0.44
4	LC81740532013201LGN00	2013	7	20	41.7	15.3	0.59
5	LC81740532013265LGN00	2013	9	22	20.5	98.1	0.74
6	LC81740532013329LGN00	2013	11	25	0.0	100.0	0.44
7	LC81740532013361LGN00	2013	12	27	0.0	100.0	0.38
8	LC81740532014012LGN00	2014	1	12	0.0	100.0	0.41
9	LC81740532014044LGN00	2014	2	13	0.0	100.0	0.28
10	LC81740532014076LGN00	2014	3	17	5.6	91.1	0.30
11	LC81740532014092LGN00	2014	4	2	25.2	89.2	0.32
12	LC81740532014108LGN00	2014	4	18	44.1	1.7	0.35
13	LC81740532014172LGN00	2014	6	21	59.4	2.6	0.58

Nb.	Landsat Scene ID						
14	LC81740532014220LGN00	2014	8	8	41.9	45.7	0.68
15	LC81740532014236LGN00	2014	8	24	2.6	99.9	0.72
16	LO81740532013153LGN00	2013	6	2	4.7	100.0	0.37

Table A3: Landsat-7 scenes used for vegetation cover analysis in Maban County.

Nb.	Landsat Scene ID	Date			Data gaps	Burnt area	NDVI
		Y	*M*	*D*	*(%)*	*(%)*	*(mean)*
1	LE71720532000352SGS00	2000	12	17	16.6	24.5	0.24
2	LE71720532002357SGS00	2002	12	23	28.1	27.7	0.23
3	LE71720532003328ASN01	2003	11	24	18.0	14.4	0.34
4	LE71720532004331ASN00	2004	11	26	16.1	8.5	0.28
5	LE71720532005333ASN00	2005	11	29	16.7	13.7	0.30
6	LE71720532006352ASN00	2006	12	18	16.6	22.6	0.29
7	LE71720532007355ASN00	2007	12	21	16.8	22.1	0.28
8	LE71720532008342ASN00	2008	12	7	15.2	14.6	0.31
9	LE71720532011350ASN00	2011	12	16	15.8	11.7	0.32
10	LE71720532012353PFS00	2012	12	18	14.7	18.7	0.31
11	LE71720532013339SG100	2013	12	5	14.8	14.9	0.32

Table A4: Landsat-7 scenes used for vegetation cover analysis in Pariang County.

Nb.	Landsat Scene ID	Date			Data gaps	Burnt area	NDVI
		Y	*M*	*D*	*(%)*	*(%)*	*(mean)*
1	LE71740532000334EDC00	2000	11	29	0.1	16.9	0.29
2	LE71740532003358ASN01	2003	12	24	18.9	26.2	0.28
3	LE71740532004345ASN00	2004	12	10	17.7	27.4	0.28
4	LE71740532005331ASN00	2005	11	27	17.6	14.9	0.35
5	LE71740532006350ASN00	2006	12	16	17.9	20.7	0.31
6	LE71740532008340ASN00	2008	12	5	16.5	15.1	0.33
7	LE71740532009342ASN00	2009	12	8	18.1	22.3	0.32
8	LE71740532010345ASN00	2010	12	11	16.6	13.3	0.38
9	LE71740532011332PFS00	2011	11	28	16.4	12.4	0.39
10	LE71740532012351ASN00	2012	12	16	16.5	21.2	0.33

Table A5: Landsat-7 scenes used for vegetation change analysis in Maban County.

Nb.	Landsat Scene ID	Date			Data gaps	Burnt area	NDVI
		Y	*M*	*D*	*(%)*	*(%)*	*(mean)*
1	LE71720532008054ASN00	2008	2	23	20.3	2.6	0.11
2	LE71720532008086ASN01	2008	3	26	15.9	2.7	0.13
3	LE71720532008182ASN00	2008	6	30	16.3	0.0	0.50
4	LE71720532008294ASN00	2008	10	20	18.8	0.0	0.47

5	LE71720532009136ASN00	2009	5	16	16.4	0.3	0.15
6	LE71720532009264ASN00	2009	9	21	16.0	0.0	0.57
7	LT51720532008254MLK00	2008	9	10	3.5	0.0	0.62
8	LT51720532009352MLK00	2009	12	18	0.0	24.1	0.18

Table A6: Landsat-7 and 5 scenes used for vegetation change analysis in Pariang County.

Nb.	Landsat Scene ID	Date			Data gaps	Burnt area	NDVI
		Y	*M*	*D*	*(%)*	*(%)*	*(mean)*
1	LE71740532007305ASN00	2007	11	1	17.4	0.0	0.43
2	LE71740532008084ASN00	2008	3	24	17.5	2.8	0.17
3	LE71740532009038ASN00	2009	2	7	18.3	10.8	0.17
4	LE71740532009150ASN00	2009	5	30	17.2	2.3	0.17
5	LE71740532009246ASN00	2009	9	3	21.8	0.0	0.59
6	LT51740532008268MLK00	2008	9	24	1.8	0.0	0.47
7	LT51740532009350MLK00	2009	12	16	0.1	24.7	0.23

Table A7: Landsat-7 scenes used for vegetation change analysis in Maban County.

Nb.	Landsat Scene ID	Date			Data gaps	Burnt area	NDVI
		Y	*M*	*D*	*(%)*	*(%)*	*(mean)*
1	LE71720531999269SGS01	1999	9	26	9.6	0.0	0.70
2	LE71720532000096EDC00	2000	4	5	10.3	36.7	0.19
3	LE71720532000256SGS00	2000	9	12	0.0	0.0	0.77
4	LE71720532001098SGS00	2001	4	8	4.2	43.5	0.19
5	LE71720532002277SGS00	2002	10	4	2.9	0.1	0.58
6	LE71720532002309SGS00	2002	11	5	0.3	0.7	0.46
7	LE71720532003024SGS01	2003	1	24	0.1	35.2	0.20
8	LE71720532003136ASN00	2003	5	16	0.5	18.0	0.21

Table A8: Landsat-7 scenes used for vegetation change analysis in Pariang County.

Nb.	Landsat Scene ID	Date			Data gaps	Burnt area	NDVI
		Y	*M*	*D*	*(%)*	*(%)*	*(mean)*
1	LE71740531999299AGS00	1999	10	26	11.3	0.2	0.56
2	LE71740532000126SGS00	2000	5	5	1.8	22.9	0.24
3	LE71740532000334EDC00	2000	11	29	0.1	16.9	0.29
4	LE71740532001272EDC00	2001	9	29	7.9	0.1	0.67
5	LE71740532002067SGS00	2002	3	8	0.1	43.8	0.21
6	LE71740532002307SGS00	2002	11	3	0.0	0.4	0.47
7	LE71740532002355SGS00	2002	12	21	1.8	16.9	0.24

B) Classification results

Confusion Matrix: SVM classification / Maban / validation

Overall Accuracy = (10772/17196) 62.6425%
Kappa Coefficient = 0.4351

Ground Truth (Pixels)

Class	EVF: Layer: f	EVF: Layer: f	EVF: Layer: f	EVF: Layer: f	Total
Unclassified	0	0	0	0	0
EVF: Layer: f	1849	230	173	541	2793
EVF: Layer: f	3109	1511	2	14	4636
EVF: Layer: f	1902	95	7405	0	9402
EVF: Layer: f	358	0	0	7	365
Total	7218	1836	7580	562	17196

Ground Truth (Percent)

Class	EVF: Layer: f	EVF: Layer: f	EVF: Layer: f	EVF: Layer: f	Total
Unclassified	0.00	0.00	0.00	0.00	0.00
EVF: Layer: f	25.62	12.53	2.28	96.26	16.24
EVF: Layer: f	43.07	82.30	0.03	2.49	26.96
EVF: Layer: f	26.35	5.17	97.69	0.00	54.68
EVF: Layer: f	4.96	0.00	0.00	1.25	2.12
Total	100.00	100.00	100.00	100.00	100.00

Class	Commission (Percent)	Omission (Percent)	Commission (Pixels)	Omission (Pixels)
EVF: Layer: f	33.80	74.38	944/2793	5369/7218
EVF: Layer: f	67.41	17.70	3125/4636	325/1836
EVF: Layer: f	21.24	2.31	1997/9402	175/7580
EVF: Layer: f	98.08	98.75	358/365	555/562

Class	Prod. Acc. (Percent)	User Acc. (Percent)	Prod. Acc. (Pixels)	User Acc. (Pixels)
EVF: Layer: f	25.62	66.20	1849/7218	1849/2793
EVF: Layer: f	82.30	32.59	1511/1836	1511/4636
EVF: Layer: f	97.69	78.76	7405/7580	7405/9402
EVF: Layer: f	1.25	1.92	7/562	7/365

Confusion Matrix: SVM classification / Pariang / calibration

Overall Accuracy = (2488/2504) 99.3610%
Kappa Coefficient = 0.9899

Ground Truth (Pixels)

Class	EVF: Layer: p	EVF: Layer: p	EVF: Layer: p	Total
Unclassified	0	0	0	0

EVF: Layer: p	755	7	1	763
EVF: Layer: p	7	1171	1	1179
EVF: Layer: p	0	0	562	562
Total	762	1178	564	2504

Ground Truth (Percent)

Class	EVF: Layer: p	EVF: Layer: p	EVF: Layer: p	Total
Unclassified	0.00	0.00	0.00	0.00
EVF: Layer: p	99.08	0.59	0.18	30.47
EVF: Layer: p	0.92	99.41	0.18	47.08
EVF: Layer: p	0.00	0.00	99.65	22.44
Total	100.00	100.00	100.00	100.00

Class	Commission (Percent)	Omission (Percent)	Commission (Pixels)	Omission (Pixels)
EVF: Layer: p	1.05	0.92	8/763	7/762
EVF: Layer: p	0.68	0.59	8/1179	7/1178
EVF: Layer: p	0.00	0.35	0/562	2/564

Class	Prod. Acc. (Percent)	User Acc. (Percent)	Prod. Acc. (Pixels)	User Acc. (Pixels)
EVF: Layer: p	99.08	98.95	755/762	755/763
EVF: Layer: p	99.41	99.32	1171/1178	1171/1179
EVF: Layer: p	99.65	100.00	562/564	562/562

C) Pre- and postseason fire frequency

Maps of the pre- (Jan.-Jul.) and post-rain (Aug.-Dec.) season fire frequency in the focus areas:

SouthSudan - Fire Frequency (Jan-Jul)

SouthSudan - Fire Frequency (Aug-Dec)

UpperNile - Fire Frequency (Jan-Jul)

UpperNile - Fire Frequency (Aug-Dec)

Unity - Fire Frequency (Jan-Jul)

Unity - Fire Frequency (Aug-Dec)

Pariang - Fire Frequency (Jan-Jul)

Pariang - Fire Frequency (Aug-Dec)

Maban - Fire Frequency (Jan-Jul)

Maban - Fire Frequency (Aug-Dec)